EXPERIMENTAL EVALUATION OF THE BOND DEPENDENT COEFFICIENT
AND PARAMETERS WHICH INFLUENCE CRACK WIDTH IN GFRP
REINFORCED CONCRETE

by

Brittany McCallum

Submitted in partial fulfilment of the requirements
for the degree of Master of Applied Science

at

Dalhousie University
Halifax, Nova Scotia
March 2013

DALHOUSIE UNIVERSITY

DEPARTMENT OF CIVIL AND RESOURCE ENGINEERING

The undersigned hereby certify that they have read and recommend to the Faculty of Graduate Studies for acceptance a thesis entitled "EXPERIMENTAL EVALUATION OF THE BOND DEPENDENT COEFFICIENT AND PARAMETERS WHICH INFLUENCE CRACK WIDTH IN GFRP REINFORCED CONCRETE" by Brittany McCallum in partial fulfilment of the requirements for the degree of Master of Applied Science.

Dated: March 28, 2013

Supervisor: _____

                     Dr. John Newhook

Readers: _____

                     Dr. Yi Liu

                     _____

                     Dr. Darrel Doman

DALHOUSIE UNIVERSITY

DATE: March 28, 2013

AUTHOR: Brittany McCallum

TITLE: Experimental Evaluation of the Bond Dependent Coefficient and Parameters which Influence Crack Width in GFRP Reinforced Concrete

DEPARTMENT OR SCHOOL: Department of Civil and Resource Engineering

DEGREE: MASc   CONVOCATION: May   YEAR: 2013

_____
Signature of Author

To my parents – Robert and Heather McCallum:
Dad – Thanks for being the world's best engineer and giving
me such a high standard to strive for.
Mom – Thanks for instilling in me all the motivation and
inspiration I could ever need.
Thanks for helping me realize my dreams.
I love you both XOXO

TABLE OF CONTENTS

LIST OF TABLES

LIST OF FIGURES

ABSTRACT

Reinforcement of concrete flexural components has been traditionally provided by steel rebar; however, durability concerns and life maintenance costs of this product have powered the emergence of fibre reinforced polymers (FRP) as reinforcement in concrete. FRP products hold tremendous promise but their application can be constrained due to design challenges resulting from a reduced modulus of elasticity. The ability to meet serviceability behavior, such as crack width and deflection, is commonly the limiting factor for design. Therefore, the area of FRP reinforcement provided is often greater than the amount required for strength alone and this has significant impacts on the project economics. The bond dependent coefficient (k_b) of FRP is required for serviceability design purposes in order to account for the bonding capability of FRP to concrete. The values of this coefficient reported in experimental studies are highly variable, resulting in unreliable crack response predictions. Therefore, a more consistent interpretation and calculation must be found for the bond dependent coefficient due to its critical importance in design.

The bond dependent coefficient, as well as physical parameters which influence crack width in GFRP reinforced concrete, were investigated experimentally in this study using a total of 33 specimens. The test procedure was taken from a procedure being developed by the American Concrete Institute (ACI) Committee 440 and was evaluated and modified as required during testing. Phase I testing was used to investigate and determine the physical parameters which had the most significant influence on cracking behaviour and bonding capability. Using significant findings from Phase I, Phase II testing was structured to focus on the interpretation of the bond dependent coefficient and the statistical variation in a set of 5 identical test specimens. Current design equations, as recommended by ACI 440.1R-06 and CHBDC CAN/CSA-S6-06, were used for the calculation of the bond dependent coefficient for all specimens. Interpretation of the bond dependent coefficient was considered using the stress-level approach and newly developed slope approach.

Results of the study indicated that the high variability of k_b was likely due to its interpretation. Current design equations force a zero intercept, neglecting the fact that concrete does not crack immediately upon loading. In addition, clear definitions of service stress and maximum crack width are ambiguous, further complicating the calculation of the bond dependent coefficient. This resulted in a range of k_b values for a given beam despite the fact that k_b is inherently a material property of the bar. The behaviour of specimens following load cycling was also very different than the initial loading cycle and consequently, k_b was also significantly different. As structures in the field will be subjected to continual loading and unloading, the effect of cyclic loading becomes a consideration in the calculation of k_b.

LIST OF ABBREVIATIONS AND SYMBOLS USED

A	average effective concrete area around a reinforcing bar
AASHTO	American Association of State Highway and Transportation Officials
ACI	American Concrete Institute
A_{frp}	area of FRP reinforcement
AFRP	aramid fibre reinforced polymer
A_r	concrete area surrounding one tension bar equal to the total effective tension area of concrete surrounding reinforcement and having same centroid, divided by number of bars
ASTM	American Society for Testing and Materials
Avg.	average
c	depth to centroid of crack section
CEB	Comité Euro-International du Béton
CFRP	carbon fibre reinforced polymer
CHBDC	Canadian Highway Bridge Design Code
COV	coefficient of variation
CRCP	continuously reinforced concrete pavement
CSA	Canadian Standards Association
d	depth to centroid of tension reinforcement
d*	controlling cover dimension
d_b	bar diameter
d_c	thickness of cover from tension face to center of closest bar
d_s	side cover
E_c	elastic modulus of concrete
E_f	tensile modulus of elasticity of FRP reinforcement
E_s	elastic modulus of steel reinforcement
f'_c	28 day concrete compressive strength
f_{frp}	stress in FRP reinforcement
FOS	fibre optic sensor
FRC	fibre reinforced concrete
FRP	fibre reinforced polymer

f_s	stress in steel reinforcement
f_u	guaranteed ultimate tensile strength of FRP reinforcement
GFRP	glass fibre reinforced polymer
H	horizontal
h_2, h_1	distance from neutral axis to tensile face, distance from neutral axis to center of reinforcement
HPC	high performance concrete
I_{cr}	cracked moment of inertia
ID	identification
ISIS	Intelligent Sensing for Innovative Structures
k_b	bond dependent coefficient
kd	distance from compression face to neutral axis in a cracked section
kg	kilogram
kN	kilo newton
L	span
LVDT	linear variable displacement transducer
m^3	cubic metre
M	applied moment
M_{cr}	cracking moment
mm	millimeter
MN	mega newton
M_n	nominal moment
MOR	modulus of rupture
MPa	megapascal
MTQ	Ministry of Transportation Quebec
NA	neutral axis
NEFMAC	2-D grid-type reinforcement consisting of glass and carbon fibers impregnated with resin
No.	number
P_{cr}	cracking load
R	h_2/h_1

RC	reinforced concrete
s	bar spacing
SCC	self-consolidating concrete
SD	standard deviation
t_b	bottom cover measured from the center of the lowest bar
t_s	side cover measured from the center of the outer bar
V	vertical
w	crack width
w_{38}	crack width corresponding to specimen with 38 mm cover
w_{50}	crack width corresponding to specimen with 50 mm cover
w_{60}	crack width corresponding to specimen with 60 mm bar spacing
w_{100}	crack width corresponding to specimen with 100 mm bar spacing
w_{150}	crack width corresponding to specimen with 150 mm bar spacing
w_{200}	crack width corresponding to specimen with 200 mm bar spacing
w_b	maximum bottom crack width in constant moment region
w_s	maximum side crack width at level of steel centroid in constant moment region
$\bar{y}_{cr}$	depth to centroid of crack section
z	crack control parameter
β	h_2/h_1
γ	ratio between the neutral axis and tension face to distance between neutral axis and centroid of reinforcement
ρ	reinforcement ratio
ρ_b	balanced reinforcement ratio
ρ_{frp}	FRP reinforcement ratio

ACKNOWLEDGEMENTS

Let me start by first thanking my supervisor, Dr. John Newhook, for providing me with such a wonderful learning opportunity. I can honestly say that I have learned from the best and his enthusiasm towards research has been inspiring.

I would like to thank NSERC for providing the financial support that enabled me to conduct this research. I would also like to acknowledge the contributions provided by Pultrall Inc. and Hughes Brothers Ltd. who provided materials for the project.

Thank you to Dr. Yi Liu and Dr. Darrel Doman, my committee members, for taking the time to review this thesis.

I would also like to thank the civil technicians for all their help in the lab, with a special shout out to Brian Liekens for his endless patience throughout this master's degree, as well as his friendship.

I would also like to thank my fellow graduate students for their help in the lab and for moral support in the office. This is especially true for Phil Vickers and Justin Clarke who have come to understand "grad students helping grad students" all too well!

Finally, I would like to thank my parents, Robert and Heather, my "ginger" siblings, Anne, Meg and Michael, and my niece, Lauren for their never wavering support.

CHAPTER 1 :   INTRODUCTION

Concrete is rarely used without the addition of reinforcement due to its low tensile strength and thus, brittle behaviour. Tensile strength in reinforced concrete has been traditionally provided by steel reinforcement; however, due to durability, corrosion and life maintenance costs, fibre reinforced polymers (FRP) have been emerging since the 1950's as an alternative to steel reinforcement. Despite the fact that FRP applications hold tremendous promise, design constraints can limit their application. Increased deflection and crack width due to a reduced modulus of elasticity of FRP are problematic in selecting an efficient design. The design of glass fibre reinforced polymer (GFRP) reinforced concrete is typically governed by serviceability criteria as the modulus of elasticity of GFRP is approximately 25% of that of steel reinforcement. Therefore, the area of GFRP reinforcement provided is often greater than what is required for strength alone which can have a significant impact on project economics.

The current design approach, as recommended by ACI 440.1R-06 and CHBDC CAN/CSA-S6-06, requires a bond dependent coefficient (k_b) to be used in prediction of the serviceability behaviour of FRP reinforced concrete. This coefficient is meant to capture the bonding capability of FRP to concrete and is highly dependent on physical properties such as surface treatment. The surface treatment of FRP is not regulated and can therefore vary dramatically depending on the manufacturer. A variety of the surface treatments that have been used in the industry are shown in Figure 1.1.

Figure 1.1 - Various surface treatments for FRP

This coefficient is critically important for reliable and consistent crack width predictions based on the current design standards. However, this coefficient has been reported as highly variable as it is dependent upon physical properties. To accurately calculate k_b, the physical parameters affecting cracking and thus the bonding behaviour of FRP to concrete must be investigated in order to determine their relationship to the bond dependent coefficient. A more consistent interpretation and calculation approach must be found for the bond dependent coefficient due to its critical importance in design.

1.1 RESEARCH OBJECTIVES

In 2010, a test method was proposed to ACI Committee 440 for the purposes of achieving consistency in the experimental determination of the bond dependent coefficient of FRP. The test method was evaluated in this study using the experimental testing of 33 concrete specimens reinforced with GFRP, while modifications were made as required. Various parameters impacting cracking and bonding behaviour were examined in two phases of testing.

The specific physical parameters that were investigated include:
- Reinforcement ratio/bar diameter,
- Concrete cover,
- Bar spacing,
- Member type (slab/beam),
- Synthetic fibre content, and
- Surface treatment.

One of the two main objectives of this research was to examine and explain the significant variability of reported k_b values. A literature review was completed to identify possible interpretation and calculation approaches for this coefficient. Using the results from this study, the second main objective was to determine an evaluation method for k_b in order to achieve consistency in its calculation.

A secondary objective was to examine the statistical variability of cracking behaviour and k_b in FRP reinforced specimens. A test series of five identical specimens was used to examine this variation. The k_b values calculated from this analysis were also applied and used to predict the bond behaviour of other specimens with identical reinforcement. Cyclic loading was also investigated to examine the effect of reloading behaviour on the calculation of k_b.

CHAPTER 2 :   LITERATURE REVIEW FOR FRP AND CRACKING

This chapter discusses relevant information pertaining to the composition of FRP bars, and identifies current applications for these products. In addition, there will be a focus on the mechanics of crack formation and control in reinforced concrete, including the properties that affect bond behaviour.

2.1   FIBRE REINFORCED POLYMERS

FRP products are composite materials that are comprised of a matrix and reinforcing fibres. FRP exhibits a much different stress-strain relationship than steel and is a brittle material that does not exhibit yielding.   As shown in Figure 2.1, the stress-stain relationship of FRP and its constituents is essentially linear up to failure with the fibres being much stronger than the matrix. Contrast this to the stress-strain relationship for steel shown in Figure 2.2; a yielding plateau occurs following a linear elastic range due to the material ductility.
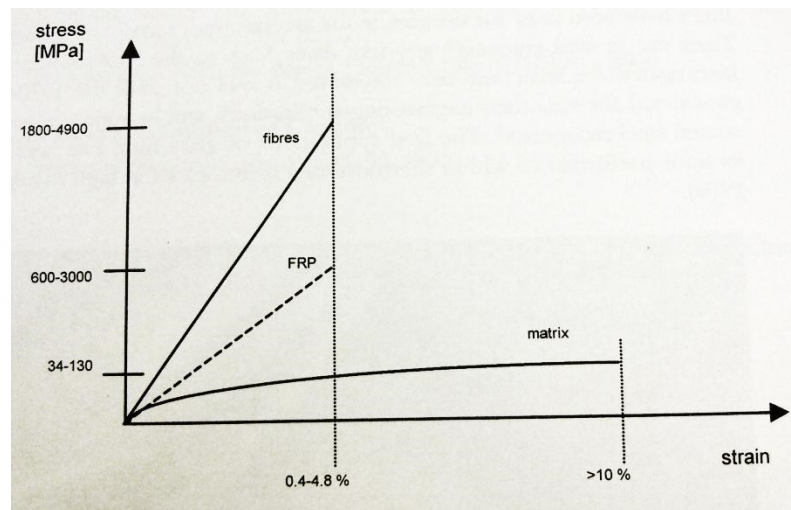
Figure 2.1 - Stress-strain relationship for FRP and its constituents (ISIS Canada Corporation, 2001)
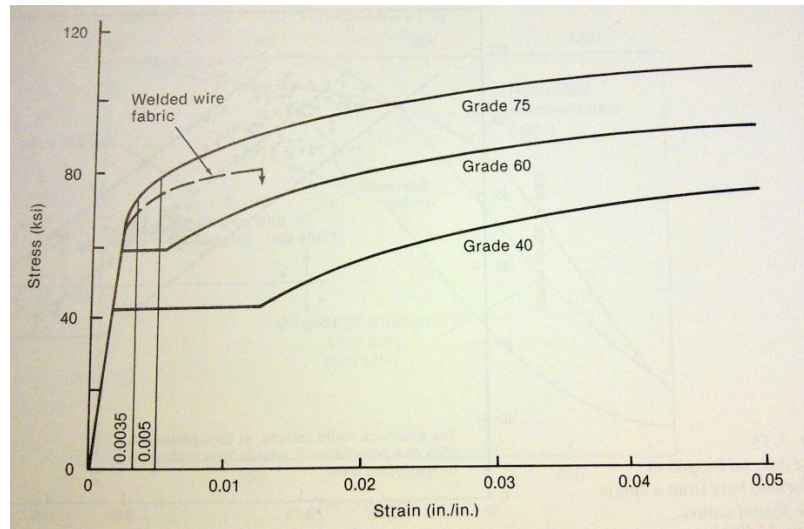
Figure 2.2 - Stress-strain relationship for reinforcing steel (Wight & MacGregor, 2009)

Due to the differences in their stress-strain relationships, there are also different design practices for FRP and steel reinforced concrete. Steel reinforced concrete is typically designed to be reinforced such that the steel yields prior to concrete crushing. However, for FRP reinforced concrete, it is preferable to fail in concrete crushing mode without tension rupture of the FRP.

2.1.1 Fibre types

The most common types of fibres for FRP are carbon (CFRP), glass (GFRP) and aramid (AFRP). CFRP are the most widely used in high-performance concrete structures due to their superior tensile strength. In addition, CFRP also has the highest modulus of elasticity of the three common fibre types. These fibres are extremely anisotropic, where the modulus in the longitudinal direction can be 29 times the modulus in the transverse direction (Campbell, 2010). Carbon fibres were first introduced in the 1960's and it was found that a bar surface treatment was required to exhibit adhesion to the epoxy matrix.

GFRP is composed of glass fibres and have moduli of elasticity in tension approximately 20 to 25 percent of steel reinforcement. This low modulus produces increased deflections and crack widths which propose significant design challenges. E-glass is the most

affordable option for high performance fibres, and thus, is used most in commercial composite applications.

AFRP is composed of organic fibres with stiffness and strength intermediate between glass and carbon. Aramid fibres are formed by the reaction between a carboxylic acid and an amine group to form aromatic polyamides. This ring structure contributes high thermal stability (Campbell, 2010). However, aramid fibres are not surface treated as no acceptable treatment has yet been developed.

2.1.2 Matrix

In order to form FRP, the fibres must be bound by a matrix. The matrix transfers the load directly to the fibres and provides toughness, impact and abrasion resistance (Campbell, 2010). Two types of polymeric matrices are widely used for FRP composites: thermosetting and thermoplastic. Thermosetting polymers are more commonly used and are composed of low molecular weight liquids whose molecules are joined by chemical cross-links (ISIS Canada Corporation, 2001). Once set, a rigid three-dimensional structure is formed that cannot be reshaped using pressure or heat. Common thermosetting polymers are epoxy, polyester and vinyl ester, whose properties are shown in Table 2.1. Thermoplastic matrix polymers are made from molecules in a linear structural form held in place by weak secondary bonds that are easily destroyed by heat or pressure if reshaping is required.

Table 2.1 - Properties of Typical Thermosetting Resins (ISIS Canada Corporation, 2001)

Resin	Specific Gravity	Tensile Strength (MPa)	Tensile Modulus (GPa)	Cure Shrinkage (%)
Epoxy	1.20 – 1.30	55 – 130	2.75 – 4.10	1 – 5
Polyester	1.10 – 1.40	34.5 – 103.5	2.10 – 3.45	5 – 12
Vinyl Ester	1.12 – 1.32	73 - 81	3 – 3.35	5.2 – 10.3

2.1.3 Manufacturing Processes

Commercially, filament winding and pultrusion are the most commonly used fabrication processes for FRP. Filament winding, as shown in Figure 2.3, has been in continuous use

since the mid 1940's and is a highly repeatable process used to fabricate bodies of practically any geometry and size. Dry tows are drawn through a liquid resin, assembled into a band and wound on a rotating mandrel. The band of fibres must be passed through a series of guides and spreader bars which is then delivered to the part. Low tension aids to reduce abrasion and minimizes the possibility of tow breakage (Campbell, 2010).
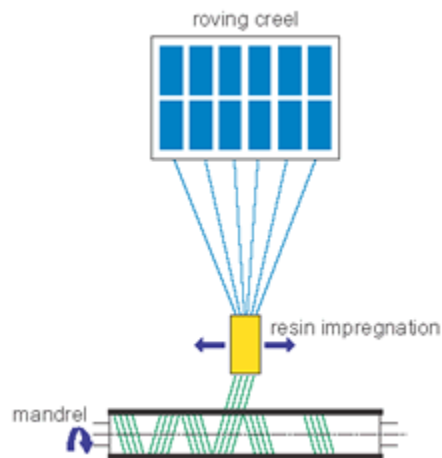
Figure 2.3 - Filament winding fabrication process (Owens Corning Composite Materials, 2011)

Pultrusion is the primary process used for manufacturing FRP bars, where the products are formed using a continuous process where the base reinforcement material is pulled through a resin bath and then a heated dye, as shown in the schematic in Figure 2.4. This process allows for a wide variety of shapes, length and properties by modifying the resin and reinforcement materials. The end product produced by pultrusion is non-corrosive, non-conductive, neutral to electromagnetic fields and is also a thermal insulator (Pultrall Inc., 2007). The main disadvantage of the pultrusion process is that the resin provides a smooth surface which produces a low quality bond in concrete and reduces the load transfer between the concrete and FRP reinforcement (Esfandeh *et al.*, 2008). However, the FRP can be surface treated to improve the bond. Examples of surface treatments are sand-coated, ribbed, helically wrapped, or braided.
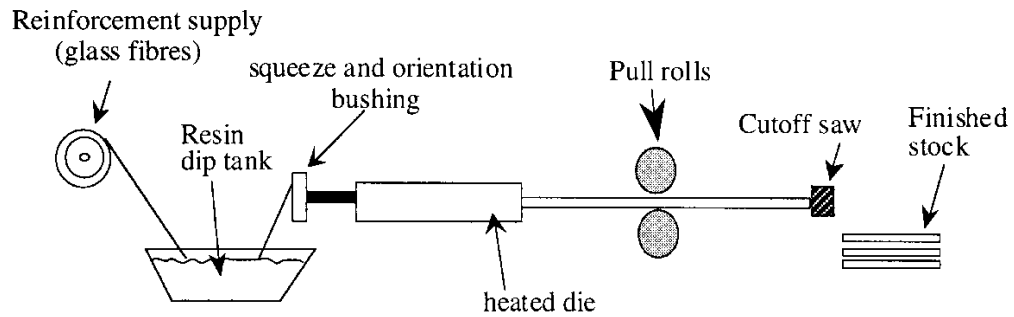
Figure 2.4 - Pultrusion process for FRP (Tighouart *et al.*, 1998)

2.2 FRP APPLICATIONS

Due to the various advantages associated with the use of FRP, the applications for these products continue to increase. Real life applications include bridge decks, wharfs and pavement reinforcement. Another major application of FRP involves rehabilitation of existing concrete, steel, timber or masonry structures. Since the late 1990's, designers have chosen to move towards these innovative technologies to mitigate corrosion problems and reduce overall life maintenance costs. However, meeting serviceability criteria such as maximum crack width and deflection can be difficult to achieve and is commonly the limiting factor in design.

2.2.1 Bridge Decks

According to Cheng & Van Zwol (2005), forty percent of the bridges in Canada were constructed more than 30 years ago and significant deterioration of the deck has resulted due to corrosion of internal steel reinforcement. Concrete bridge decks are in direct exposure to harsh environments and de-icing chemicals, resulting in an accelerated deterioration process. For this reason, FRP is being employed in bridge deck design in order to extend the service life of the structure.

In 1997, the first continuous steel-free deck was constructed as part of the Crowchild Trail Bridge in Alberta. This deck replaced the existing superstructure, although the piers and abutments were first built in the 1960's (Cheng & Van Zwol, 2005).

In December of 1997, the Joffre Bridge, shown in Figure 2.5(a), in Downtown Sherbrooke, Quebec opened to vehicle traffic over the St. François River. The bridge had dimensions of 164.4 m in length and 16.8 m in width and was composed of five spans of continuous steel girders. The deck slab for this bridge was 260 mm thick and was reinforced with CFRP NEFMAC grids in the top mat, as shown in Figure 2.5(b). This bridge was instrumented at critical locations using fibre optic sensors (FOS) to monitor the deck behavior and performance during and following construction to ensure structural integrity. Since 1997, the use of FRP reinforced concrete bridge decks has grown across Canada and the United States.

| (a) | (b) |

Figure 2.5 - Joffre Bridge: (a) After construction; and (b) CFRP grids (Benmokrane *et al.***, 2004)**

2.2.2 Pavement

As of 2006, continuously reinforced concrete pavements (CRCP) with GFRP reinforcement had never been used on a highway with regular traffic. However, in 2006, MTQ Pavement Division and the University of Sherbrooke initiated a test project on Highway 40 East near Montreal. For this study, 18 full scale slabs, ranging from 280 – 350 mm in thickness were installed over 3 lanes of traffic, as shown in Figure 2.6.

150 m

22 m

| B | A4 | A3 | A2 | A1 | S1 | CRCP-Steel | Lane 1 |

D = 280 mm
p = 1.16 %-2#20
D = 280 mm
p = 1.32 %-2#20
D = 280 mm
p = 1.16 %-2#20
D = 280 mm
p = 1.16 %-2#20
D = 280 mm
p = 1.05 %-2#20
D = 280 mm
p = 0.74 %-1#20

Lane 2

| D3 | D2 | D1 | C2 | C1 | S2 | CRCP-Steel |

D = 280 mm
p = 0.97 %-1#22
D = 280 mm
p = 1.27 %-1#25
D = 280 mm
p = 1.27 %-1#25
D = 280 mm
p = 1.07 %-1#25
D = 280 mm
p = 1.57 %-2#22
D = 280 mm
p = 0.74 %-1#20

Lane 3

| G | F | E2 | E1 | D4 | S3 | CRCP-Steel |

D = 350 mm
p = 0.93 %-1#20 (2L)
D = 350 mm
p = 0.93 %-2#20
D = 280 mm
p = 1.03 %-1#25
D = 280 mm
p = 1.16 %-1#20
D = 280 mm
p = 0.77 %-1#20
D = 280 mm
p = 0.74 %-1#20

p : Percent of Reinforcement;   # : Bar Diameter (mm);   D: Pavement Thickness

Figure 2.6 - Layout of test slabs on Highway 40 East (Benmokrane *et al.*, 2008)

Instrumentation on the bars was completed in order to monitor the performance of the pavement following construction. After one year in service, satisfactory performance was achieved with no pumping, faulting, spalling or punch-out failure in the slab surface. Crack spacing and crack width were also monitored as these are the critical factors that control pavement performance. It was found that crack widths ranged from 0.75 – 0.9 mm, which is less than the current AASHTO design limits.

2.2.3 Wharf

Hall's Harbour is the only safe harbour on the Fundy Shore and is located north of Digby in Nova Scotia. It is also home to the first marine structure in Canada utilizing GFRP reinforcement and a steel-free deck (Newhook, 2006). This design was initiated due to a collapse of the mid-section of the wharf during a storm in 1998. Due to the extreme environmental exposure conditions, FRP was suggested as a feasible solution. This innovative design was approximately 4.5% more based on the total project cost than its steel counterpart and extended service life from 30 years to between 60 and 80 years. In terms of the design, the piles were composed of steel free concrete encased in a GFRP jacket. The deck panels were composed of fibre reinforced concrete (FRC), utilizing arching to resist tension forces and also contained GFRP rods to reinforce against the uplift force created by the waves. Fibre optic monitoring technology was also embedded in the glass rods in order to allow ISIS Canada to monitor the performance of the structure over time.

2.2.4 Rehabilitation and Retrofit

Many structures in Canada require rehabilitation due to corroded steel reinforcement or increases in load due to changes in the use of the structure. To demolish a structure and rebuild can be very costly and is not always a viable solution. Many structures are facing this challenge today and with minimal intrusion, FRP strengthening proposes a viable solution in order to preserve aesthetics in the form of FRP wraps and externally bonded FRP laminates.

Galati *et al.* (2006) investigated the flexural strengthening of a bridge superstructure located on Route 0039 in Washington County, Missouri. The bridge was a 4 span RC slab 17.8 m long and 4.3 m wide with a 178 mm thick concrete slab. Visible damage was found on the North edge of the deck in the form of concrete spalling, resulting in exposed steel reinforcement. It was also deemed that cracking at midspan was due to insufficient longitudinal reinforcement. CFRP laminates were proposed and analyzed using AASHTO specifications as a solution to the current situation. The laminates were externally bonded on the bridge as shown in Figure 2.7. The entire application was completed by a certified contractor in 48 hours without any disruption to traffic. Following installation, the load posting of the bridge was increased from 4.5 to 16 tons (a 320% enhancement).
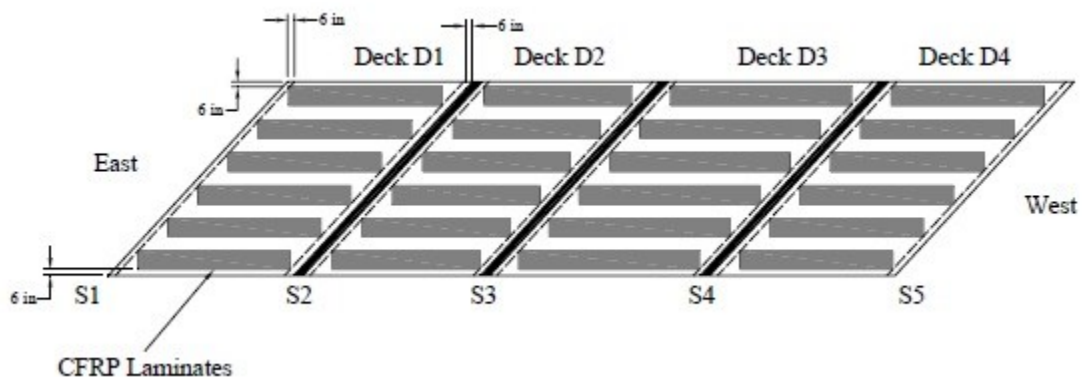
Figure 2.7 - Location of CFRP Laminates for Bridge Strengthening (Galati *et al.*, 2006)

After one year in service, cracking was observed in a high rise structure in the slabs, foundation walls, beams and columns as shown in Figure 2.8. Likely causes were differential settlement of the foundation, shear reinforcement deficiency in the beams, excessive cover to main reinforcement in foundation walls, smaller than specified thickness of the walls and the presence of clay backfill behind the wall (Sheikh & Homam, 2004). Repair of the structure was required as the factor of safety against shear ranged from 0.45 – 1.28, while design values were 1.65. To minimize interference with residents, retrofit with CFRP wraps and sheets was chosen. As of 2004, the repaired components had satisfactory performance without any problems for 4 years.

(a)   (b)
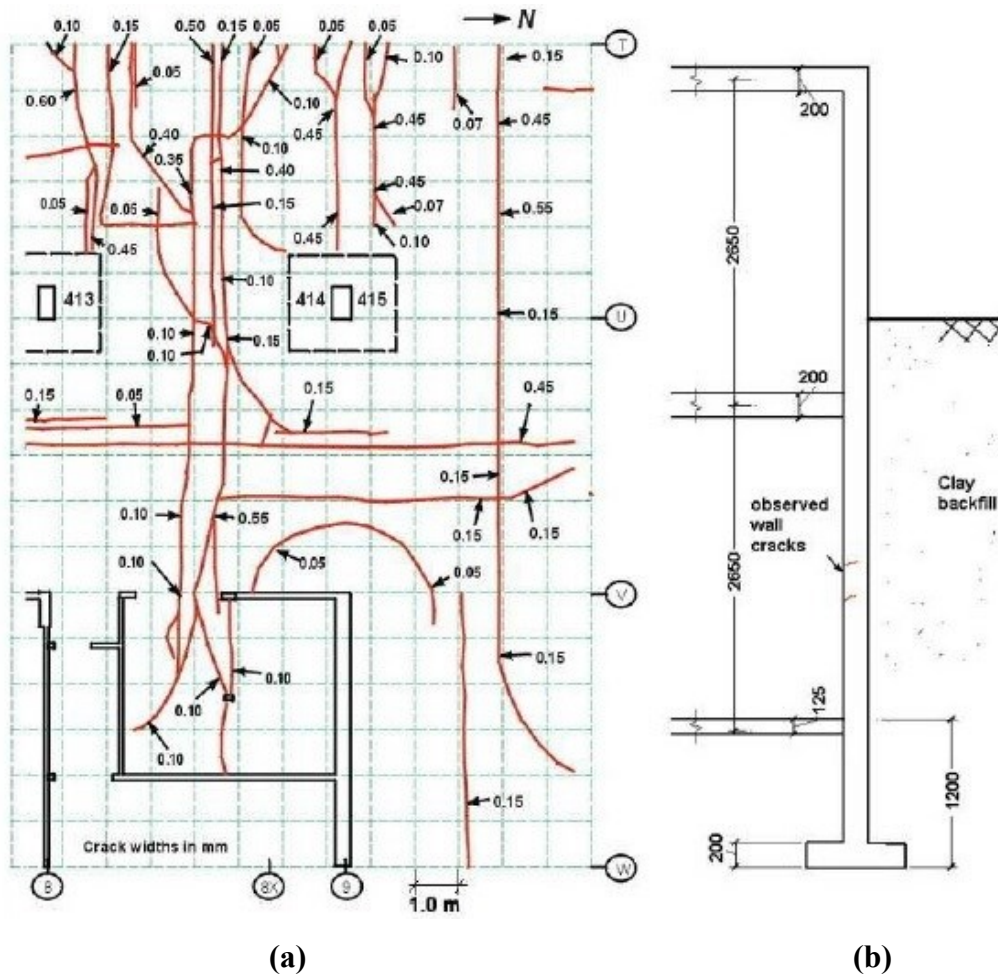
Figure 2.8 - Observed cracks in: (a) the slab; and (b) the foundation wall (Sheikh & Homam, 2004)

2.2.5 Design Challenge

In steel reinforced concrete, crack control is important to protect the reinforcement from corrosion; however, FRP bars have excellent corrosion resistance and therefore, maximum crack width limits are primarily for aesthetics. However, meeting these serviceability limits with FRP can be a challenge due to its reduced modulus of elasticity, making cracking a very important consideration in design. There are many methods to approach crack control in FRP reinforced concrete which will be discussed in Section 2.6.

2.3 PROPERTIES AFFECTING CRACKING BEHAVIOUR

Many of the crack width equations that have been formulated by researchers in the past have shown that stress in the reinforcement is the single most important variable in predicting crack width. However, based on statistical or physical models, researchers have found varying results for properties such as surface treatment, reinforcement ratio/bar diameter, clear cover and fibre content. This section discusses the literature to date on these parameters and the reported results of their variation on cracking behaviour.

2.3.1 Surface Treatment

In FRP reinforced concrete, the bond between FRP and concrete is dependent on adhesion and friction, unlike deformed steel reinforcement which relies heavily on mechanical bearing (Tighouart *et al.*, 1998). Because friction controls the quality and strength of the bond, the surface configuration of the FRP rebar has a large impact on the bond formed. Pull-out resistance is linked to a combination of both the static and friction loads as well as normal forces attributed to surface configuration that are exerted on the rebar and the surrounding concrete, as shown in Figure 2.9. Esfandeh *et al.* (2008) confirmed these phenomena with a series of pull-out tests on FRP rebars with four types of surface configurations: one with a smooth surface, sand-coated surface, helically wound ribs and a combination of sand-coated and helically wound ribs In this study, the addition of any type of texture resulted in an increase in pull-out resistance. Based on pull-out and load-displacement behaviour, the FRP bar with the sand-coated surface and helically wound ribs had the best overall performance. Research carried out by

Masmoudi *et al.* (1996) also determined differences in crack width and crack spacing depending on the surface configuration of GFRP rebars.
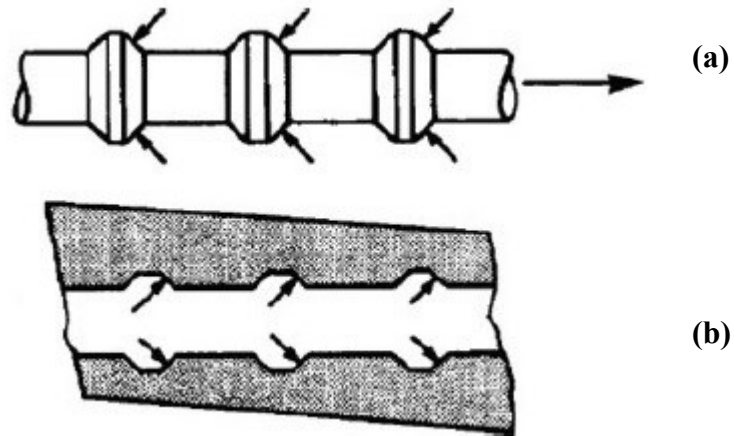
Figure 2.9 - Schematic of forces on (a) deformed rebar; and (b) concrete during pull-out testing (Esfandeh *et al.*, 2008)

2.3.2 Reinforcement Ratio/Bar Diameter

Lee *et al.* (2010) found no clear correlation between bond and reinforcement ratio or bar size when evaluating k_b. However, Masmoudi *et al.* (1996) found that an increase in reinforcement ratio resulted in more numerous cracks in the constant moment region of the specimen and thus, decreased crack spacing. These researchers also found that an increase in reinforcement ratio resulted in decreased crack widths. Further investigations by Tighouart *et al.* (1998) revealed that FRP rebar, similar to steel, exhibited a loss in maximum bond strength as the diameter of the bar increased. This occurrence can be further explained by the fact that as the diameter increases, more bleeding water from the concrete can be trapped beneath the bar, reducing the contact area available for bond. With a smaller contact area, bond strength will be decreased in pull-out testing. This was confirmed by Alves *et al.* (2011) where the bond strength of No.16 (ϕ15.875 mm) bars was 30-50% greater than No.19 (ϕ19.05 mm) GFRP bars with identical surface configurations.

2.3.3 Concrete Cover

The majority of the research completed to date on the effects of cover for FRP has been focused on durability, as FRP proposes increased durability to conventional steel reinforcement. Based on work completed by Galati *et al.* (2006), small covers were more susceptible to micro cracking due to stresses induced by thermal treatment. In addition, local bond slip relationships were improved with increases in cover. Concrete cover was also determined to be important in decreasing the temperature gradient and thus, the expansion of the cross section of the bar (Alves *et al.*, 2011).

Although the behaviour of steel is fundamentally different than FRP, the same crack width prediction equations are used for both materials with variable bond dependent coefficients. Cover is one of the variables used in crack control for steel and FRP reinforced concrete and therefore, some conclusions can be drawn from steel reinforced members. Broms (1965) determined that crack spacing in steel reinforced members was determined primarily by the maximum concrete cover. Experimentally, the observed crack spacing at the level of reinforcement was approximately two times the thickness of the cover to the center of the reinforcing bar.

2.3.4 Synthetic Fibre Content

Fibre reinforced concrete (FRC) dates as far back as 4900 B.C. when civilization in Mesopotamia used straw to reinforce their mud brick buildings (Campbell, 2010). In present times, fibre reinforced concrete refers to concrete that is reinforced with randomly distributed fibres. Common materials for these fibres include steel, glass, synthetic and natural and they can be deformed or have mechanical anchorage to improve their bond to the concrete matrix. The behaviour of FRC depends on the ability of the fibres to maintain a good bond to concrete when they are being pulled in tension across crack openings (Wight & MacGregor, 2009). Since the 1980's, FRC has been used in non-structural uses due to lack of design codes; however, in 2008, ACI allowed for steel fibres to be used as minimum shear reinforcement in beams.

The addition of fibres to FRP reinforced concrete has been investigated by several researchers to determine the improvements they may provide for serviceability. Due to the large variation of fibre materials commercially available, several types of fibres have been tested in varying percentages. Wang & Belarbi (2005) used 0.5% by volume, fibrillated, polypropylene fibres with FRP reinforcement and determined that there was a negligible change in crack spacing between plain and FRC specimens at ultimate. However, at a service stress of 40% of ultimate, the FRC specimens had more numerous cracks and therefore, a 20% smaller crack spacing. The crack spacing in FRC specimens was smaller as less bond stress was required to attain the cracking stress due to the tensile component from the bridging of the fibres, as shown in Figure 2.10. The researchers also found that the FRC specimens exhibited higher ultimate strains and failed in a more ductile manner than the plain specimens that failed in a brittle, explosive manner. By increasing the volume of fibres to 1% (polypropylene, crimped), a reduction in crack width was observed, as well as increased bonding due to a lower value of k_b for FRC specimens over plain concrete specimens (Lee *et al.*, 2010). It was also found that over-reinforced beams with FRC had more numerous cracks due to the addition of fibres that prevented localization of cracking. A 30-70 polyolefin-steel combination was used at a volume of 2% and increased the modulus of rupture by 72.52% and the load carrying capacity by 75.42% over plain concrete (Eswari *et al.*, 2008). At ultimate and service loads, the deflection was increased by 137.5% and 187.49% respectively and the FRC specimens also exhibited increased ductility. Experimentally, more cracks were formed and there was an observed 80% reduction in crack widths. Yang *et al.* (2012) conducted testing on six high-strength concrete beams with GFRP or CFRP flexural reinforcement, and either 2.0% synthetic or 1.0% steel fibre content by volume. As predicted, the FRC specimens exhibited smaller crack widths at equivalent load levels compared to plain specimens. The researchers also observed that the FRC specimens had delayed initiation of cracking, with the cracking loads being approximately twice those of the plain concrete. Crack widths were only controlled by the fibres up to a load of 100 kN; however, the ductility index at failure was 70 - 80% higher for FRC specimens. As a final conclusion, the researchers found that the synthetic fibers were more effective for controlling cracking response than the steel fibers in CFRP.
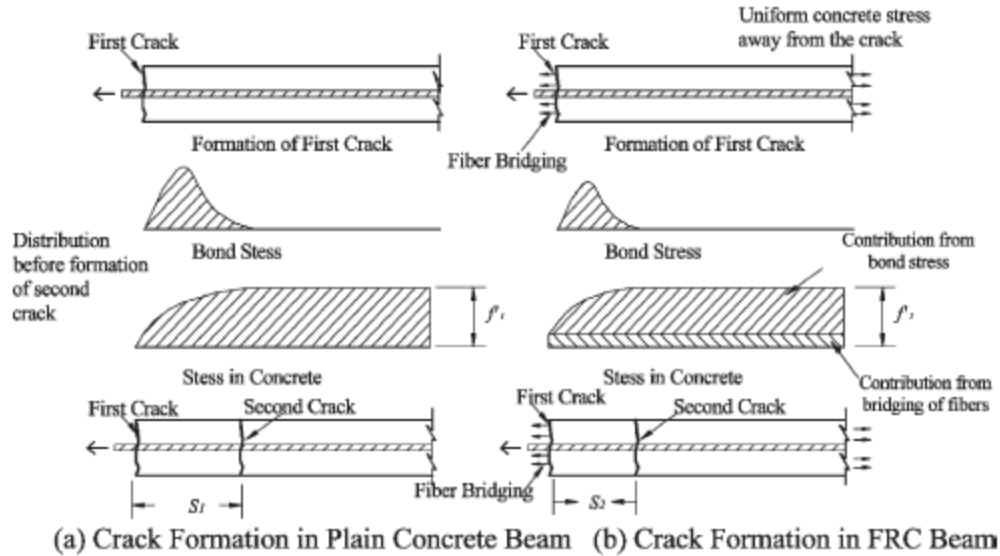
Figure 2.10 - Crack formation in concrete (Wang & Belarbi, 2005)

2.4 MECHANICS OF CRACK FORMATION

In concrete members, the mechanism of cracking begins by the formation of tensile stresses due to applied load, moment, shear and torsion. The crack patterns resulting from these induced loads are very distinctive, as shown in Figure 2.11. The formation of a crack occurs when the tensile stress developed in the concrete exceeds the tensile strength of the concrete. At the crack location, the reinforcement begins to accept the tensile force. As the distance extends from the crack, the stress is gradually transferred from the reinforcement to the concrete through bonding until the formation of another crack occurs due to re-attaining the tensile strength within the concrete. With increases in load, this process can be repeated until the distance between cracks is not large enough for the tensile stress of concrete to be reached and therefore, the formation of cracks is ceased.
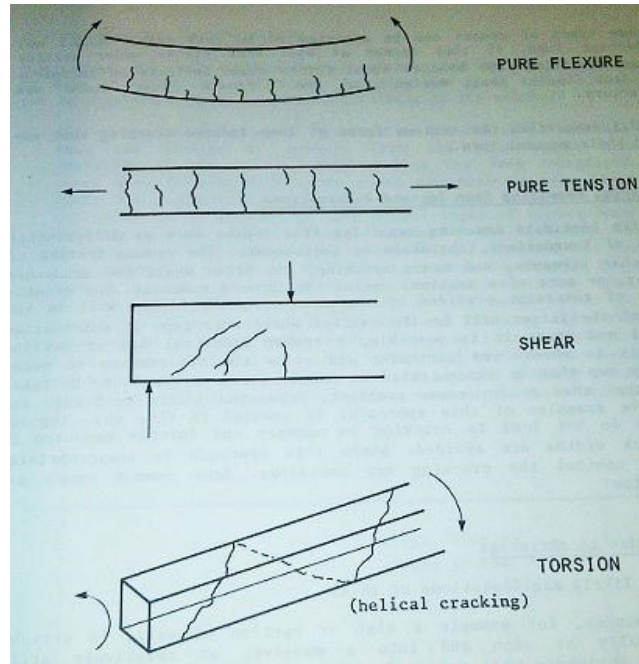
Figure 2.11 - Load induced cracks (Comité Euro-International du Béton (CEB), 1985)

Cracking can also be initiated by imposed deformations such as differential settlement of foundations, shrinkage or temperature. A common solution to minimizing cracking due to imposed deformations is to remove the restraint and allow deformation to occur at concentrated points where measures have already been taken to avoid problems. This can be achieved in a variety of ways, such as the use of control joints or the addition of shrinkage reinforcement. Another major cause of cracking is attributed to the temperature gradient within members and to the cooling of members due to the hydration of cement (Comité Euro-International du Béton (CEB), 1985).

2.5 CRACK WIDTH PREDICTION IN STEEL REINFORCED CONCRETE

Serviceability performance of reinforced concrete infrastructure relies on maintaining acceptable crack control and deflection. Excessive cracking is not only undesirable for aesthetic purposes, but can also enable substances, such as chlorides or salts, to penetrate through the concrete and corrode the steel reinforcement, compromising durability. Several crack width equations have been proposed by researchers since the 1960's as a means to address these concerns and since 1971, the American Concrete Institute (ACI) has required control of flexural cracking in steel reinforced concrete.

18

2.5.1 Gergely-Lutz Equation

In 1968, Peter Gergely and Leroy Lutz statistically derived the Gergely-Lutz equation for predicting crack widths in steel reinforced concrete. With the data collected by several researchers, Gergely and Lutz performed a multiple regression analysis to determine the variables that contributed most to crack width. The data consisted of 612 observations of bottom crack widths, and 355 observations of side crack widths (Gergely & Lutz, 1968). It was concluded that steel stress was the most important variable in the evaluation of crack width. Two equations, [2.1] and [2.2], were considered to best predict the maximum probable crack width at the side and bottom (tension) faces:

$$w_s = 0.091 \frac{\sqrt[3]{t_s A}}{1 + \frac{t_s}{h_1}} (f_s - 5) \qquad\qquad [2.1]$$

$$w_b = 0.091 \sqrt[3]{t_b A} R (f_s - 5) \qquad\qquad [2.2]$$

where,

w_s is the maximum (measured or calculated) side crack width at the level of the steel centroid in constant moment region, in

w_b is the maximum (measured or calculated) bottom crack width in constant moment region, in

t_s is the side cover measured from the center of the outer bar, in

t_b is the bottom cover measured from the center of the lowest bar, in

A   is the average effective concrete area around a reinforcing bar ($=A_e$/# of bars), in^2

f_s is the steel stress calculated by elastic cracked section theory, psi

R   is the ratio of h_2/h_1

h_1 is the distance from neutral axis to center of reinforcement, in

h_2 is the distance from neutral axis to tensile face, in

Although the equations presented above best predicted the most probable crack width, a more simplistic approach (Equation [2.3]) was suggested by these researchers for design purposes:

$$w = 0.076\beta f_s \sqrt[3]{d_c A} \qquad\qquad [2.3]$$

where,

w	is the most probable crack width, in
β	is the ratio of h_2/h_1
h_2	is the distance from neutral axis to tensile face, in
h_1	is the distance from neutral axis to center of reinforcement, in
d_c	is the thickness of cover from tension face to bottom of closest bar, in

The Gergely-Lutz equation was adopted by ACI in 1971 for steel reinforced concrete using the z-factor approach (ACI Committee 318, 1971). By using a common value of 1.2 for β, the following equation (Equation [2.4]) was recommended for crack control using a steel stress of approximately 60% of ultimate, where z is limited to 30000 N/mm for interior exposure and 25000 N/mm for exterior exposure:

$$z = f_s \sqrt[3]{d_c A} \qquad\qquad [2.4]$$

2.5.2 Frosch Equation

In contrast to the Gergely-Lutz equation, the crack width equation proposed by Frosch is based on a physical model. Robert Frosch (1999) re-evaluated the crack data used by Gergely and Lutz and determined that their statistical equation was only workable at low values of cover; however, increased cover and high performance concrete are desirable as they can mitigate durability concerns. A cracking model was developed and compared to the well-known Gergely-Lutz equation. For cracks on the bottom face, the controlling cover dimension was determined by the larger of the side cover, or the bar spacing as shown in Figure 2.12. The results from this comparison showed that no method demonstrated better accuracy than the others when analyzing the ratio of calculated to measured crack width, as shown in Figure 2.13.

20
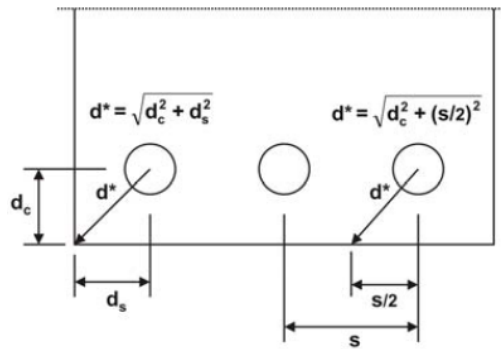
Figure 2.12 - Controlling cover dimension (Frosch, 1999)
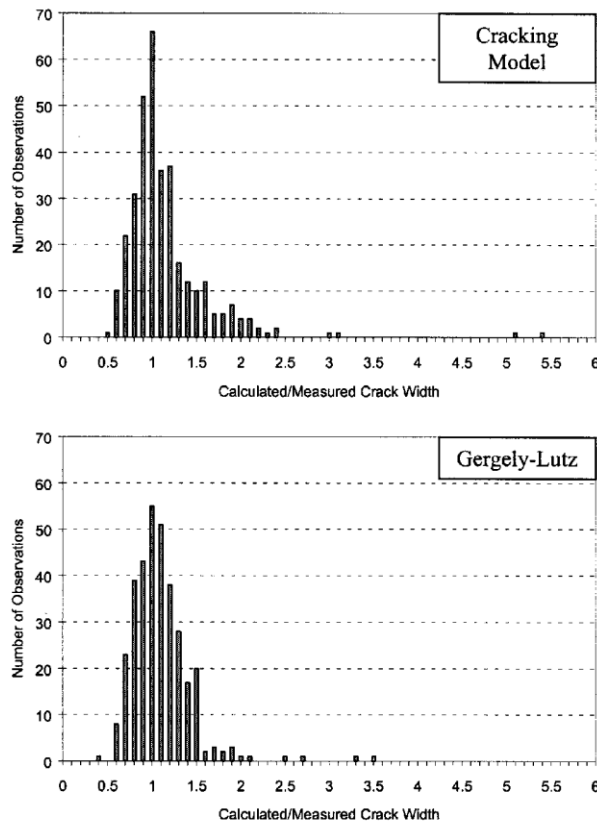
Figure 2.13 - Maximum bottom crack width comparison (Frosch, 1999)

Based on the results found from the cracking model, both cover and spacing of the bars were shown to affect crack width and spacing. The following equation (Equation [2.5]) was proposed by Frosch for uncoated steel reinforcement:

$$w = 2\frac{f_s}{E_s}\beta\sqrt{d_c^2 + \left(\frac{s}{2}\right)^2} \qquad\qquad \textbf{[2.5]}$$

where,

      w is the maximum crack width at tension face, mm

      f_s is the stress in the steel reinforcement, MPa

      E_s is the tensile modulus of elasticity of the steel reinforcement, MPa

      β is the ratio between the neutral axis and tension face to distance between neutral axis and centroid of reinforcement

      d_c is the thickness of cover from tension face to center of closest bar, mm

      s is the bar spacing, mm

Based on the tests conducted by Treece and Jirsa (1989), Frosch felt confident that epoxy coated reinforcement resulted in increased crack width and spacing in the range of approximately two times that of the uncoated reinforcement. For this reason, Frosch recommended the equation presented above be multiplied by a factor of two when epoxy coated reinforcement was used. ACI adopted this approach in their Building Code Requirements for Structural Concrete in 1999 by rearranging the equation to determine the maximum allowable bar spacing to control cracking (ACI Committee 318, 1999).

2.6   FLEXURAL CRACKING PREDICTIONS IN FRP REINFORCED CONCRETE

With the increasing use of fibre reinforced polymers (FRP) in concrete, previous crack width equations require modifications due to the differences in physical and mechanical behaviour of steel and FRP. Four methods of crack prediction in FRP reinforced concrete will be discussed in this section.

2.6.1 Gergely-Lutz Equation

Until 2001, design and construction standards were not available for concrete reinforced with FRP bars. ACI published the first guide in 2001 and specified a modified version of the Gergely-Lutz equation for prediction of crack widths with the addition of a corrective

coefficient meant to capture the bond behaviour of FRP. The modified Gergely-Lutz equation (Equation [2.6]) for FRP is as follows:

$$w = \frac{2.2}{E_f} \gamma k_b f_f \sqrt[3]{d_c A} \qquad\qquad \textbf{[2.6]}$$

where,

       w   is the maximum crack width at tension face, mm

       f_f is the stress in the FRP reinforcement, MPa

       E_f is the tensile modulus of elasticity of the FRP reinforcement, MPa

       γ is the ratio between the neutral axis and tension face to distance between neutral axis and centroid of reinforcement

       k_b is the bond dependent coefficient

       d_c is the thickness of cover from tension face to center of closest bar, mm

       A   is the average effective area of concrete, mm^2

2.6.2 Modified Frosch Equation

In 2006, ACI 440.1R-06 and CHBDC CAN/CSA-S6-06 adopted the Frosch equation for FRP reinforced concrete with the addition of a bond quality coefficient, k_b, to account for the bond between the FRP and concrete (Equation [2.7]). Maximum crack width guidelines were defined as 0.5 mm for exterior exposure and 0.7 mm for interior exposure.

$$w = 2 \frac{f_f}{E_f} \beta k_b \sqrt{d_c^2 + \left(\frac{s}{2}\right)^2} \qquad\qquad \textbf{[2.7]}$$

where,

       w   is the maximum crack width at tension face

       f_f is stress in the FRP reinforcement

       E_f is the tensile modulus of elasticity of the FRP reinforcement

       β is the ratio between the neutral axis and tension face to distance between neutral axis and centroid of reinforcement

d_c is the thickness of cover from tension face to center of closest bar

s is the bar spacing

2.6.3 Moment Equation

Lee *et al.* (2010) noticed a fundamental difference in behaviour between experimental test data and the design equation recommended by ACI 440.1R-03 when studying the impact of FRC on the cracking behaviour of beams containing FRP longitudinal reinforcement. Equation [2.6] forces a zero intercept; however, the behaviour of concrete specimens indicates that cracking does not occur immediately upon loading but rather when the cracking moment of the concrete is reached. To address this issue, the researchers modified the Gergely-Lutz equation for FRP to include a non-zero intercept using a regression analysis forced through the experimental cracking moment of the beam. In addition, the equation was also modified to include moment instead of reinforcement stress, as shown in Equation [2.8].

$$w = \frac{2.2}{E_c} \times \frac{d - \overline{y}_{cr}}{I_{cr}} \gamma k_b (M - M_{cr}) \sqrt[3]{d_c A_r} \qquad M > M_{cr} \qquad \textbf{[2.8]}$$

where,

w is the maximum crack width at tension face

E_c is the elastic modulus of concrete

d is the depth from top of beam to centroid of tension reinforcement

$\overline{y}_{cr}$ is the depth from top of beam to centroid of crack section

γ is the ratio between the neutral axis and tension face to distance between neutral axis and centroid of reinforcement

k_b is the bond dependent coefficient

M is the applied moment

M_{cr} is the experimentally observed cracking moment

d_c is the thickness of cover from tension face to center of closest bar

A_r is the concrete area surrounding one tension bar equal to total effective tension area of concrete surrounding reinforcement and having same centroid, divided by number of bars

2.6.4 Indirect Flexural Crack Control Approach

Indirect methods of crack control involve controlling crack widths by specifying maximum permissible reinforcement bar spacing. Ospina & Bakis (2007) proposed an indirect approach resulting from a rearrangement of flexural crack control provisions by Frosch from ACI 440.1R-06. The proposed model accounts for the dominant effects (bar cover, FRP reinforcement stress, stiffness and bond properties) on flexural cracking. There are two advantages to this method: 1) bar spacing dependence allows the designer to choose the level of flexural cracking that is to be controlled; and 2) if the bar spacing is constrained, flexural cracking can also be controlled by prescribing a stress limit in the FRP. Equation [2.9] represents the proposed model for interior exposure conditions, while Figure 2.14 graphically demonstrates this model as a function of concrete cover (d_c).

$$s = 0.8 \frac{E_r}{f_r k_b} - 2.5 d_c \leq 0.7 \frac{E_r}{f_r k_b} \qquad \textbf{[2.9]}$$

where,

s	is the maximum bar spacing
d_c	is the clear cover
E_r	is the modulus of elasticity of the FRP (assumed value of 40 GPa)
f_r	is the stress in the FRP (assumed value of 80 MPa)
k_b	is the bond dependent coefficient of FRP (1.4)
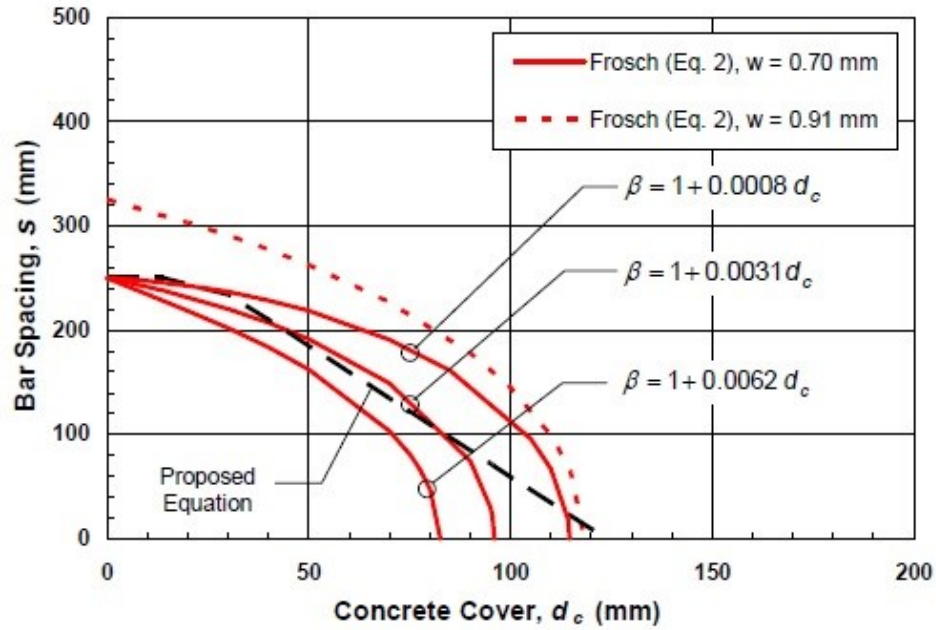
Figure 2.14 - Proposed flexural crack control provisions for GFRP RC (Ospina & Bakis, 2007)

The maximum bar spacing provisions are based on the β relationships that represent conditions typical of shallow members $(1+0.0062d_c)$ and deeper members $(1+0.0008d_c)$, as well as the value assumed by Frosch for steel reinforced concrete design $(1+0.0031d_c)$. In addition, the value of 0.91 mm shown in Figure 2.14 corresponds to a 30% variation in the crack width limit of 0.7 mm.

The effect of bond quality on these provisions was investigated using k_b values of 1.0 and 1.4. As shown in Figure 2.15, the higher k_b value of 1.4 requires a smaller bar spacing to meet maximum crack width limits.
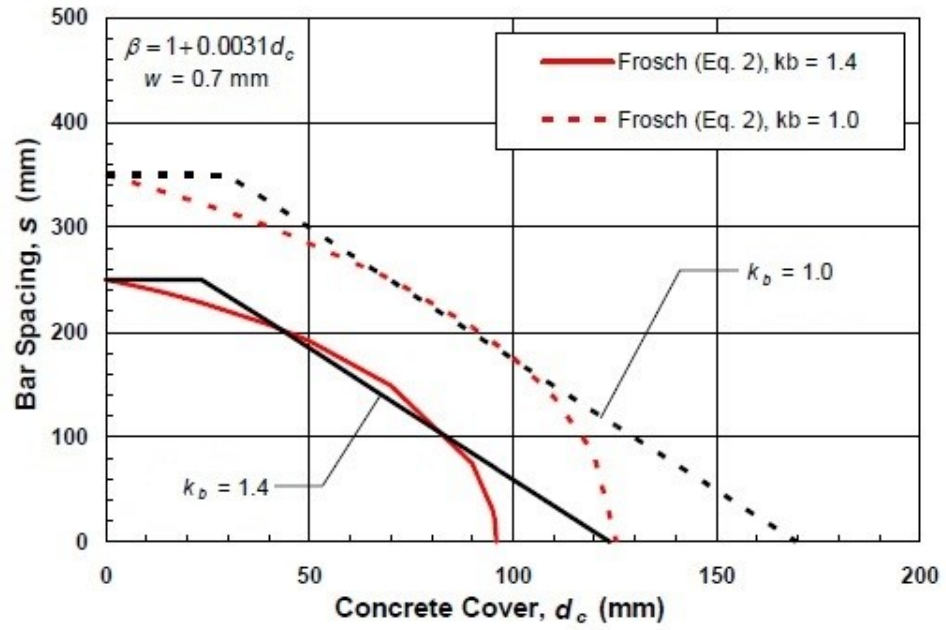
Figure 2.15 - Effect of bond quality on FRP flexural crack control (adapted from Ospina & Bakis, 2007)

CHAPTER 3 :   LITERATURE   REVIEW   ON   THE   BOND DEPENDENT COEFFICIENT

This chapter discusses the current calculation method for k_b at service stress and newly developed slope approach. Additionally, literature on previously completed research on the bond dependent coefficient will be presented, as well as case studies where k_b is calculated using a slope approach to increase the current database of results. Lastly, there is a detailed discussion on the ACI 440 test method that will be used in this study.

3.1   BOND DEPENDENT COEFFICIENT AT SERVICE STRESS

The approach used in literature involves determination of k_b at a specific service stress using the corresponding crack width. Using Equation [2.7] and crack width data recorded during testing, k_b can be calculated when geometric properties of the specimen are known. As an example, Figure 3.1 depicts the typical cracking behaviour of a specimen where k_b is calculated at 30% of the ultimate tensile strength of the bars (205 MPa) at a corresponding crack width of 0.54 mm. Equation [2.7] forces a zero intercept and calculates the bond dependent coefficient as the secant at the point of interest based on the current linear format.
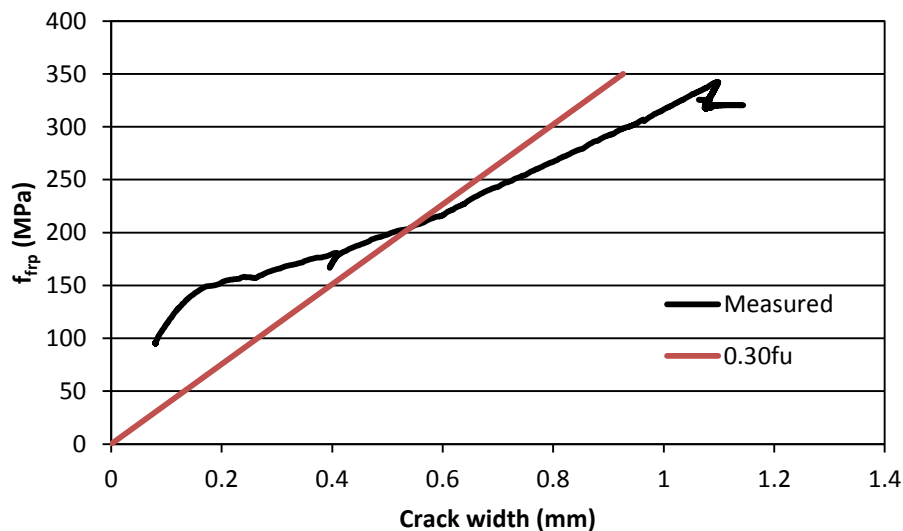
Figure 3.1 - Calculation of k_b using stress-level approach

There are many issues with this method resulting from the lack of a consistent definition of service stress and maximum crack width in current design standards. The service stress of FRP reported in the literature and design documents ranges in value from 15 –

30% of the guaranteed ultimate tensile strength of the bars. As the value of k_b depends highly on the service stress chosen for its calculation, this approach can result in a large range of k_b values which significantly impacts crack width prediction. This approach of determining k_b is also inherently unable to represent a large range of data as it is only representative of one specific data point. In addition, as multiple cracks form within the specimen, there have been different interpretations of maximum crack width:

- 90th percentile crack width (mean plus 1.28 times the standard deviation) as reported by Bakis *et al.* (2006), Giernacky (2002), Newhook (2000) and Thiagarajan (2003).

- Maximum crack width at a service moment equal to 30% of the nominal moment of the section as reported by Kassem *et al.* (2011).

- Widest crack across the length of the flexural zone as reported by Kassem (2004), Masmoudi *et al.* (1998), Theisz (2004), Lee *et al.* (2010) and Theriault & Benmokrane (1998).

3.2 BOND DEPENDENT COEFFICIENT USING SLOPE APPROACH

Based on the issues identified with the stress-level approach, an alternative slope approach can also be used for determination of k_b. Lee *et al.* (2010) briefly discussed this method in their research findings where approximate plot linearity was observed in terms of cracking behaviour that could be well represented using a line of best fit. Using a reinforcement stress (or one of its derivatives) versus crack width plot, the slope (w/f_{frp}) can be found using linear regression which can be used to back calculate k_b. To expand the current database of results in literature, case studies were completed where k_b was calculated using this method and the results can be found in Section 3.4.

3.3 FRP CRACK WIDTH PREDICTION AND THE BOND DEPENDENT COEFFICIENT

The bond dependent coefficient of FRP has been investigated by many researchers that have reported values that are highly variable. The studies presented in this section depict the large variability of k_b and cracking behaviour in specimens reinforced with FRP.

A meeting of ACI Committee 440 in October of 2004 prompted a collaborative study to compare the effects of k_b in previous and proposed equations for predicting crack widths in FRP reinforced concrete members. At the time, ACI 440 was considering the adoption of the Frosch equation from the current Gergely-Lutz equation. However, because the forms of the two equations are different, the k_b value that should be used in the absence of experimental data is also different. Bakis *et al.* (2006) conducted this study to cover a range of FRP types – GFRP, CFRP and AFRP. A total of 15 different experimental studies were used for this analysis in a collaborative effort, using both bar strains that were measured as well as those calculated using a cracked elastic section analysis depending on the data available. Summaries of these experimental studies are shown in Table 3.1 as well as the calculated k_b values.

Table 3.1 - Summary of experiments and calculated k_b values (Bakis *et al.,* 2006)

Bar Type (source of data)	Surface Treatment	Bar Strain ($\mu\varepsilon$)	Mean Gergely-Lutz k_b	Mean Frosch k_b	Ratio of k_b's, F/GL
Hughes Aslan 100 E-glass/ vinylester (Giernacky, 2002)	Spiral indent, sand coating	2000-2100	0.92	1.10	1.20
Marshall Ind. C-Bar E-glass/ PET-polyester (Trejo et al. 2005)	Molded ribs	1600-4500	1.39	1.72	1.24
Pultrall E-glass/ vinylester (Trejo et al. 2005)	Sand coating	1200-3500	1.07	1.27	1.18
Hughes Aslan 100 E-glass/ vinylester (Trejo et al. 2005)	Spiral indent, sand coating	1100-3600	1.33	1.58	1.19
Marshall Ind. C-Bar E-glass/ PET-polyester (Thériault et al. 1998)	Molded ribs	2300-9000	0.58	0.60	1.03
Marshall Ind. C-Bar E-glass/ PET-polyester (Masmoudi et al. 1998)	Molded ribs	2200-7900	1.00	1.14	1.13
Pultrall E-glass/ vinylester (Newhook, 2000)	Sand coating	2400-4300	0.76	0.84	1.12
Hughes Aslan 200 carbon/ vinylester (Theisz, 2004)	Spiral indent, scrim texture	2400-8800	0.92	1.09	1.19
DFI carbon/ epoxy (Thiagarajan, 2003)	Sand-blasted	1300-9800	1.07	1.16	1.08
Pultrall E-glass/ vinylester (El-Salakawy and Benmokrane, 2004)	Sand coating	1300-3400	0.60	0.67	1.12
Pultrall Carbon/ vinylester (El-Salakawy and Benmokrane, 2004; Kassem, 2004)	Sand coating	1100-3200	0.64	0.79	1.23
Marshall Ind. C-Bar E-glass/ PET-polyester (Kassem, 2004)	Molded ribs	2100-3000	0.83	1.10	1.33
Marshall Ind. C-Bar Carbon/ PET-polyester (Kassem, 2004)	Molded ribs	1300-2800	0.82	1.09	1.32
Arapree Aramid/ epoxy (Kassem, 2004)	Sand coating	3400-4300	0.92	1.22	1.33
Steel (El-Salakawy and Benmokrane, 2004; Kassem, 2004)	Ribbed	800-1200	0.72	0.90	1.26
FRP Maximum			*1.39*	*1.72*	*1.33*
FRP Minimum			*0.58*	*0.60*	*1.03*
FRP Mean			*0.92*	*1.10*	*1.19*
FRP Std. Dev.			*0.25*	*0.31*	*0.093*
FRP CV (%)			*27*	*28*	*8*

The researchers found k_b to vary with bar strain and recommended that k_b be investigated over a range of strain values typical for field applications. Mean k_b values were also found to be scattered for different beams, and also for any one beam at different load levels. To calculate the default k_b value that should be used for the modified Frosch equation, the researchers used the mean F/GL ratio and multiplied it by 1.2, as that is the value recommended for the Gergely-Lutz equation. A k_b value of 1.4 is conservative in all but one case from this experimental study where reinforcement containing molded ribs was used. However, the researchers noted a necessity to carry out further analysis in order to be able to make definitive statements on the cause for the large variation in k_b found.

A total of 12 concrete beams reinforced with GFRP and CFRP were tested by Lee *et al.* (2010). All specimens were 125 x 250 mm (width x depth) with a simply supported span of 1830 mm. Each specimen contained a single layer of two reinforcing bars ranging in size from #2 (ϕ6.35) - #4 (ϕ12.7). Half of the specimens also contained polypropylene fibres at a volume fraction of 1% due to the aim of the study which involved determining improvements provided to FRP with FRC. The researchers found k_b to range from 1.04 – 2.98 depending on reinforcement ratio/bar diameter and fibre material (carbon or glass) using the slope to calculate k_b with Equation [2.8].

Toutanji & Deng (2003) conducted a study in order to verify design equations in ACI 440.1R-01 using three series of RC beams with GFRP longitudinal reinforcement. Each series contained two identical test specimens that were 180 x 300 x 3000 mm (width x depth x length) and contained 12.7 mm diameter bars although the configuration and quantity of the bars varied between series. The researchers found that the provisions from ACI 440.1R-01 (using the then recommended k_b value of 1.2) were accurate in predicting crack widths when the reinforcement was placed in one layer (GB1 and 2 series). However, the provisions underestimated crack widths when reinforcement was placed in two layers (GB3). These results were improved when k_b was modified to 1.4 and are denoted by an asterix in Table 3.2. The average results for each series are shown graphically in Figure 3.2.

Table 3.2 - Comparison of crack widths, mm (adapted from Toutanji & Deng, 2003)

Beam #	ρ (%)	Experimental		Theoretical	
		30% M_n	90% M_n	30% M_n	90% M_n
GB1 – 1	0.52	1.3	3.3	1.1	3.3
GB1 – 2	0.52	1.2	3.5	1.1	3.3
GB2 – 1	0.79	0.6	2.3	0.7	2.0
GB2 – 2	0.79	0.7	2.3	0.7	2.0
GB3 – 1	1.10	0.6	1.8	0.6	1.7*
GB3 – 2	1.10	0.5	1.9	0.6	1.7*

*modified crack width (k_b = 1.4)
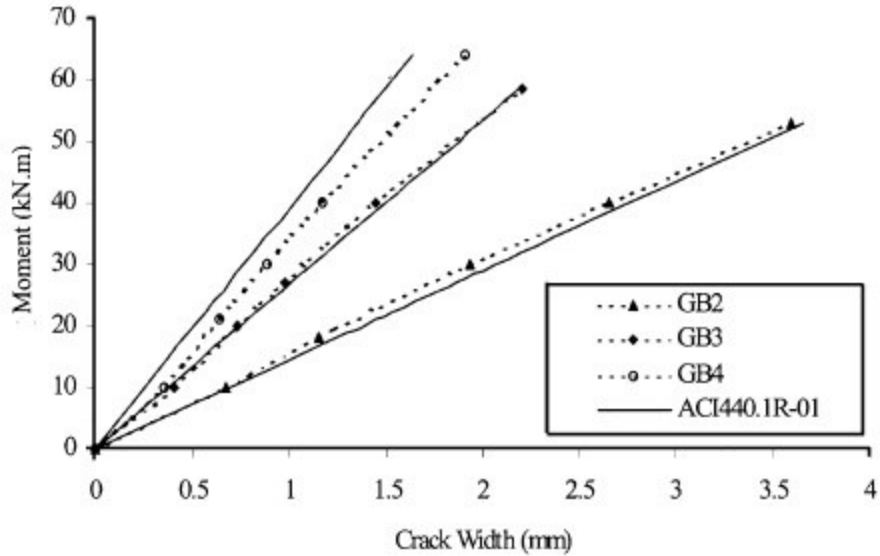
Figure 3.2 - Comparison of experimental and theoretical crack widths predicted by ACI 440.1R-01 (Toutanji & Deng, 2003)

3.4 CASE STUDIES

A literature review was conducted on crack width prediction and the bond dependent coefficient of FRP in order to identify case studies that could be used for comparison of calculated k_b values. The case studies investigated in this section were chosen as the necessary plots and parameters were provided in the paper to calculate k_b. In this section, k_b results calculated by the researchers will be presented in addition to a comparison with values calculated using an alternative slope approach. Detailed information regarding the test specimens and material properties of the reinforcement used in the case studies can be found in Appendix A, as well as calculations and associated plots.

3.4.1 Case Study 1

The researchers in this study (Lee *et al.*, 2010) used a modified Gergely-Lutz equation, Equation [2.8], for calculation of the bond dependent coefficient in order to account for the non-zero intercept observed in experimental testing.

The data collected from the specimens was analyzed using linear regression and lines of best fit were forced through y-axis at the location of the experimentally measured cracking moment of the beam. The slope of the regression lines were then used to back-

calculate k_b using Equation [2.8] and the results are summarized in Table 3.3. As can be seen in Table 3.3, there is substantial variation for k_b depending on fibre type, as well as bar size. In addition, the k_b values found for the FRC specimens are significantly lower than plain concrete, indicating better bond behaviour and thus, smaller crack widths.

Table 3.3 - k_b results for slope method with forced intercept (adapted from Lee *et al.*, 2010)

Bar type	Bar size	k_b		$k_{b,FRC}/k_{b,plain}$
		Plain	FRC	
GFRP	#2	1.57	0.67	0.42
	#4	1.04	0.57	0.55
CFRP	#2	1.74	0.92	0.53
	#4	2.98	0.76	0.26

3.4.2 Case Study 2

For determination of the bond dependent coefficient, the researchers in this study (Kassem *et al.*, 2011) used the maximum crack width exhibited within the specimen at a service moment equal to 30% of the nominal moment (M_n). It should be noted that $0.3M_n$ does not represent any standard service stress condition defined in design codes and guidelines. The modified Frosch equation was used for this calculation in accordance with ACI 440.1R-06 and CHBDC CAN/CSA-S6-06. The results of this calculation are shown in Table 3.4. The k_b results are fairly consistent with identical fibre types regardless of bar diameter. Two different types of CFRP and GFRP were used in this study and the differences in mechanical properties and surface treatments do not have a large effect on the results for k_b.

Table 3.4 - k_b values at $0.3M_n$ (Kassem *et al.*, 2011)

Specimen	k_b
C1-4	0.95
C1-6	0.88
C1-8	0.99
C2-4	0.97
C2-6	0.86
C2-8	0.86
G1-6	1.07
G1-8	1.08
G2-6	1.04
G2-8	1.02
AR-6	1.27
AR-8	1.32

3.4.3 Calculation of k_b from Other Published Works

To increase the current database of results, a slope method was used to calculate k_b values for both case studies using the modified Frosch equation, Equation [2.7]. This approach involved using experimental plots of reinforcement stress (or one of its derivatives) versus crack width to determine a slope which can be used to back calculate k_b. The non-zero intercept was neglected in this analysis as the current design equation cannot accommodate this due to its mathematical form. All related calculations and plots can be found in Appendix A.

The k_b values found using this method, as shown in Table 3.5, are significantly variable depending on fibre type and bar diameter. In addition, this analysis was performed for each crack within the specimen. For instance, in a beam where 4 cracks were reported, 4 sets of results were calculated along with the average of all 4. The variability that occurs within cracks occurring in the same specimen can be demonstrated from this analysis.

Table 3.5 - Case Study 1 k_b results using slope method

Specimen	Crack	Slope (x10^{-9})	Constant (x10^{-8})	k_b
G2N0	1	268.0		1.04
	2	494.0	25.8	1.92
	Average	381.0		1.48
G2P1	1	290.0		1.12
	2	311.0	25.8	1.20
	Average	301.0		1.16
G4N0	1	74.5		1.37
	2	72.1		1.33
	3	59.0	5.4	1.08
	Average	68.5		1.26
G4P1	1	43.9		0.80
	2	28.3		0.52
	3	33.9		0.42
	4	29.9	5.5	0.55
	5	9.1		0.17
	6	25.3		0.46
	Average	28.4		0.52
C2N0	1	142.0		1.96
	2	140.0	7.3	1.93
	Average	141.0		1.95
C2P1	1	93.1		1.28
	2	74.1		1.02
	3	83.7	7.3	1.15
	Average	83.6		1.15
C4N0	1	85.8		4.40
	2	63.0		3.19
	3	64.2	2.0	3.30
	Average	70.7		3.63
C4P1	1	22.8		1.17
	2	17.0		0.87
	3	8.4	2.0	0.43
	4	12.5		0.64
	Average	15.2		0.78

The k_b values calculated for Case Study 2 using a slope approach, as shown in Table 3.6, yielded variability based on both fibre type and bar diameter. For these specimens, moment versus crack-width relationships for the first crack width formed in the specimen were used to calculate k_b using a slope approach.

Table 3.6 - Case Study 2 k_b values using slope approach

Specimen	Slope (x10^{-8})	Constant (x10^{-8})	k_b
C1-4	2.27	2.10	1.09
C1-6	1.63	99.4	1.64
C1-8	1.11	68.4	1.63
C2-4	2.35	2.01	1.17
C2-6	1.58	1.01	1.56
C2-8	9.16	71.9	1.27
G1-6	2.77	1.51	1.83
G1-8	1.23	1.08	1.13
G2-6	2.49	1.89	1.31
G2-8	1.14	1.34	0.85
AR-6	3.19	2.13	1.50
AR-8	3.26	1.46	2.24

3.4.4 Comparison and Discussion of k_b

Shown in Tables 3.7 and 3.8 are the comparisons between the k_b values calculated by the researchers and the k_b values calculated using a slope approach. It is important to note that both researchers calculated their k_b values using different equations and interpretation approaches which introduces further variability into the results.

Table 3.7 - Comparison for Case Study 1

Specimen	k_b from Paper	Slope k_b
G2N0	1.57	1.48
G2P1	0.67	1.16
G4N0	1.04	1.26
G4P1	0.57	0.49
C2N0	1.74	1.95
C2P1	0.92	1.15
C4N0	2.98	3.63
C4P1	0.76	0.78

Table 3.8 - Comparison for Case Study 2

Specimen	k_b from Paper	Slope k_b
C1-4	0.95	1.09
C1-6	0.88	1.64
C1-8	0.99	1.63
C2-4	0.97	1.17
C2-6	0.86	1.56
C2-8	0.86	1.27
G1-6	1.07	1.83
G1-8	1.08	1.13
G2-6	1.04	1.31
G2-8	1.02	0.85
AR-6	1.27	1.50
AR-8	1.32	2.24

For the first case study, the general trend was that k_b values calculated using the slope approach with zero intercept were larger, and therefore more conservative, than those calculated with a forced intercept through the experimental cracking moment of the beam (M_{cr}). This difference was more pronounced for the FRC samples; however, this is likely due to the influence of crack bridging from the addition of the fibres. In addition, the researchers used a modified form of the Gergely-Lutz equation (Equation [2.8]) to calculate their k_b results, while the k_b values found using the slope approach were calculated using the modified Frosch equation (Equation [2.7]) as recommended by current design standards. The major difference between these two equations is that different geometric parameters are defined as the major contributors to crack width. For the Gergely-Lutz equation, the geometric parameters defined to influence crack width are cover and effective area of concrete, while the Frosch equation emphasizes cover and bar spacing. It is also important to note that the Gergely-Lutz equation is based on a statistical model, while the Frosch equation is based on a physical model due to inconsistencies with Gergely & Lutz's equation (Frosch, 1999).

For the second case study, the k_b values found using the slope approach are also more conservative than those calculated using the maximum crack width at $0.3M_n$. In this study, the researchers used a conventional stress-level approach and therefore, the differences in k_b values can be mostly attributed to interpretation method as the modified

Frosch equation was used for both methods. Current design guidelines recommend using a k_b value of 1.4 when experimental data is not available. For this case study, this value would be conservative for all specimens using the stress-level approach; however, this value would underestimate the expected crack widths in half of the specimens when using the slope approach.

For both case studies, it is apparent that k_b calculated using a stress-level approach would significantly vary between specimens. This is because k_b, based on current design standards, is calculated as the secant at each stress value. This general trend will be observed in all specimens until a service stress is clearly defined at which this calculation should take place. However, the loading behaviour of all specimens is essentially linear although there are variations in slopes and intercepts, as shown by the plots in Appendix A.

3.5 ACI COMMITTEE 440 TEST METHOD

The test method that will be evaluated is entitled *Test Method for Determining the Bond-Dependent Coefficient of Fibre-Reinforced Polymer (FRP) Rods (Second Draft)* (Benmokrane, 2010) and was presented to ACI Committee 440 (K Subcommittee) in March of 2010. This test method specifies requirements for determining k_b of FRP rods used as reinforcement in concrete flexural members. A copy of the test method can be found in Appendix B, while this section will discuss the most significant aspects of the experimental test.

The test method suggests beam dimensions of 200 x 300 x 3000 mm (width x height x length) in order to be representative of real structural members. Reinforcement should be comprised of GFRP bars ranging from #3 - #8 or CFRP bars #3 - #5. The shear span should be at least equal to a third of the span between supports or three times the height of the beam but should not be smaller than 500 mm and shear reinforcement is to be provided to prevent shear failure; however, the maximum moment region may be free of stirrups to avoid confinement effect. The concrete used for these specimens should be of a standard mix, with a minimum strength of 28 MPa. Clear concrete cover should be

dependent on the diameter of the bars, with 38 mm of cover recommended for bar sizes #2 - #5 and 50 mm for bar sizes #6 - #8. Crack monitoring should be done using LVDT's or similar apparatuses. FRP bars at midspan are to be instrumented with two electrical strain gauges. The test should also be conducted in a standard laboratory atmosphere temperature and humidity.

The test is to be carried out on beams that are simply supported and tested in two points loading, as shown in Figure 3.3. Load is applied until the formation of the first flexural crack. At this stage, the load is held constant to allow for measurements of the initial crack width using a microscope. A displacement meter is then installed at the level of reinforcement to monitor crack growth during testing. Loading is then resumed until the second flexural crack forms and the process is repeated. At this point, the beam should be loaded until both monitored crack widths reach 1 mm or until beam failure, depending on whether ultimate performance is desired.

Using the data collected from the test, k_b is then determined using measured crack widths and strains in the FRP bars at service stage. The modified Frosch equation (Equation [2.7]) is to be used for this calculation. If strain readings are poor or bad, it is acceptable to use stress values calculated with elastic crack theory. A maximum crack width of 0.7 mm should be used for calculation of k_b.
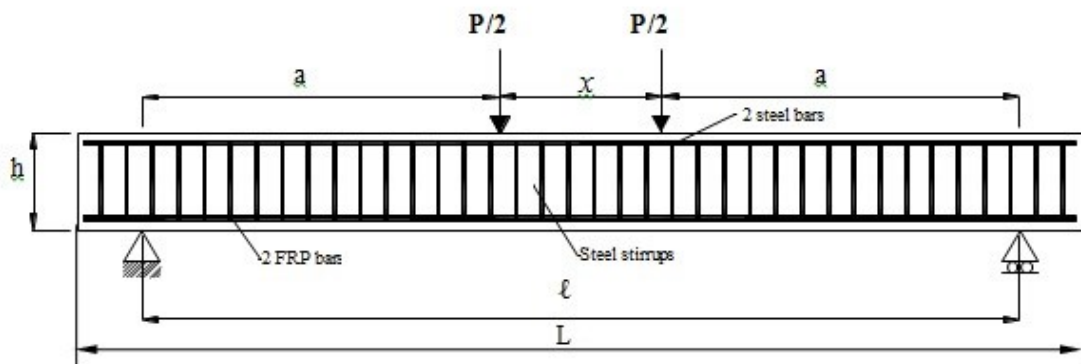
Figure 3.3 - Setup for k_b test method (Benmokrane, 2010)

CHAPTER 4 : EXPERIMENTAL PROGRAM

For this study, two types of GFRP reinforcement were used: 1) V-Rod manufactured by Pultrall Inc.; and 2) Aslan 100 manufactured by Hughes Brothers Inc. as shown in Figure 4.1. The V-Rod GFRP are a composite rebar that is manufactured to conform to CSA S807-10 using a pultrusion process that combines glass fibres to provide high strength, and a vinyl ester resin to provide corrosion resistance and is finished with a sanded surface (Pultrall Inc., 2007). While the Aslan 100 GFRP rebar also consists of a vinyl ester matrix and is manufactured using pultrusion, its surface treatment consists of deformations as well as a sand coated finish in order to achieve both a mechanical and chemical bond to concrete (Hughes Brothers Inc., 2011). Material properties of the reinforcement are shown in Tables 4.1 and 4.2. Bar testing certifications from the manufacturers can be found in Appendix C to verify tensile properties.

| (a) | (b) |
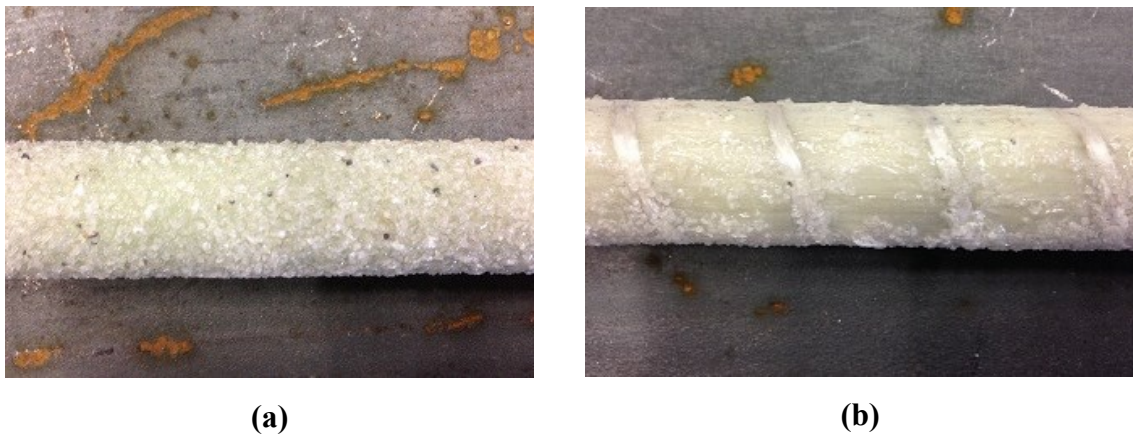
Figure 4.1 - Photos of surface treatment for: (a) V-Rod; and (b) Aslan 100

Table 4.1 - V-Rod GFRP Material Properties (Pultrall Inc., 2007)

Bar size	Nominal Diameter (mm)	Cross Sectional Area (mm^2)	Tensile Modulus of Elasticity (GPa)	Guaranteed Tensile Strength (MPa)
#3	9.5	71.3	45.4	765
#4	12.7	126.7	46.3	708
#5	15.9	197.9	48.2	683
#6	19.1	285	47.6	656
#8	25.4	506.7	51.9	597

Table 4.2 - Aslan 100 GFRP Material Properties (Hughes Brothers Inc., 2011)

Bar size	Nominal Diameter (mm)	Cross Sectional Area (mm^2)	Tensile Modulus of Elasticity (GPa)	Guaranteed Tensile Strength (MPa)
#5	15.9	197.9	46	724
#6	19.1	285	46	690

Concrete compressive strength was determined using cylinder compressive testing completed at various stages during curing and testing. All results are reported in Appendix D, as well as those from modulus of rupture (MOR) testing complying with ASTM C78-10.

Manual crack width measurements were also taken throughout the duration of the test to validate those recorded using crack gauges. These results can be found in Appendix E.

4.1 PHASE I

Testing for this phase comprised a total of 23 specimens for investigative purposes in order to determine the parameters that had the most impact on cracking behaviour and bonding capability. The parameters investigated were: reinforcement ratio/bar diameter, concrete cover, bar spacing, member type (slab/beam) and synthetic fibre content. The test specimens, the test method used and significant results from testing will be presented.

4.1.1 Test Specimens

The tests of 14 beams and 9 slabs were completed for this investigation. Beams were designed to examine the effects of cover and fibre content on crack width, as well as the applicability of the k_b equation to these variations. The dimensions of the beams were 200 x 300 x 3000 mm (width x height x length). Slabs were designed primarily to examine the effect of bar spacing and slab thickness on crack width and the k_b equation by maintaining approximately the same reinforcement ratio in each specimen. The dimensions of the slabs were 600 x 150 x 3000 mm, 600 x 200 x 3000 mm, and 600 x 225 x 3000 mm, respectively and contained V-Rod GFRP reinforcement. Grade 400 10M (ϕ11.3) steel stirrups were used for shear reinforcement in the 14 beam specimens and conformed to CSA G30.18-09. Stirrups were not provided in the maximum moment

region to avoid confinement effect.   Shown in Figure 4.2 are the typical cross sections
for the specimens with a summary of detailed properties shown in Table 4.3.

(a)   **(b)**
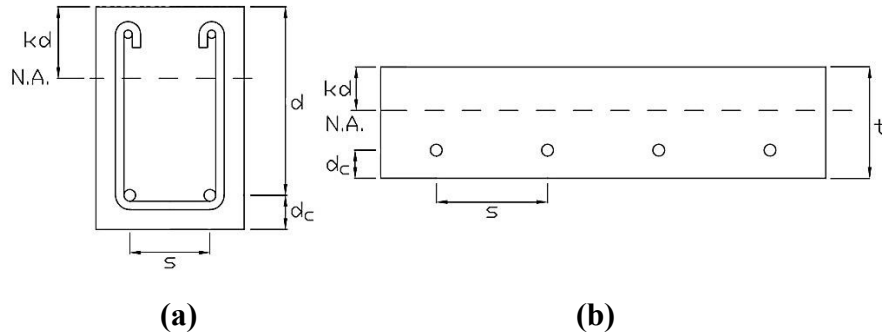
Figure 4.2 - Typical cross sections for: (a) beam specimens; and (b) slab specimens

Table 4.3 - Detailed Properties of Test Specimens for Phase I

ID #	Dimensions (width x height x length)	Longitudinal Reinforcement			Concrete		
		Bar sizes	ρ (%)	Cover (mm)	f'_c (MPa)	kd (mm)	Fibre content (kg/m^3)
B1		2 - #5	0.78	38	31	55	0
B2		2 - #6	1.19	50	31	62	0
B3		2 - #5	0.78	38	36	52	1.8
B4		2 - #6	1.19	50	36	58	1.8
B5		2 - #5	0.82	50	36	50	0
B6		2 - #6	1.13	38	36	60	0
B7	200 x 300 x 3000	2 - #5	0.78	38	32	54	2.4
B8		2 - #6	1.19	50	32	61	2.4
B9		2 - #5	0.78	38	32	54	3.6
B10		2 - #6	1.19	50	32	61	3.6
B13		2 - #5	0.78	38	28	57	4.6
B14		2 - #6	1.19	50	28	64	4.6
B15		2 - #5	0.78	38	28	57	6.9
B16		2 - #6	1.19	50	28	64	6.9
S1		10 - #3	1.11	38	31	26	0
S2	600 x 150 x 3000	6 - #4	1.2	38	31	26	0
S3		4 - #5	1.27	38	36	26	0
S4		3 - #6	1.39	38	36	27	0
S5		10 - #3	0.76	38	30	33	0
S6	600 x 200 x 3000	6 - #4	0.81	38	30	34	0
S7		4 - #5	0.86	38	29	36	0
S8		3 - #6	0.93	38	29	34	0
S9	600 x 225 x 3000	3 - #8	1.56	50	25	52	0

The specimens from Table 4.3 containing FRC will be used in a limited discussion in Chapter 5 as it relates only to the bond dependent coefficient.

4.1.2 Test Methodology

The ACI 440 test method discussed in Section 3.5 was used for this phase of testing. The specimens were simply supported and tested in four-point bending, as shown in Figure 4.3, with a shear span of approximately 933 mm. The specimens were tested with a 1.0 MN servo-controlled hydraulic actuator and values were recorded using a16 bit data acquisition card. A steel distribution beam was used to distribute the load to the two third-span points. A linear variable displacement transducer (LVDT) was used at midspan to record the deflection of each specimen. Beams B9 and B10 were also instrumented with strain gauges at midspan to record the strains in the GFRP longitudinal reinforcement. Crack width transducers were installed in the constant moment region of the specimen in order to record the growth of the cracks for the duration of the test. Values from the crack gauges and LVDT's were recorded to three decimal places (one thousandth of a millimetre) which is within the resolution of the system.
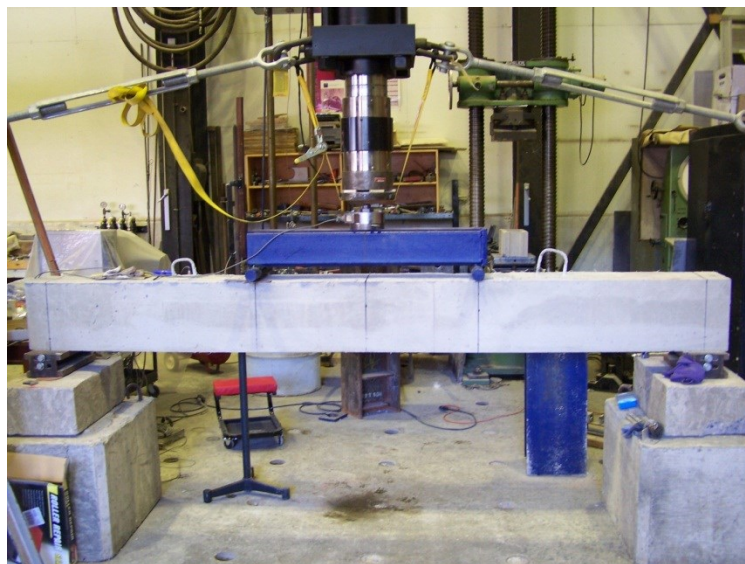
Figure 4.3 - Flexural Test Configuration

At the appearance of two flexural cracks, the load was held constant to allow for initial measurements of crack widths. PI displacement transducers, shown in Figure 4.4, were then installed over these two cracks at the level of reinforcing to record growth over the

remainder of the test. If possible, the specimens were loaded until both cracks reached 1 mm. All cracks within the constant moment region were then manually read using a microscope. Measurements were recorded at the level of reinforcing on the front and back side, as well as at quarter points on the underside (tension face) of the specimen. To investigate the effects of repeated loading, the specimen was then cycled at a frequency of approximately 0.3 Hz (beams) or 0.1 Hz (slabs) to its maximum load a total of 100 times and the cracks widths prior to and following cycling were used for comparison.

Figure 4.4 - PI crack gauges (Tokyo Sokki Kenkyujo Co. Ltd., 2011)

With the exception of slabs S1 – S8, the specimens were loaded to failure in four-point bending recording both load and deflection at midspan. To avoid shear failure, slabs S1 – S8 were loaded to failure in single point loading at midspan, as shown in Figure 4.5.

Figure 4.5 - Failure Arrangement for Slabs S1 – S8

4.1.3 Test Results

All specimens exhibited a typical cracking behaviour upon loading, shown in Figure 4.6. This plot represents the load history of specimen B9, with the vertical axis representing the stress in the FRP reinforcement calculated using elastic cracked section theory and the horizontal axis representing the average crack width that was measured during experimental testing. Similar plots for the remaining specimens can be found in Appendix F, while calculations relating to the elastic cracked section theory can be found in Appendix G. There is an initial cracking phase, followed by a linear portion of crack growth. However, the overall behaviour of this specimen demonstrates approximate plot linearity that can be well represented using the line of best fit shown on the figure. It is important to note that the line of best fit does not pass through the origin.
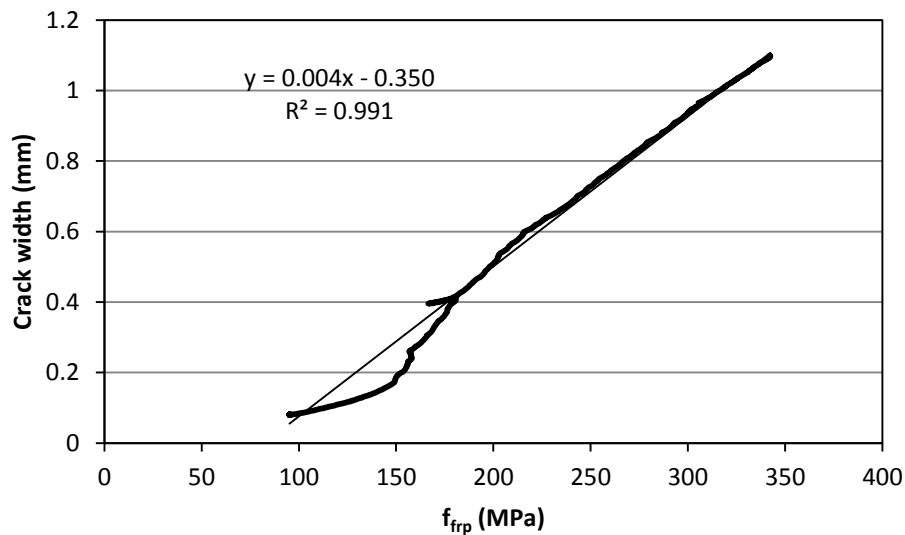
Figure 4.6 - Typical cracking behaviour for specimen B9

As two of the specimens were instrumented with strain gauges, a comparison between measured and calculated stresses was possible. As shown in Figure 4.7, there is good correlation between the measured and calculated stresses with a slight deviation at the beginning of loading. The calculated stresses were calculated based on a fully cracked section; however, at this stage of loading, the section is not fully cracked and therefore, the calculated stresses are higher as the theory assumes the FRP reinforcement has taken

all the tensile stress and that the concrete has become ineffective below the neutral axis. Details of these calculations can be found in Appendix G.
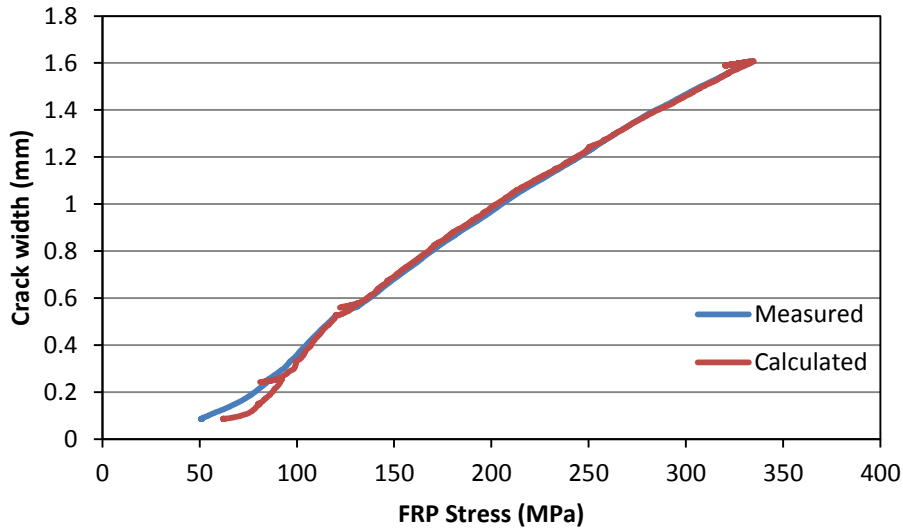
Figure 4.7 - Measured versus calculated stress for specimen B10

4.1.3.1   Cover

According to ACI 440.5-08, the recommended cover to primary reinforcement for beams is 50 mm. However, according to the test methodology used, the recommended cover is dependent upon the diameter of the bars: 38 mm for #5 bars, and 50 mm for #6 through #10 bars. A total of 4 specimens were constructed to investigate the results of varying cover. Beams were constructed with 2-#5 bars, or 2-#6 bars with both 38 and 50 mm cover. For comparison, ratios of crack widths for 50 mm cover to 38 mm cover (w_{50}/w_{38}) were compared from experimental testing to the predicted values from the modified Frosch equation. Detailed results by service stress level are provided in Tables 4.4 and 4.5, with a summary shown in Table 4.6. As shown in Table 4.6, the average crack width values observed in experimental testing are much less than those predicted using the modified Frosch equation. However, the maximum values taken at low service stresses (approximately 0.1 - 0.15f_u) are very similar to the predicted results. It can be seen that the w_{50}/w_{38} ratio decreases as the stress increases until it becomes nearly constant at high values of service stress. Based on these results, the modified Frosch equation accurately captures the effects of varying cover at low values of service stress, but is not applicable beyond approximately 0.15f_u.

Table 4.4 - w_{50}/w_{38} ratios from experimental testing for specimens with #5 bars

Stress level	Stress	Cover = 38 mm			Cover = 50 mm			w_{50}/w_{38}
		Crack 1	Crack 2	Average	Crack 1	Crack 2	Average	
$0.10f_u$	68	-	-	-	-	-	-	-
$0.125f_u$	85	0.06	0.08	0.07	-	-	-	-
$0.15f_u$	102	0.08	0.10	0.09	0.09	0.10	0.09	1.07
$0.175f_u$	120	0.15	0.14	0.15	0.13	0.13	0.13	0.86
$0.20f_u$	137	0.32	0.23	0.28	0.17	0.17	0.17	0.60
$0.225f_u$	154	0.48	0.34	0.39	0.23	0.24	0.23	0.59
$0.25f_u$	171	0.55	0.48	0.51	0.29	0.33	0.31	0.62
$0.275f_u$	188	0.63	0.62	0.62	0.36	0.41	0.38	0.63
$0.30f_u$	205	0.75	0.78	0.77	0.42	0.48	0.45	0.59
$0.325f_u$	222	0.86	0.90	0.88	0.47	0.56	0.51	0.58
$0.35f_u$	239	0.95	1.01	0.98	0.52	0.62	0.57	0.58
$0.375f_u$	256	1.04	1.12	1.08	0.57	0.68	0.62	0.58
$0.4f_u$	273	1.11	1.21	1.16	0.61	0.73	0.67	0.58

Table 4.5 - w_{50}/w_{38} ratios from experimental testing for specimens with #6 bars

Stress level	Stress	Cover = 38 mm			Cover = 50 mm			w_{50}/w_{38}
		Crack 1	Crack 2	Average	Crack 1	Crack 2	Average	
$0.10f_u$	66	0.12	0.04	0.08	0.07	0.09	0.08	1.01
$0.125f_u$	82	0.15	0.06	0.10	0.11	0.14	0.12	1.18
$0.15f_u$	98	0.22	0.13	0.18	0.14	0.18	0.16	0.91
$0.175f_u$	115	0.26	0.20	0.23	0.18	0.22	0.20	0.86
$0.20f_u$	131	0.32	0.27	0.30	0.21	0.26	0.24	0.79
$0.225f_u$	148	0.38	0.35	0.36	0.24	0.30	0.27	0.75
$0.25f_u$	164	0.44	0.41	0.43	0.27	0.34	0.31	0.72
$0.275f_u$	180	0.50	0.47	0.49	0.30	0.38	0.34	0.71
$0.30f_u$	197	0.56	0.54	0.55	0.33	0.42	0.38	0.69
$0.325f_u$	213	0.61	0.60	0.60	0.36	0.46	0.41	0.68
$0.35f_u$	230	0.66	0.66	0.66	0.40	0.50	0.45	0.68
$0.375f_u$	246	0.73	0.72	0.72	0.42	0.54	0.48	0.67
$0.4f_u$	262	0.77	0.79	0.78	0.44	0.58	0.51	0.65

Table 4.6 - Predicted versus experimental average w_{50}/w_{38} ratios

	Predicted using modified Frosch equation	Experimental testing		
		Average	Minimum	Maximum
#5 bars	1.01	0.66	0.58	1.08
#6 bars	1.03	0.79	0.65	1.18

It is important to also note that the spacing of the bars was varied as much as 24 mm due to maintaining the same top and side cover within each specimen. The spacing of the bars was accounted for in the predicted values using the modified Frosch equation; however, the results found by experimental testing may have been influenced by both a variation in cover and spacing. Further testing could be completed with varying only the bottom cover of the specimens and maintaining the same side covers in order to determine the effects from varying bottom cover only as it is the variable found in the modified Frosch equation.

4.1.3.2   Bar Spacing

The slab specimens were designed to investigate the effects of varying reinforcement spacing. For each thickness (150 or 200 mm), 4 specimens were constructed using #3, #4, #5 and #6 bars such that the reinforcement ratio would remain as constant as possible. A bar spacing of 200 mm was used as the base for comparison to 60, 100 and 150 mm bar spacings. As shown in Table 4.7, the w_{60}/w_{200} and w_{100}/w_{200} ratios increase as the stress in the reinforcement increases; however, this trend is opposite for the w_{150}/w_{200} ratios which decrease as the reinforcement stress increases. Crack width measurements at the level of reinforcement were used for this comparison with a β value of 1.

Table 4.7 - Crack width ratios for: (a) 150 mm slabs; and (b) 200 mm slabs

(a)   **(b)**

Stress (MPa)	w_{60}/w_{200}	w_{100}/w_{200}	w_{150}/w_{200}	Stress (MPa)	w_{60}/w_{200}	w_{100}/w_{200}	w_{150}/w_{200}
75	-	-	-	75	-	-	-
100	0.18	0.44	2.03	100	-	-	1.07
125	0.41	0.89	1.68	125	0.20	0.22	1.46
150	0.89	1.08	1.60	150	0.19	0.34	1.11
175	1.23	1.24	1.60	175	0.23	0.38	0.98
200	1.33	1.16	1.54	200	0.32	0.36	0.92
225	1.33	1.11	1.47	225	0.30	0.34	0.91
250	1.19	1.10	1.43	250	0.31	0.34	0.91
Average	0.94	1.00	1.62	Average	0.26	0.33	1.05
Frosch	0.45	0.59	0.79	Frosch	0.45	0.59	0.79

Varying the spacing parameter, s, in Equation [2.7] and assuming all other values to be constant, the ratio of crack widths can be determined and is labeled as 'Frosch' in Table 4.7. This can then be compared against the 'Average' of the experimental values. According to the Frosch equation, smaller crack widths are expected with closer bar spacing. For this set of specimens, crack width ratios for bar spacings of 60 (w_{60}/w_{200}) and 100 mm (w_{100}/w_{200}) were underestimated in the thinner slab and were overestimated in the thicker slab, while there was a very significant increase in observed crack width at a bar spacing of 150 mm.

4.1.3.3   Slab Thickness

The slab specimens also permitted the investigation of the effect of slab thickness on crack width. Slabs S1 – S4 were 150 mm in thickness, whereas slabs S5 – S8 were 200 mm in thickness and contained the following reinforcement: 10 - #3, 6 - #4, 4 - #5 or 3 - #6 yielding approximately the same reinforcement ratio. For the specimens reinforced with #3 and #4 bars, there was a large decrease in crack width when using a thicker slab as shown in Figure 4.8(a). However, for the #5 and #6 bars, the 150 mm thickness exhibited much smaller crack widths than the 200 mm thickness, as shown in Figure 4.8(b).
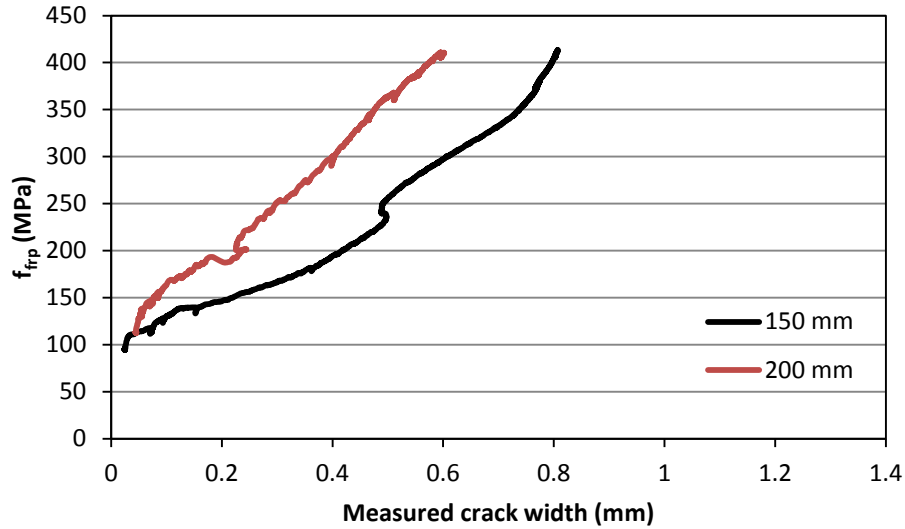
(a)
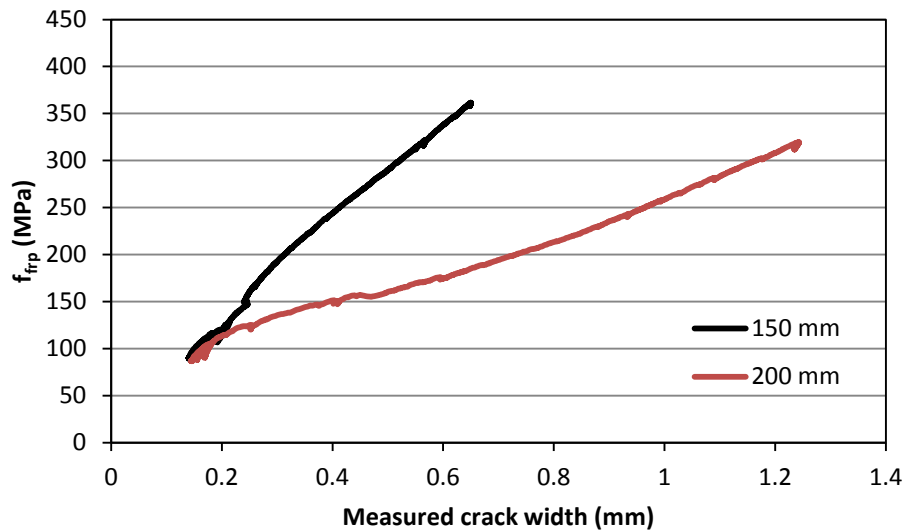
(b)

Figure 4.8 - Effect of slab thickness for: (a) #3 bars; and (b) #6 bars

The manual measurements taken for the slab specimens indicated that thinner slabs (150 mm) had more cracks in the constant moment region, and therefore, smaller crack spacing. Specimen S9 (thickness = 225 mm) had the least amount of cracks of all the slab specimens; however, this could also be due to the large diameter bars in the specimen.

4.1.3.4   Cyclic loading

An addition to the test methodology was to use cyclic loading to investigate crack stabilization. The specimens were loaded in the first load cycle up to a crack width of 1 mm. The beam was then unloaded and loaded back up to this same point a total of 100 times and the 25th, 50th, 75th and 100th cycle are shown plotted in Figure 4.9. For specimen B9, only crack 1 is used for this analysis as the second crack gauge came loose during cycling. It was found that the behaviour prior to and following cycling are very different. Following cycling, there is plot linearity as crack stabilization has been achieved.
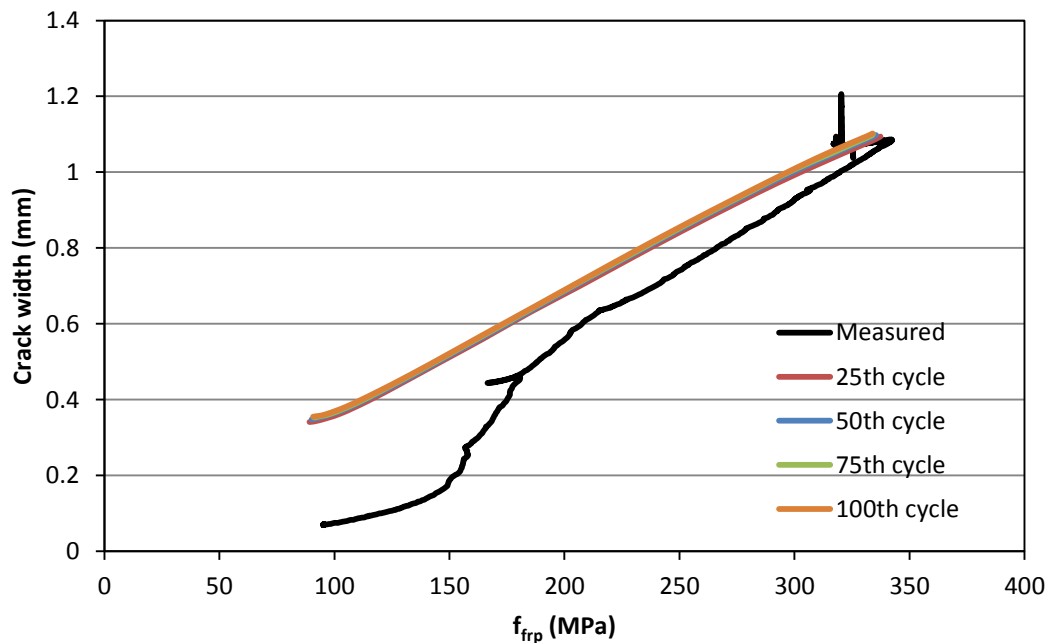
Figure 4.9 - Behaviour of specimen B9 following cycling

4.1.4 Recommendations for Future Testing

After the completion of testing in Phase I, several issues were deemed problematic and required modification prior to moving forward with testing:

- The test methodology dictated that the first two flexural cracks that form within the constant moment region of the specimen be selected for analysis. However, there is no guarantee that these cracks will necessarily be the largest in the specimen following testing simply because they were the first to form. This was

proven by taking manual measurements during testing and comparing them to the data collected from the crack gauges. These two cracks can also follow very different paths (i.e. slopes) during growth making the decision random as to which crack should be analyzed for determination of k_b.

- PI displacement transducers were used to monitor the growth of cracks for the duration of the test. However, it was observed that often more than one crack would form in the gauge opening, and therefore, the recorded measurements may not be completely accurate. This was especially true for the mixes containing FRC as decreased crack spacing was observed.

- Initially, super glue had been used to install the crack gauges to the specimen. However, after several attempts, the paste continued to pull off of the specimen and a good bond could not be formed. In order to continue testing, the alternative was to anchor the gauges using plastic plugs and screws. After anchoring the gauges into the specimen, cracks through the screw holes often formed and several of the crack gauges came loose, especially during cyclic loading. Potential error in the recording of crack width measurements could also be due to the relative twisting of the crack gauges. In addition, to safely install the crack gauges the specimen had to be unloaded. The test procedure dictated that the crack gauge be installed without unloading and this reloading cycle could affect the crack width measurements, especially considering the significant change in behavior prior to and following cycling that was observed during this phase of testing.

- Measured stresses found using strain gauges on the FRP bars compared well to values calculated using elastic cracked section theory. The deviation at the beginning was due to the fact the section was not fully cracked and therefore, calculated stresses were higher than those actually exhibited by the specimen.

4.2 PHASE IIA

The second phase of testing directly focused on the calculation and the interpretation of the bond dependent coefficient, as these results were the most significant from Phase I,

by expanding to two different surface treatments. In addition, the variability of cracking behaviour and k_b for a set of identical specimens was investigated.

4.2.1 Test Specimens

Testing of 8 specimens was completed for this phase. All specimens had dimensions of 200 x 300 x 2810 mm (width x height x length) to maintain consistency in cross sectional area with previous beams tested in Phase I. Based on the project objectives, a set of five identical beams were cast with #5 GFRP V-Rod rebar to examine statistical variation in cracking behaviour when properties and loading conditions were maintained. The remaining three specimens were cast in order to compare the behaviour of the specimens to variability in surface treatment. Two different reinforcement types, shown in Figure 4.10, were used in this phase in order to determine the effect of surface treatment on cracking and bonding behavior: 1) V-Rod GFRP reinforcement manufactured by Pultrall Inc.; and 2) Aslan 100 GFRP reinforcement manufactured by Hughes Brothers Ltd. Grade 400 10M (ϕ11.3) steel stirrups were used for shear reinforcement in the specimens and conformed to CSA G30.18-09. Stirrups were not provided in the maximum moment region to avoid confinement effect. Table 4.8 provides specimen details.

(a)

(b)

Figure 4.10 - Surface treatments for: (a) V-Rod; and (b) Aslan 100

Table 4.8 - Detailed Properties of Test Specimens for Phase IIA

ID #	Dimensions (width x height x length)	Longitudinal Reinforcement			Concrete	
		Bar sizes	ρ (%)	Cover (mm)	f'$_c$ (MPa)	kd (mm)
B1V5	200 x 300 x 2810	2 - #5	0.79	38	29	56
B2V5		2 - #5	0.79	38	29	56
B3V5		2 - #5	0.79	38	29	56
B4V5		2 - #5	0.79	38	29	56
B5V5		2 - #5	0.79	38	32	54
BA5		2 - #5	0.78	38	32	53
BV6		2 - #6	1.19	50	32	60
BA6		2 - #6	1.19	50	32	61

4.2.2 Test Methodology

The specimens in this phase were tested in an identical test configuration as those in Phase I, with the exception that the length of the distribution beam was reduced to 870 mm to account for the change in specimen length. All specimens were also instrumented with strain gauges at midspan to record the strains in the GFRP longitudinal reinforcement.

As discussed in Section 4.1.4, some modifications to the testing procedure and equipment were deemed necessary following issues identified in Phase I testing. The major issue identified in Phase I was the shortfalls of the PI displacement transducers for this type of testing. To rectify the issue, 10 mm stroke LVDT's were used with the addition of a fixture to aid in the application to the concrete specimen. This assembly is shown in Figure 4.11(a), and as can be seen in the photo, the fixture enabled parallel application of the two brackets using a dummy LVDT. Brackets were separated from the fixture following the adhesive setting time and the true LVDT was installed as shown in Figure 4.11(b). To avoid intrusion and compromising the crack formation of the sample by unloading, a two part acrylic adhesive, Red Head A7 (Illinois Tool Works, 2013), was used to secure the LVDT brackets. Several adhesives were tested on smaller concrete samples in order to determine the adhesive best suited for the application prior to testing.
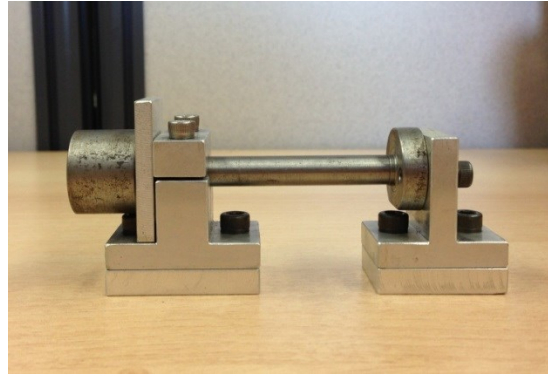
(a)

(b)

Figure 4.11 - LVDT fixture assembly: (a) prior to installation with dummy LVDT; and (b) after installation on specimen

The test procedure as specified by ACI Committee 440 was also used for this phase of testing with two modifications. As cracks on the tension face are of primary concern to designers, a third crack gauge was installed on the tension face of the specimen. This gauge was placed as close to the transition from vertical to horizontal as possible in the specimen. The other two LVDT gauges were installed at the level of reinforcement. As done in Phase I, the behaviour of the specimens following cyclic loading was also investigated in this phase using 25 loading and unloading cycles at a frequency of 0.1 Hz. Only 25 cycles were chosen for this phase as results from Phase I demonstrated that plot linearity was achieved on the second reloading cycle and therefore, 25 cycles were more than sufficient for characterization of this behaviour.

4.2.3 Test Results

The results for this phase of testing are subdivided into two main categories based on the project objectives: results for the five identical beam specimens, as well as the results relating to the difference in surface treatment between the Aslan and V-Rod reinforcement.

4.2.3.1   Five Identical V-Rod Specimens

In terms of raw cracking behaviour, the set of specimens exhibited fairly consistent crack growth within the service range of the bars up to 25 to 30% of ultimate (175 - 200 MPa). Beyond this point, there continued to be some correlation especially with the cracks at the level of reinforcement. However, the cracks on the tension face (bottom) began to further deviate around this point as shown in Figure 4.12(b). As a general observation, there is a larger variability in the cracks on the tension face than those at the level of reinforcement.
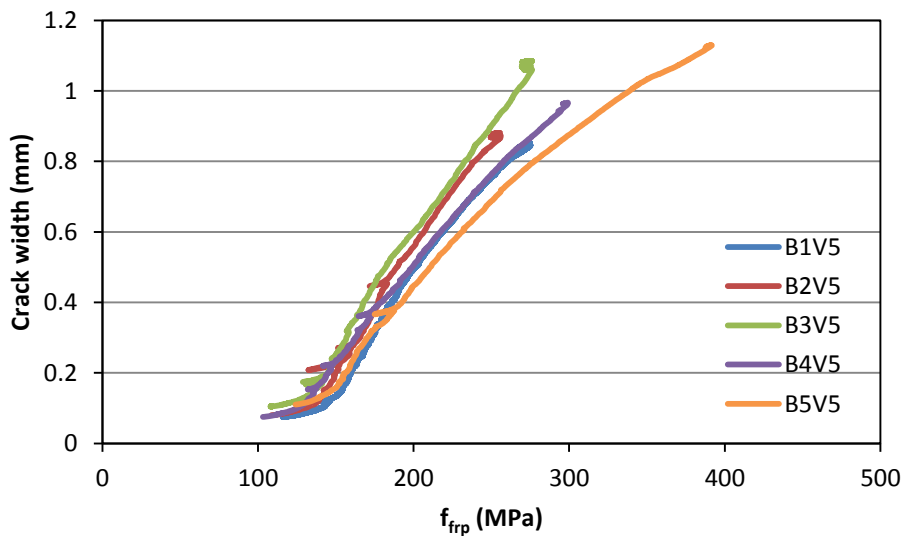
(a)
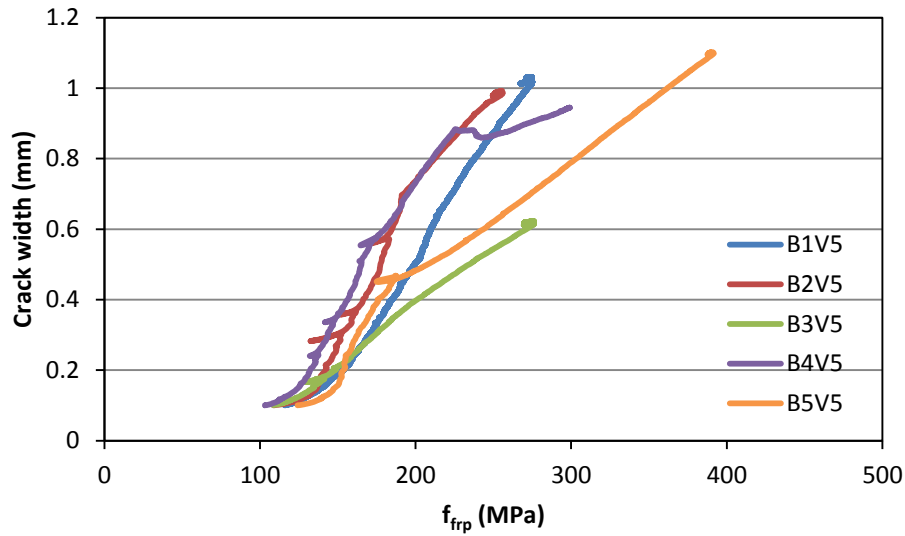
(b)

Figure 4.12 - Reinforcement stress versus crack width plots for: (a) average side crack width; and (b) tension face crack width

For all specimens, there was a major difference in behaviour between the first and subsequent loading cycles. As shown in Figure 4.12, the plots from the 1st load cycle demonstrate an initial cracking phase followed by the formation of cracks with an overall approximately linear relationship. Shown in Figure 4.13 are the plots following 25 loading cycles that depict a much more linear relationship with significant changes in slopes and y-intercepts from the first loading cycle. There is still some variation between specimens; however, this may be due to the fact that each specimen was loaded to slightly different crack widths which could affect the slope of the linear reloading curve.
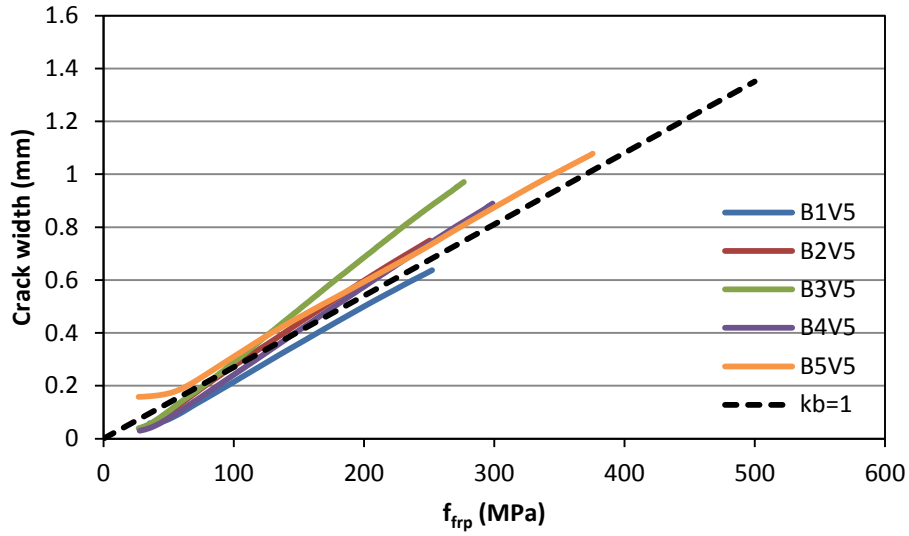
(a)
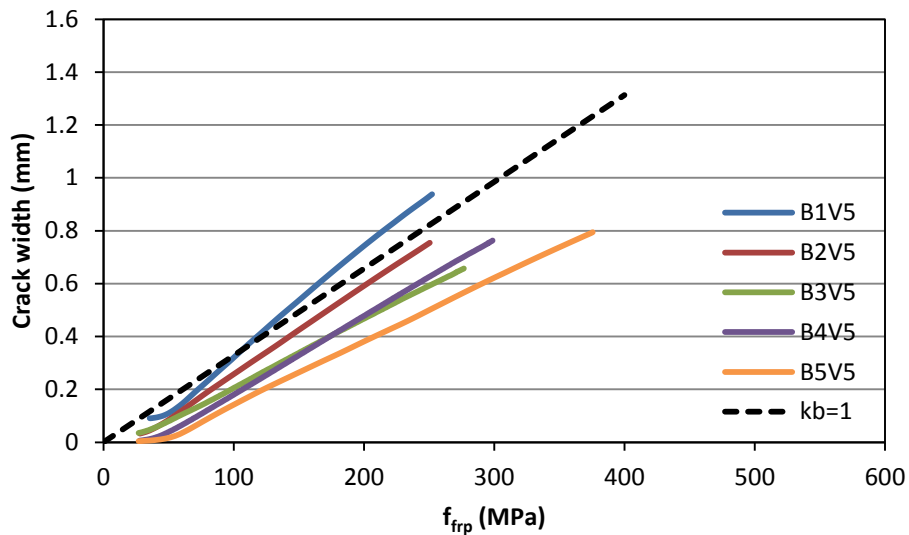
(b)

Figure 4.13 - Reinforcement stress versus crack width plots following 25 loading cycles for: (a) average side crack width; and (b) tension face crack width

4.2.3.2   Aslan versus V-Rod

Although multiple specimens had 2 - #5 bars for reinforcement, specimen B5V5 was chosen for comparison with BA5 as both specimens were cast in the same pour and the variability of concrete strength could be ignored from the analysis.   Based on raw cracking behaviour, the specimens behaved very similarly regardless of the type of

longitudinal reinforcement used. As shown in Figure 4.14, the behaviour of specimens B5V5 and BA5 were very consistent for cracks at the level of reinforcement whereas there are some deviations for the crack on the tension face.
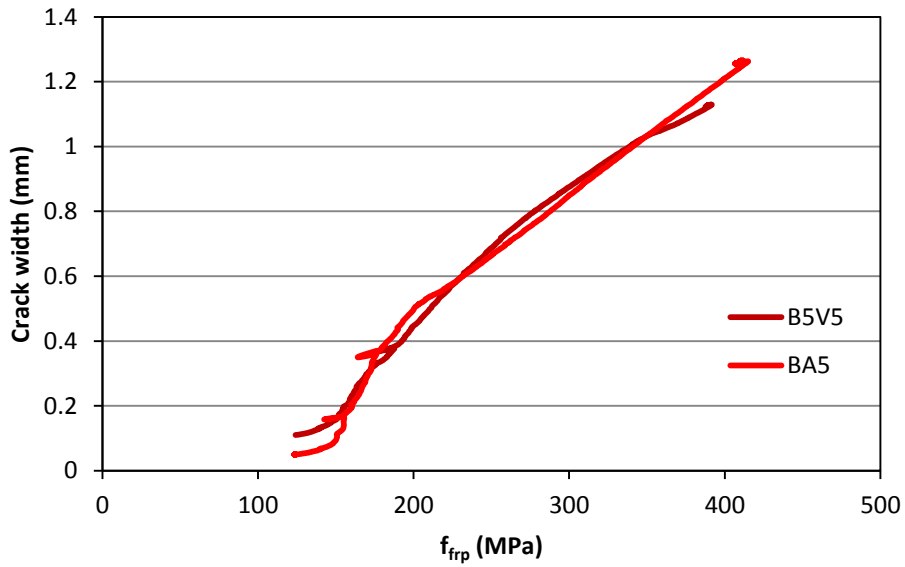
(a)
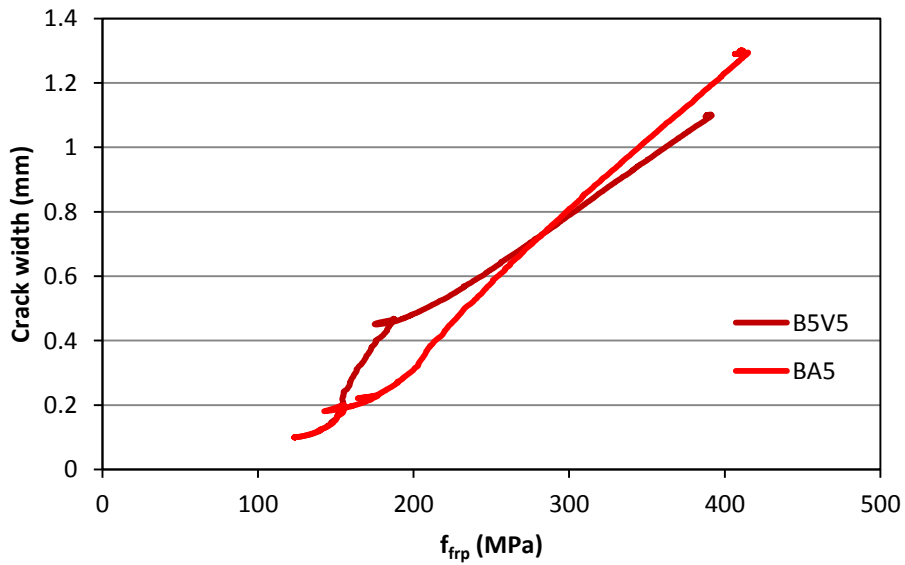
(b)

Figure 4.14 - Plots for B5V5 and BA5 comparison: (a) average side crack width; and (b) tension face crack width

Based on raw cracking behaviour, the specimens reinforced with #6 bars also behaved similarly regardless of the type of longitudinal reinforcement. As shown in Figure 4.15, specimens BV6 and BA6 have similar trends in crack growth for all cracks monitored using gauges.
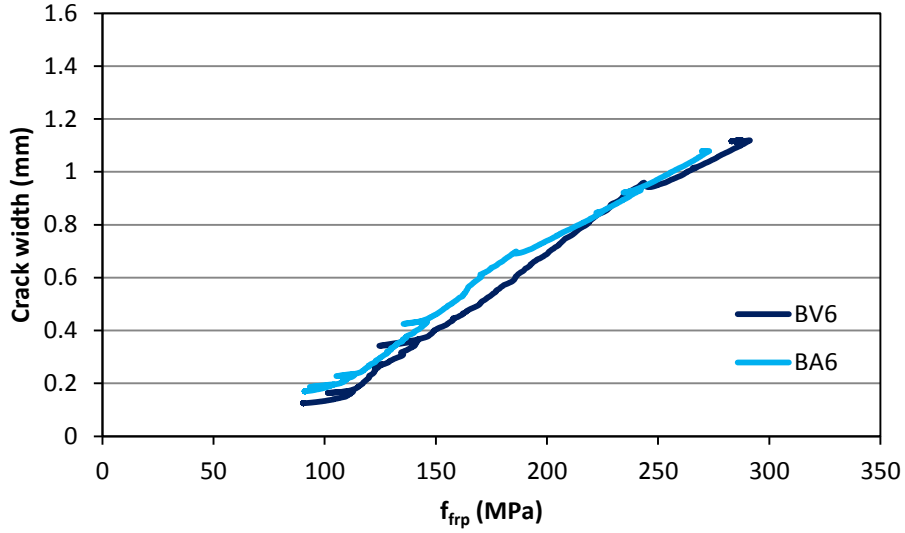
(a)
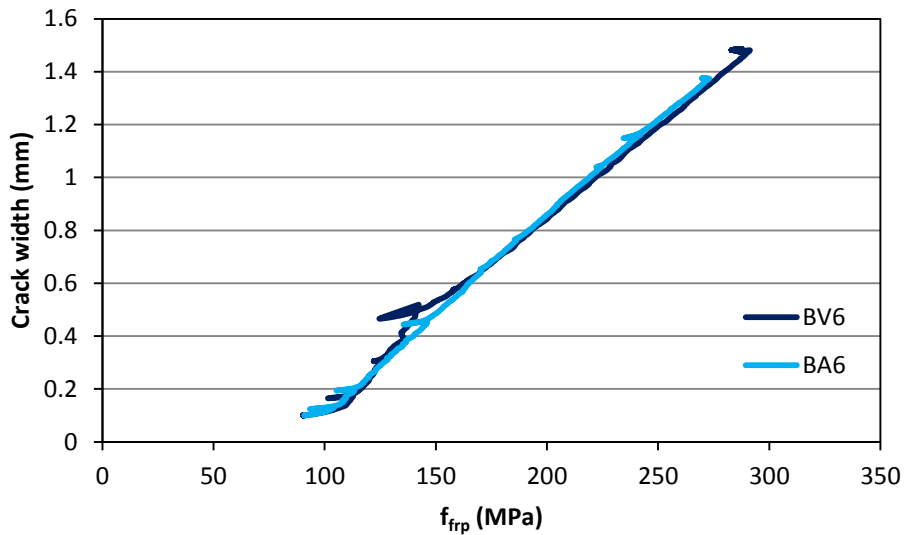
(b)

Figure 4.15 - Plots for BV6 and BA6 comparison: (a) average side crack width; and (b) tension face crack width

When comparing the behaviour of the #5 and #6 bars, it can be observed that the larger diameter bars (#6) have inferior bond performance to the #5 bars as shown in Figure 4.16 where larger crack widths are observed at equivalent stresses. However, this can also be attributed to the changes in concrete cover as the specimens with #5 bars have 38 mm cover, while the specimens with #6 bars have 50 mm cover.
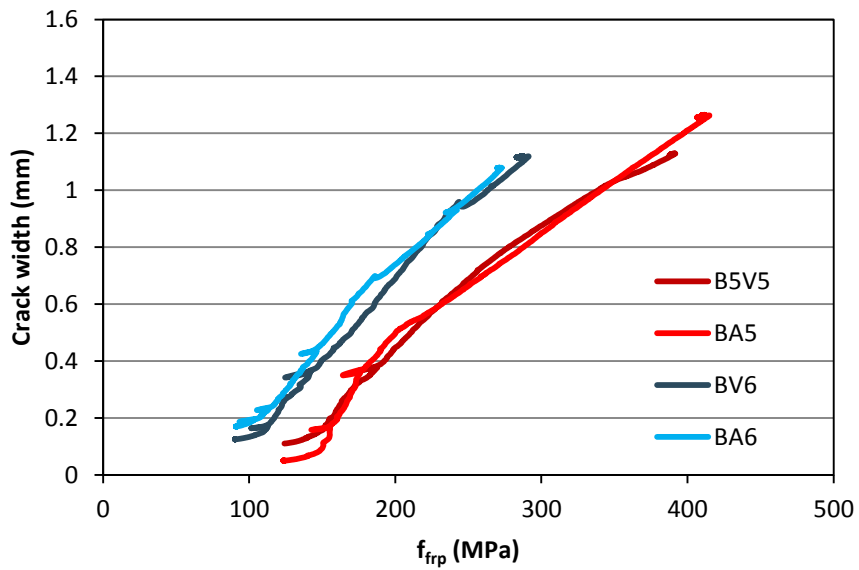
(a)
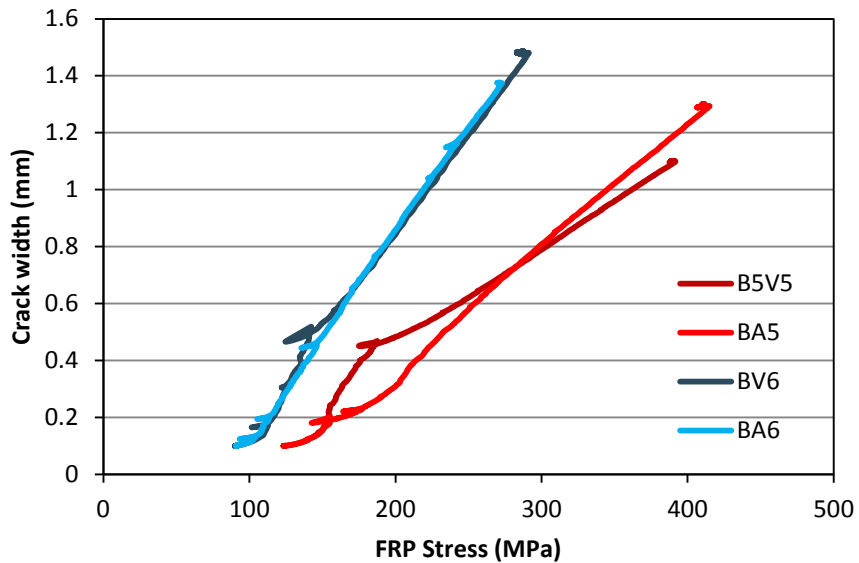
(b)

Figure 4.16 - V-Rod and Aslan 100 comparison for #5 and #6 bars: (a) average side crack width; and (b) tension face crack width

4.2.4 Recommendations for Future Testing

Although many issues were rectified prior to this phase of testing, there were significant issues observed with the strain gauges during testing. In Phase I, the strain gauges were applied for investigative purposes on only two of the samples and of the two samples, only one exhibited functional strain gauges on both bars during testing. One gauge broke prior to loading and no strain data was acquired. Entering this phase of testing, there were concerns on whether or not the gauges would function when applied to a large number of specimens due to the results from Phase I:

- The strain gauges for this phase were applied to the GFRP longitudinal reinforcement following removal of the surface coating and resin to ensure a sufficiently smooth surface. This removal was done mechanically using a grinding mill and based on the gauges' poor performance in this phase of testing, the gauges likely bonded to individual fibres as too much resin was removed. As the specimen was loaded, the gauge unbonded from individual fibres resulting in premature lifting of the gauge and therefore, the gauges broke off prior to completing the cracking phase.

- The strain data that was acquired from this phase of testing was compared to those predicted by the elastic cracked section theory. The strain values had good correlation for only two of the specimens, while the other six specimens recorded strains much lower than those predicted by the theory. It is likely that this was also due to the strain gauges starting to debond upon initial loading.

4.3 PHASE IIB

Phase IIB testing was focused on attaining measured strain values for the GFRP longitudinal reinforcement during cracking as this was unsuccessful in Phase IIA. In addition, the depth and bottom cover of the two specimens were varied in order to have two additional samples to compare to the #5 identical specimens previously cast in Phase IIA. The goal was to determine whether the bonding and cracking behavior was significantly affected by changes in parameters despite the fact identical #5 bars from the same lot were used. This was chosen as k_b is supposed to be a mechanical property of the bar.

4.3.1 Test Specimens

The tests of 2 specimens were completed for this phase. Both specimens had dimensions of 200 x 250 x 2810 mm (width x height x length) and contained 2 - #5 V-Rod GFRP rebars manufactured by Pultrall Inc. as longitudinal reinforcement. Grade 400 10M (ϕ11.3) steel stirrups were used for shear reinforcement in the specimens and conformed to CSA G30.18-09. Stirrups were not provided in the maximum moment region to avoid confinement effect. Table 4.9 shows a summary of detailed properties of the specimens.

Table 4.9 - Detailed Properties of Test Specimens for Phase IIB

| ID # | Dimensions (width x height x length) | Longitudinal Reinforcement | | | Concrete | |
		Bar sizes	ρ (%)	Cover (mm)	f'$_c$ (MPa)	kd (mm)
B38	200 x 250 x 2810	2 - #5	0.97	38	35	46
B50		2 - #5	1.03	50	35	45

To enable comparison, the objective was to maintain concrete strengths between Phases IIA and IIB. In Phase IIA, the concrete strengths were 29 and 32 MPa, whereas the specimens in Phase IIB have a slightly higher concrete strength at 35 MPa.

4.3.2 Test Methodology

Both the test configuration and the test procedure for this phase were identical to those for Phase IIA, as discussed in Section 4.2.2. For this phase, strain gauges were applied by carefully removing the outer layer of resin from the GFRP bars manually using multiple grades of sandpaper. Resin was removed until there was a sufficiently smooth surface cleared that was large enough for application of the gauge. Sanding was carefully completed to ensure only the outer resin was removed and the fibres were not exposed.

4.3.3 Test Results

The typical cracking behaviour of B38 and B50 are shown in Figure 4.17. This behaviour is consistent with the previous specimens tested and the cracks exhibit approximate plot linearity during growth as shown by the linear lines of best fit. Cracks at the level of reinforcement and cracks on the tension surface are larger for B50

immediately following loading, demonstrating the immediate effect of increased cover. As strain gauge readings were not acquired in this phase of testing, FRP stresses were calculated using elastic cracked section theory.
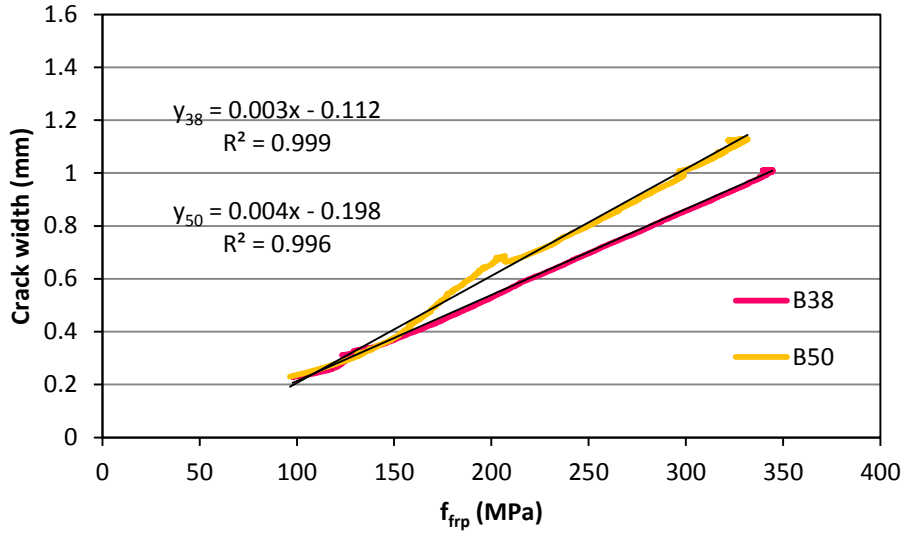
(a)
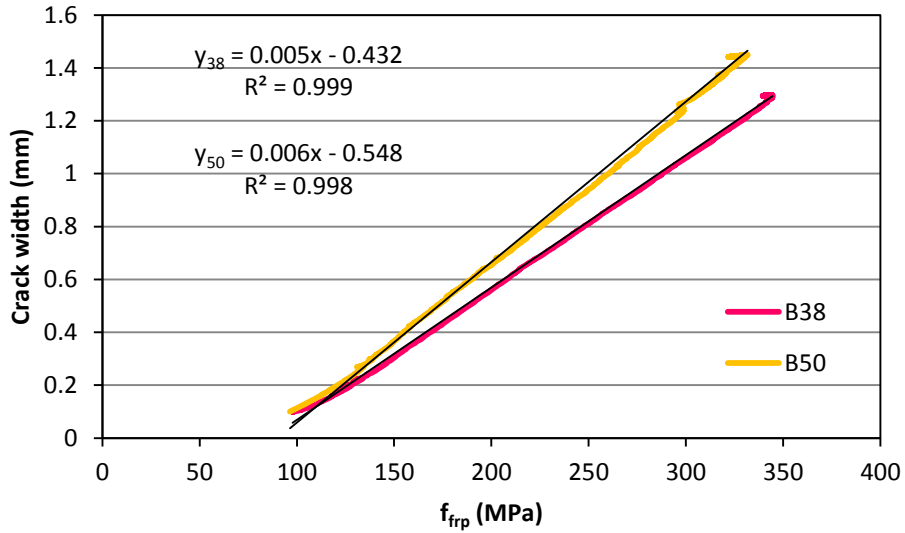
(b)

Figure 4.17 - Typical cracking behaviour and best fit lines for: (a) average side crack width; and (b) tension face crack width

4.3.3.1 Comparison with Phase IIA

As shown in Figure 4.18(a), the cracking behaviour of specimens B38 and B50 differ from the five identical V-Rod specimens at the beginning of loading for cracks on the side of the beam at the level of reinforcement. However, near 200 MPa (approximately 30% of the guaranteed ultimate tensile strength of the bars), the plots begin to converge and there is fairly good correlation for the remainder of the recorded data. For cracks on the tension face, there is an overall good correlation for the service range of the bars shown in Figure 4.18(b) with separation in behaviour following this point. The crack widths corresponding to several service stresses are shown in Tables 4.10 and 4.11.
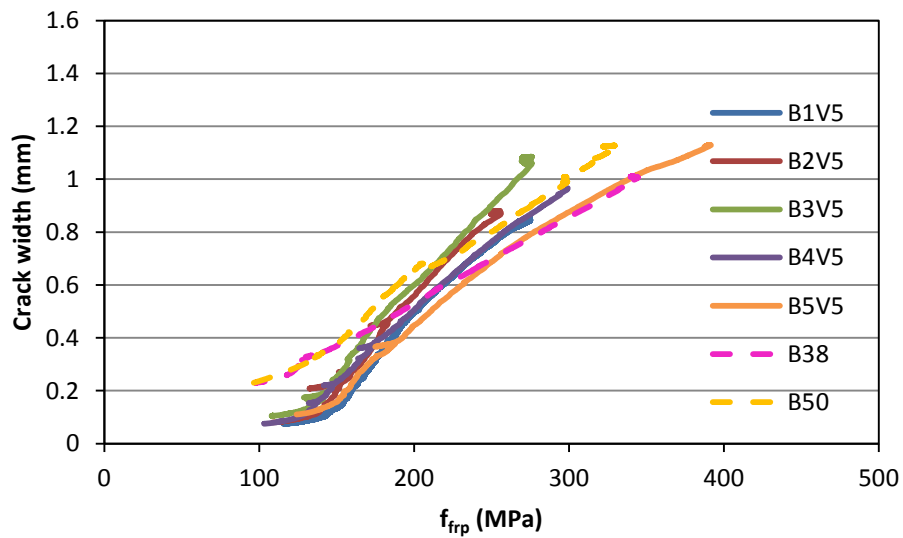
(a)
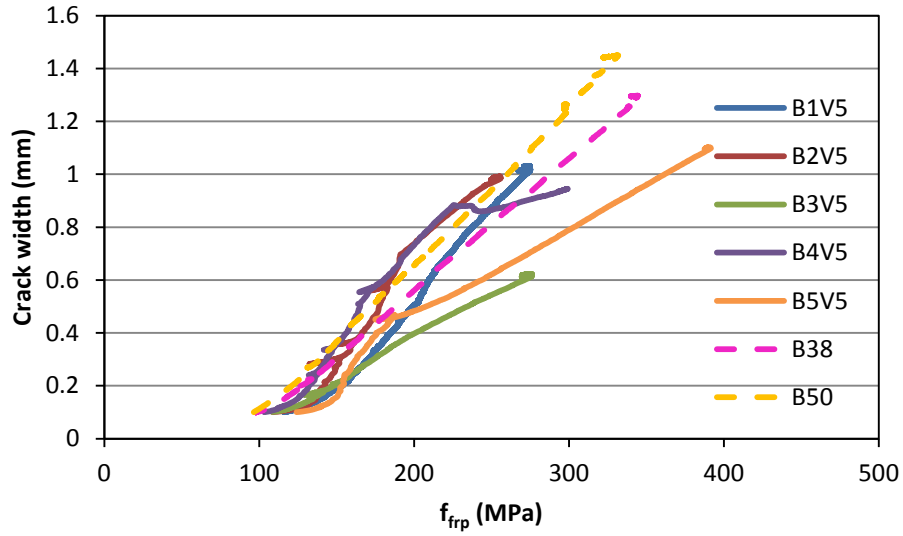
(b)

**Figure 4.18 - Comparison of Phases IIA and B specimens with #5 V-Rod bars for:
(a) average side crack width; and (b) tension face crack width**

**Table 4.10 - Average side crack widths (mm) at various stress levels for specimens
reinforced with #5 V-Rod bars in Phases IIA and IIB**

Stress (MPa)	B1V5	B2V5	B3V5	B4V5	B5V5	B38	B50
125	0.08	0.09	0.12	0.10	0.11	0.29	0.32
150	0.13	0.20	0.25	0.23	0.16	0.37	0.40
175	0.32	0.38	0.45	0.38	0.32	0.44	0.46
200	0.49	0.56	0.60	0.51	0.45	0.53	0.53
225	0.63	0.72	0.75	0.64	0.57	0.61	0.57

**Table 4.11 - Tension face crack widths (mm) at various stress levels for specimens
reinforced with #5 V-Rod bars in Phases IIA and IIB**

Stress (MPa)	B1V5	B2V5	B3V5	B4V5	B5V5	B38	B50
125	0.11	0.12	0.13	0.15	0.10	0.19	0.28
150	0.19	0.28	0.21	0.36	0.16	0.30	0.40
175	0.34	0.47	0.31	0.58	0.39	0.43	0.46
200	0.50	0.74	0.40	0.73	0.48	0.56	0.52
225	0.70	0.86	0.47	0.88	0.55	0.69	0.57

Observing the behaviour following 25 cycles, specimens B38 and B50 show better
agreement with the specimens from Phase IIA for both cracks on the side and bottom

faces as shown in Figure 4.19. For cracks at the level of reinforcement, all specimens exhibit similar slopes, while cracks on the tension face have similar y-intercepts even though the slopes do vary. In both cases, specimens B38 and B50 have the largest crack widths of all specimens for essentially the entire range of recorded data.
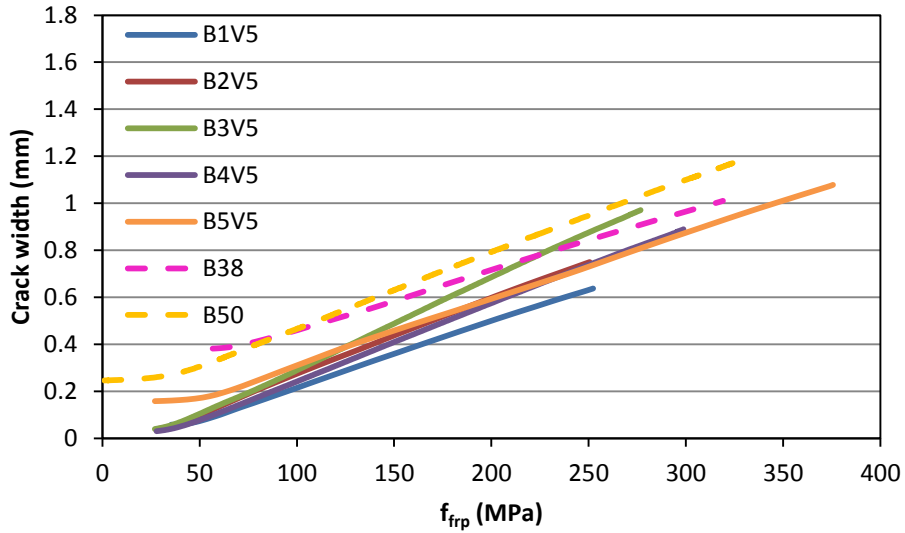
(a)
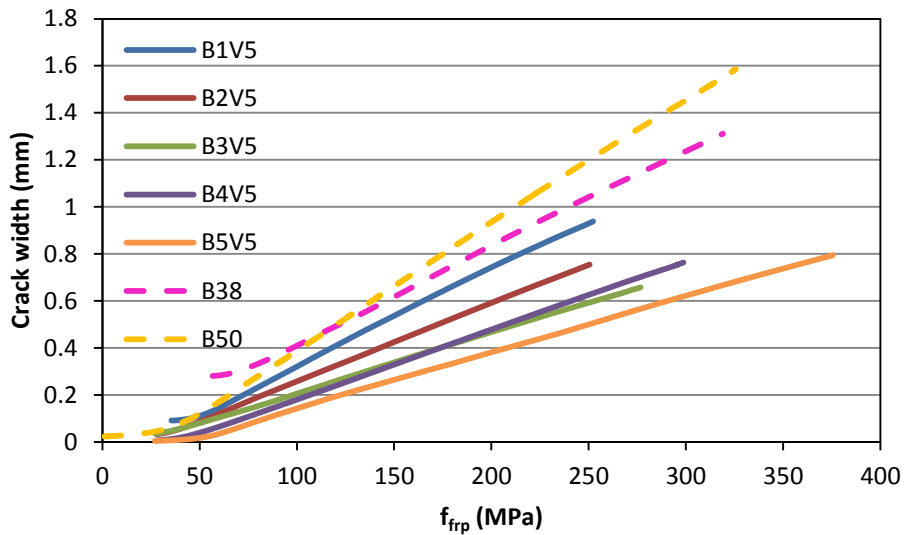
(b)

Figure 4.19 - Behaviour following cycling for Phases IIA and B specimens with #5 V-Rod bars for: (a) average side crack width; and (b) bottom crack width

When compared to the five identical test specimens, the beginning of the loading behaviour (initial cracking phase) of specimens B38 and B50 is different, which may be due to the influence of concrete strength or quality due to consolidation.

4.3.4 Recommendations for Future Testing

Following completion of Phase IIB testing, there are several recommendations that should be taken into account if additional testing was to be performed:

- The inability to collect measured strain data during testing did not allow for a direct comparison to calculated values derived from elastic cracked section theory. However, based on literature (Bakis *et al.*, 2006) and ACI 440.1R-06, both calculated and measured strains are acceptable for the calculation of k_b. In addition, the majority of the applications for the modified Frosch equation will be for design purposes where measured values will not be available.

- With the absence of measured strain data, it is not possible to make conclusive statements regarding the effect on the calculation of k_b. It is therefore required that this issue be further investigated using additional test specimens.

CHAPTER 5 :   INTERPRETATION OF EXPERIMENTAL k_b

This chapter discusses the interpretation and calculation of the bond dependent coefficient using the data collected from experimental testing in Chapter 4.

5.1   PHASE I

Two approaches were considered in order to determine the most consistent calculation method for the bond dependent coefficient: 1) the typical stress-level approach; and 2) the slope approach. The stress-level approach involves the calculation of k_b at a specific service stress using the corresponding crack width observed in testing. A slope approach was also considered where the slope of a crack width versus reinforcement stress plot would be used in order to back calculate k_b. In both cases, the modified Frosch equation (Equation [2.7]) was used for the analysis.

5.1.1 Stress-Level Approach

For the stress-level approach, k_b was calculated using the current design equation and crack width measurements recorded during testing. The bond dependent coefficient is to be calculated at service stress as these are the cracks that are of interest to designers; however, there is no uniform guidance on the service stress for FRP although it has been most commonly reported as 30% of the ultimate guaranteed tensile strength of the FRP bars. This calculation method is sensitive to the stress level chosen, and therefore, a variety of stresses ranging from 15 – 30% of ultimate were chosen in order to demonstrate the variability that results. Ignoring the variability for k_b across many specimens, there should only be one k_b value for each beam as this is a material property of the bar. However, as shown in Figure 5.1, the stress-level approach results in significant variability depending on the stress chosen for analysis. For this specimen, k_b ranges from 0.31 – 0.98, with an average k_b over this range of 0.60. The reason for such a wide fluctuation of values results from the fact that k_b at each stress level is calculated as the secant at that point according to the equation recommended by ACI 440.1R-06 and CHBDC CAN/CSA-S6-06. Complete results for all specimens are shown in Table 5.1.
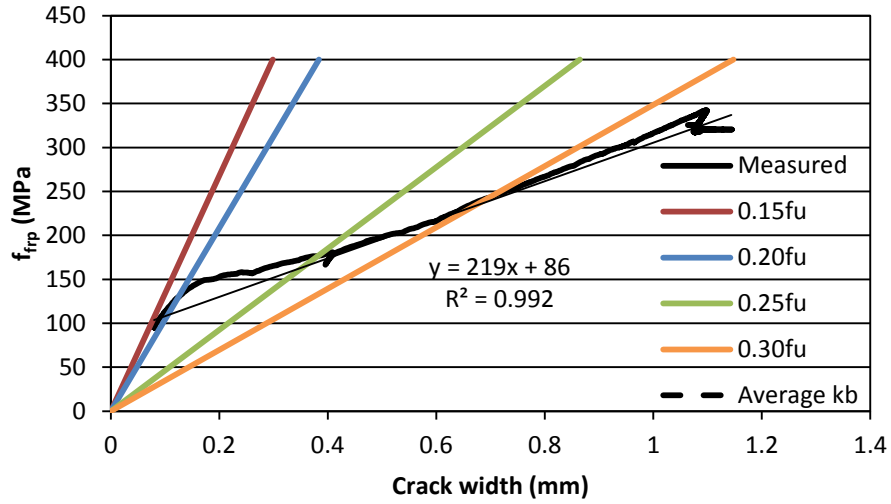
Figure 5.1 - Variability of k_b using stress-level approach for specimen B9

Table 5.1 - Values of k_b at service stress levels

	$0.1f_u$	$0.15f_u$	$0.2f_u$	$0.25f_u$	$0.3f_u$	Average k_b
B1	-	0.31	0.75	1.11	1.39	0.89
B2	0.45	0.58	0.63	0.66	0.68	0.60
B3	-	0.34	0.45	0.68	0.81	0.57
B4	0.45	0.64	0.8	0.92	0.98	0.76
B5	-	0.21	0.75	1.25	1.37	0.90
B6	0.32	0.59	0.86	0.93	0.95	0.73
B7	-	0.18	0.58	0.90	1.09	0.69
B8	0.36	0.77	0.92	0.81	0.76	0.72
B9	-	0.31	0.37	0.73	0.98	0.60
B10	0.48	1.07	1.56	1.69	1.74	1.31
B13	0.49	0.75	0.96	1.14	1.21	0.91
B14	0.43	0.84	1.05	1.09	1.11	0.90
B15	-	0.40	0.64	0.78	0.84	0.66
B16	-	0.55	0.82	0.95	0.99	0.83
S1	-	0.22	0.48	0.74	0.93	0.59
S2	-	0.25	0.72	0.64	0.63	0.56
S3	-	0.83	0.71	0.71	0.67	0.73
S4	-	0.32	0.41	0.34	0.33	0.35
S5	-	0.17	0.06	0.23	0.51	0.24
S6	-	-	0.39	0.35	0.44	0.39
S7	-	0.49	0.94	0.82	0.90	0.79
S8	-	0.35	0.61	0.52	0.73	0.55
S9	0.67	0.82	0.94	1.02	-	0.86
Average	**0.46**	**0.50**	**0.71**	**0.83**	**0.91**	**0.70**
COV (%)	**22.8**	**52.1**	**42.1**	**39.0**	**36.2**	**32.1**

All the calculated k_b lines shown in Figure 5.1 begin at the origin, as forced by current design equations. However, this is not consistent with the behaviour of the specimen, which does not crack immediately upon loading but rather when the cracking moment of the concrete is reached. In addition, the calculated k_b value is only representative of one point of the specimen's behaviour. This could explain why there has been such large variability reported by researchers, as the value used for this calculation is often ambiguous.

To further analyze these results, groups of specimens were compared depending on the bar diameter used. The comparison is shown in Figure 5.2, and demonstrates that k_b not only varies according to stress level but must also be influenced by bar diameter.
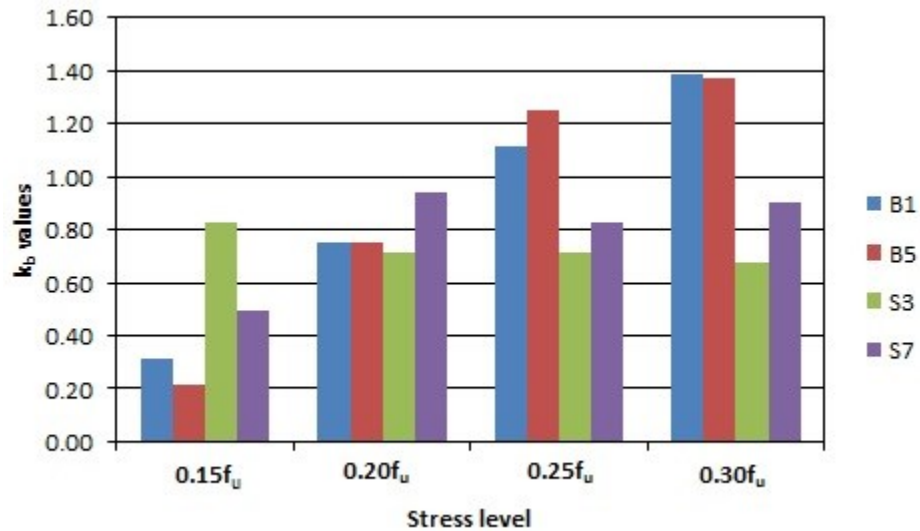
(a)
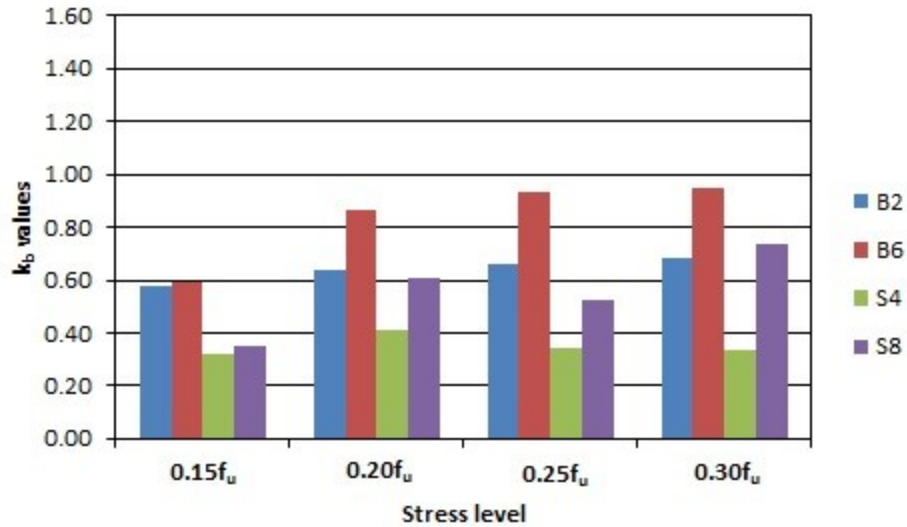
(b)

Figure 5.2 - Impact of k_b on stress level for: (a) #5 bars; and (b) #6 bars

The specimens were also compared depending on member type, either beam or slab. As can be seen in Figure 5.3, the general observation is that the slab specimens tend to have smaller average k_b values, and therefore, smaller crack widths. For these V-Rod GFRP bars, the recommended k_b from the manufacturer is 0.8 which would be a good fit for the beam specimens; however, this would over predict crack widths in the slab specimens. Despite the fact that a beam test is currently the standard for determination of k_b, the majority of FRP applications are likely to be slab specimens. Based on these results, the beam test may not be the most appropriate for determination of k_b.
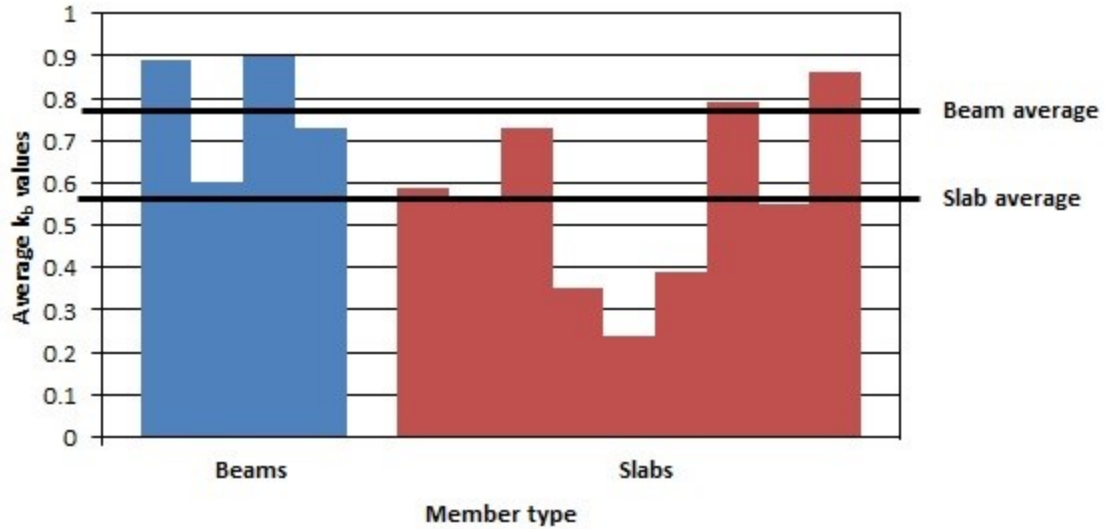
Figure 5.3 - Average k_b values for specimen member types

5.1.2 Slope Approach

Due to the issues that arose using the stress-level approach, a slope approach was also considered for the calculation of k_b in an attempt to achieve better consistency with experimental results. The approximately linear behaviour of the specimen suggests that the bond behaviour is basically unchanged during testing and therefore, there should be no significant variability for k_b. For this approach, the slope of a crack width versus reinforcement stress plot was used to back calculate a k_b that is representative of a large range of the data for each specimen. The recommended design equation (Equation [2.7]) can be rearranged to the form shown below in Equation [5.1] and the slope in conjunction with a geometric constant can be used to solve for k_b for a given beam:

$$\frac{w}{f_f} = k_b \times CONSTANT \qquad [5.1]$$

where CONSTANT = $\dfrac{2\beta}{E_f}\sqrt{d_c^2 + \left(\dfrac{s}{2}\right)^2}$

This calculated k_b value is then plotted with a dashed line in Figure 5.4 to demonstrate the result of neglecting the intercept, where predicted crack widths are much greater than those observed in testing. However, there is consistent error over the entire range of data but the calculated line needs to be shifted closer to the measured experimental values to

accurately represent the data. This would require a change in format of the equation in order to accommodate the non-zero y-intercept. This procedure was carried out on all test specimens and the results are summarized in Table 5.2 and associated plots can be found in Appendix F.
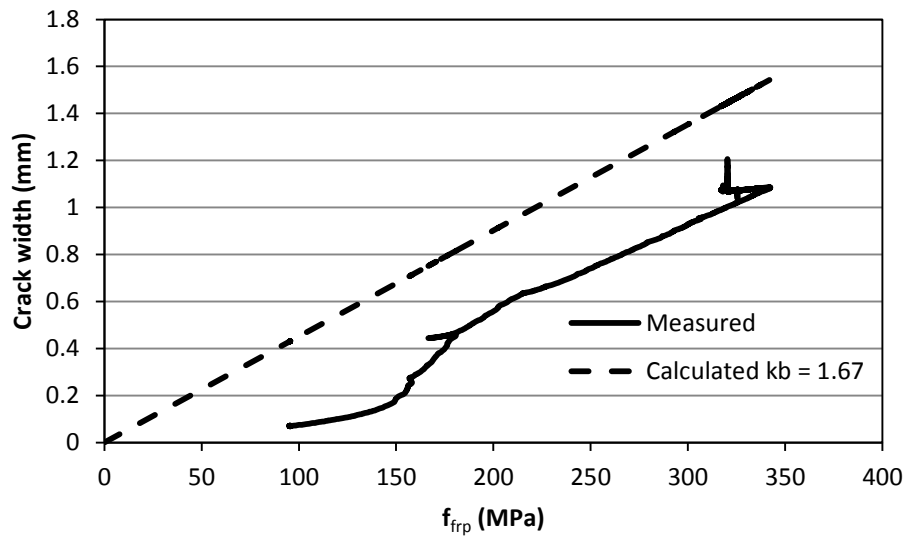
Figure 5.4 - Determination of k_b using slope method for specimen B9

Table 5.2 - Slope, w intercepts and R^2 values using slope approach

	Initial cracking			Following 100 cycles		
	Slope (x10⁻³)	Intercept	R^2	Slope (x10⁻³)	Intercept	R^2
B1	6.58	-0.599	0.995	4.14	0.240	0.998
B2	1.94	-0.026	0.997	2.99	-0.081	1.000
B3	3.27	-0.235	0.998	2.19	0.159	0.999
B4	3.76	-0.196	1.000	3.03	0.139	0.999
B5	4.51	-0.271	0.925	2.63	0.139	0.995
B6	3.11	-0.132	0.996	2.46	0.093	0.999
B7	4.78	-0.407	0.995	3.05	0.210	0.999
B8	0.90	0.164	0.765	1.28	-0.060	0.969
B9	4.26	-0.350	0.991	3.17	0.054	0.999
B10	5.59	-0.195	0.992	4.27	0.192	0.998
B13	4.17	-0.191	0.998	2.93	0.257	0.999
B14	3.55	-0.103	0.996	2.76	0.171	0.999
B15	2.59	-0.085	0.986	1.99	0.089	0.997
B16	3.69	-0.182	0.995	2.55	0.157	0.999
S1	2.49	-0.157	0.971	1.56	-0.092	0.999
S2	2.15	-0.077	0.987	1.55	0.117	0.999
S3	2.28	0.051	0.983	1.91	0.272	0.999
S4	1.86	-0.036	0.994	1.66	0.042	1.000
S5	1.92	-0.189	0.996	1.66	0.284	0.999
S6	1.77	-0.111	0.966	1.62	-0.046	1.000
S7	4.31	-0.195	0.997	2.83	0.291	0.999
S8	4.97	-0.302	0.995	3.35	0.210	0.999
S9	5.67	-0.161	0.997	3.62	0.236	0.999

5.1.2.1 k_b Following Cyclic Loading

The k_b values calculated from the 1st load cycle are shown plotted in Figure 5.5 with the data following 100 cycles. It is clear that the k_b value from the slope approach still over predicts the crack widths. The k_b value of 0.98 at 30% of ultimate actually under predicts the crack widths, where the actual cracks are larger than those predicted by the equation. **In fact, this k_b value no longer represents any point of the behaviour after the 1st cycle.** There is one major caveat however: the cyclic lines are likely dependent on the peak load and would be influenced depending on what maximum crack width was chosen.
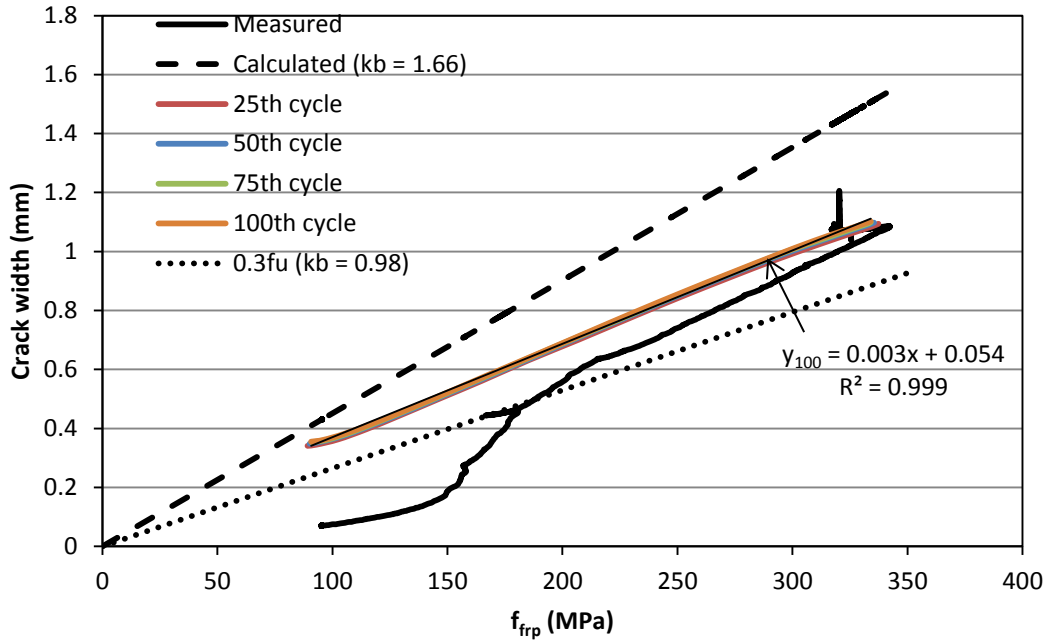
Figure 5.5 - Crack stabilization using cyclic loading

Figure 5.6 shows a summary of the k_b values for the 1st and 100th load cycle using a slope approach. Overall, cycling the specimen reduces some of the variability with the coefficient of variation (COV) dropping from 49 to 37.8%. This is likely due to the fact that the initial portion of the crack behaviour is unstable on the 1st cycle which introduces variability.

(a)
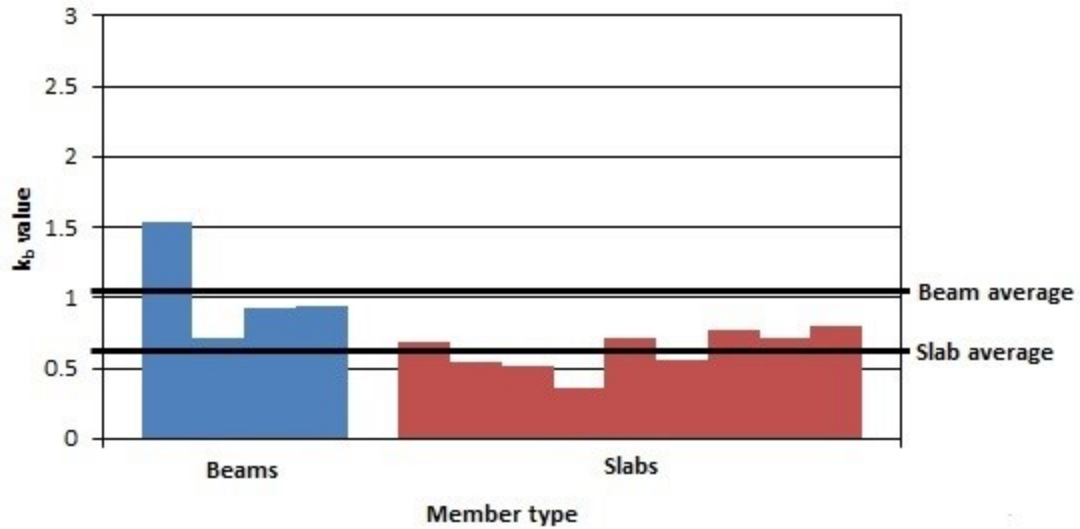
(b)

Figure 5.6 - Slope approach k_b values depending on member type for: (a) 1st load cycle; and (b) 100th load cycle

To investigate the effect of slab thickness on k_b, average k_b values obtained from the stress-level approach were used. The colors used in Figure 5.7 also correspond to the same bar size in order to further classify the samples. The beam samples, which also have the largest depth (300 mm), have overall larger k_b values than the remaining slab samples. However, there is also significant variability within groups of each depth of specimen.
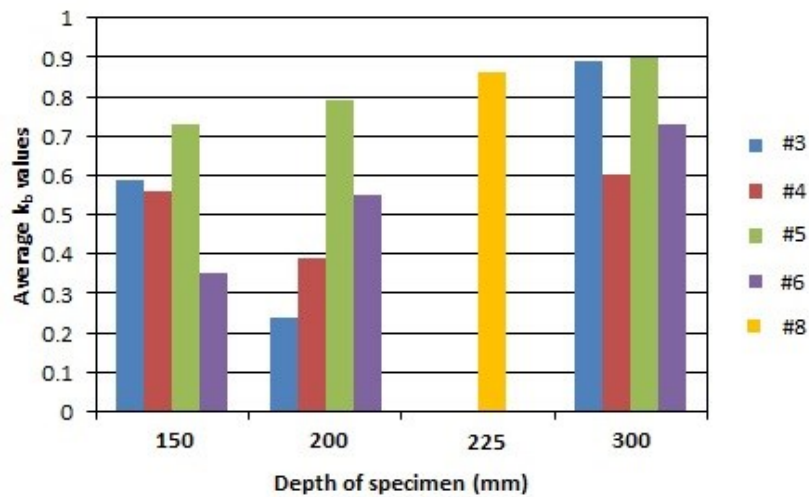
Figure 5.7 - Average k_b values depending on specimen depth

5.2 PHASE IIA

The cracks used for this analysis were the first three cracks that formed within the constant moment zone and hence, are labeled as 1, 2 and 3. For specimens B1V5 – B4V5, crack 3 was on the tension face; however, for specimen B5V5, crack 2 represents the crack on the tension face. All k_b values were calculated using the recommended equation by ACI 440.1R-06 and CHBDC CAN/CSA-S6-06 for crack width prediction in FRP reinforced concrete. This section will be further divided into two main sections: 1) the five identical specimens; and 2) the comparison of Aslan versus V-Rod.

5.2.1 Five Identical Specimens

The five identical specimens were used to examine if consistency could be achieved in the calculation of k_b. Identical reinforcement was used in all specimens and loading conditions were maintained.

5.2.1.1   Stress-Level Approach

Using the stress-level approach for the calculation of k_b yielded significant variation depending on the stress-level at which this calculation was done. As shown in Table 5.3, the general trend is that the calculated k_b values continue to increase with increases in stress for any given crack. The manufacturer of the bars, Pultrall Inc., recommends a bond dependent coefficient of 0.8, and for these test results, this occurs at a stress in the range of 25 – 30% of ultimate which is also the most commonly reported service stress limit for GFRP reinforcement. However, there is also a variation depending on which crack is chosen for analysis within a given beam.

79

Table 5.3 - Calculated k_b values using stress-level approach for Phase IIA

	Level	$0.2f_u$	$0.225f_u$	$0.25f_u$	$0.275f_u$	$0.30f_u$	Average
	Stress (MPa)	137	154	171	188	205	
B1V5	k_{b1}	0.21	0.35	0.58	0.79	0.93	0.57
	k_{b2}	0.29	0.37	0.63	0.82	0.97	0.62
	Avg. $k_{b,side}$	0.25	0.36	0.60	0.81	0.95	0.59
	k_{b3}	0.31	0.40	0.54	0.67	0.81	0.55
	Avg. $k_{b,all}$	0.27	0.37	0.58	0.76	0.91	0.58
B2V5	k_{b1}	0.20	0.35	0.55	0.85	1.00	0.59
	k_{b2}	0.41	0.77	0.93	1.08	1.13	0.86
	Avg. $k_{b,side}$	0.30	0.56	0.74	0.96	1.07	0.73
	k_{b3}	0.33	0.62	0.77	1.01	1.14	0.77
	Avg. $k_{b,all}$	0.31	0.58	0.75	0.98	1.09	0.74
B3V5	k_{b1}	0.47	0.69	0.92	1.08	1.15	0.86
	k_{b2}	0.36	0.63	0.90	1.04	1.10	0.81
	Avg. $k_{b,side}$	0.42	0.66	0.91	1.06	1.13	0.84
	k_{b3}	0.36	0.44	0.51	0.58	0.61	0.50
	Avg. $k_{b,all}$	0.40	0.59	0.78	0.90	0.95	0.72
B4V5	k_{b1}	0.40	0.58	0.77	0.87	0.98	0.72
	k_{b2}	0.43	0.62	0.75	0.87	0.96	0.72
	Avg. $k_{b,side}$	0.41	0.60	0.76	0.87	0.97	0.72
	k_{b3}	0.53	0.76	0.99	1.05	1.14	0.89
	Avg. $k_{b,all}$	0.45	0.65	0.84	0.93	1.03	0.78
B5V5	k_{b1}	0.36	0.45	0.67	0.68	0.78	0.59
	k_{b3}	0.32	0.41	0.64	0.81	0.92	0.62
	Avg. $k_{b,side}$	0.34	0.43	0.65	0.74	0.85	0.60
	k_{b2}	0.26	0.39	0.64	0.76	0.73	0.56
	Avg. $k_{b,all}$	0.31	0.42	0.65	0.75	0.81	0.59

Table 5.4 depicts the variability of k_b in two ways: 1) the variability within a beam for k_b calculated from 20 – 30% of ultimate; and 2) the variability for k_b across all specimens at a specific stress level. The coefficients of variation indicate that k_b is highly variable within a beam depending on the stress level at which the calculation is completed for both cracks at the level of reinforcement and those on the tension face. However, for the

entire set of specimens, the coefficients of variation are much smaller across a specific load level.

Table 5.4 - Coefficients of variation for k_b calculated using stress-level approach

	B1V5	B2V5	B3V5	B4V5	B5V5	Average	COV (%)
Average side cracks							
$0.20f_u$	0.25	0.30	0.42	0.41	0.34	0.34	**21.0**
$0.25f_u$	0.60	0.74	0.91	0.76	0.65	0.73	**16.3**
$0.30f_u$	0.95	1.07	1.13	0.97	0.85	0.99	**11.0**
Average	0.60	0.70	0.82	0.71	0.61	0.69	**12.9**
COV (%)	**58.3**	**54.9**	**44.3**	**39.7**	**41.9**	**47.4**	
Bottom crack							
$0.20f_u$	0.31	0.33	0.42	0.53	0.26	0.37	**28.8**
$0.25f_u$	0.54	0.77	0.91	0.99	0.64	0.77	**24.1**
$0.30f_u$	0.81	1.14	1.13	1.14	0.73	0.99	**20.5**
Average	0.55	0.75	0.82	0.89	0.54	0.71	**21.9**
COV (%)	**45.2**	**54.3**	**44.3**	**35.9**	**45.9**	**44.3**	
All three cracks							
$0.20f_u$	0.27	0.31	0.40	0.45	0.31	0.35	**21.4**
$0.25f_u$	0.58	0.75	0.78	0.84	0.65	0.72	**14.5**
$0.30f_u$	0.91	1.09	0.95	1.03	0.81	0.96	**11.3**
Average	0.59	0.72	0.71	0.77	0.59	0.68	**12.3**
COV (%)	**54.6**	**54.6**	**39.7**	**38.2**	**43.3**	**45.5**	

5.2.1.2   Slope Approach

The calculated k_b values using the slope method were much more conservative than those found using the stress-level approach. As shown in Table 5.5, all k_b values are greater than 1 which is the reference for steel reinforcement. There is also a variation within the specimens despite the fact that the properties and loading conditions are the same with average beam k_b values ranging from 1.35 – 2.2. The slopes used to calculate these k_b values, as well as y-intercepts and R^2 values to demonstrate a good linear fit are shown in Table 5.6.

Table 5.5 - k_b values using slope approach for first loading cycle

ID	k_{b1}	k_{b2}	k_{b3}	Avg. k_b
B1V5	1.89	2.26	2.04	2.06
B2V5	2.48	2.07	2.04	2.20
B3V5	2.67	2.18	1.01	1.95
B4V5	1.93	1.78	1.40	1.70
B5V5	1.67	1.10	1.30	1.35

Table 5.6 - Slopes, y-intercepts and R^2 values for 1st loading cycle

ID	Slope 1 $(x10^{-3})$	Int. 1	R^2 1	Slope 2 $(x10^{-3})$	Int. 2	R^2 2	Slope 3 $(x10^{-3})$	Int. 3	R^2 3
B1V5	5.13	-0.584	0.980	6.13	-0.735	0.996	6.71	-0.816	0.995
B2V5	7.21	-0.826	0.989	5.62	-0.544	0.990	6.73	-0.688	0.987
B3V5	7.22	-0.795	0.995	5.94	-0.635	0.996	3.34	-0.279	0.998
B4V5	5.24	-0.524	0.994	4.83	-0.480	0.996	4.64	-0.307	0.905
B5V5	5.73	-0.475	0.998	3.64	-0.306	0.984	3.51	-0.273	0.926
Avg.	6.11	-0.641	0.991	5.23	-0.540	0.992	0.50	-0.472	0.962
COV (%)	**20.0**	**25.0**	**0.7**	**19.7**	**30.0**	**0.6**	**33.5**	**54.9**	**4.5**

The slope approach was also used to calculate k_b values following the application of 25 loading cycles. The k_b values calculated from the 25th cycle are much more reasonable compared to the value of 0.8 that was provided by the manufacturer as shown in Table 5.7. From the 1st to the 25th cycle, there is a reduction in k_b ranging from 29 – 52%. In addition, the average k_b values for each beam are much less variable. The slopes, y-intercepts and R^2 values found for the 1st and 25th loading cycles are shown in Tables 5.6 and 5.8 and depict the drastic change in values, in particular the y-intercepts that occurs. The y-intercepts are reduced and begin to approach zero, similar to the current form of the recommended equation by ACI 440.1R-06 and CHBDC CAN/CSA-S6-06.

Table 5.7 - k_b values using slope approach for 25th loading cycle

ID	k_{b1}	k_{b2}	k_{b3}	Avg. k_b
B1V5	0.93	1.11	1.25	1.10
B2V5	1.18	1.19	0.97	1.11
B3V5	1.52	1.30	0.76	1.19
B4V5	1.22	1.22	0.88	1.11
B5V5	1.18	0.79	0.89	0.96

Table 5.8 - Slopes, y-intercepts and R^2 values for 25th loading cycle

ID	Slope 1 $(x10^{-3})$	Int. 1	R^2 1	Slope 2 $(x10^{-3})$	Int. 2	R^2 2	Slope 3 $(x10^{-3})$	Int. 3	R^2 3
B1V5	2.53	-0.064	0.999	3.01	-0.055	0.999	4.14	-0.084	0.999
B2V5	3.24	-0.052	0.999	3.22	-0.042	0.998	3.23	-0.059	0.997
B3V5	4.11	-0.088	0.999	3.53	-0.078	0.999	2.50	-0.044	0.999
B4V5	3.32	-0.089	1.000	3.34	-0.078	1.000	2.93	-0.108	0.999
B5V5	3.22	0.173	0.998	2.63	0.102	0.998	2.44	-0.092	0.999
Avg.	3.28	-0.024	0.999	3.14	-0.030	0.999	3.05	-0.077	0.999
COV (%)	17.4	465.0	0.1	11.0	251.0	0.1	22.6	33.3	0.1

5.2.2 Aslan versus V-Rod

Pultrall Inc. recommends a k_b value of 0.8 for the V-Rod bars, while Hughes Brothers Inc. recommends a k_b value of 0.9 for the Aslan 100 bars regardless of bar diameter. Calculation of the bond dependent coefficient using the stress-level approach produced k_b values consistent with those provided by the manufacturers of the bars. All monitored cracks in specimen B5V5 reach approximate k_b values of 0.8 near 25 – 30% of ultimate, whereas only one crack (tension face) in specimen BA5 reaches a k_b value of 0.9 at the same stress-level on the tension face as shown in Tables 5.9 and 5.10. Using the slope approach for calculation of k_b yielded a value of 1.35 for both specimens on the first loading cycle. Following 25 cycles, these k_b values were decreased to 0.96 and 1.0 respectively for specimens B5V5 and BA5.

Table 5.9 - k_b values calculated using stress-level approach for B5V5

	Level	$0.2f_u$	$0.225f_u$	$0.25f_u$	$0.275f_u$	$0.30f_u$	Average
	Stress (MPa)	136.6	153.675	170.75	187.825	204.9	
B5V5	k_{b1}	0.36	0.45	0.67	0.68	0.78	0.59
	k_{b3}	0.32	0.41	0.64	0.81	0.92	0.62
	Avg. $k_{b,side}$	0.34	0.43	0.65	0.74	0.85	0.60
	k_{b2}	0.26	0.39	0.64	0.76	0.73	0.56
	Avg. $k_{b,all}$	0.31	0.42	0.65	0.75	0.81	0.59

Table 5.10 - k_b values calculated using stress-level approach for BA5

	Level	$0.2f_u$	$0.225f_u$	$0.25f_u$	$0.275f_u$	$0.30f_u$	Average
	Stress (MPa)	144.8	162.9	181	199.1	217.2	
BA5	k_{b1}	0.19	0.43	0.63	0.65	0.63	0.51
	k_{b3}	027	0.36	0.39	0.45	0.55	0.40
	Avg. $k_{b,side}$	0.23	0.40	0.51	0.55	0.59	0.46
	k_{b2}	0.18	0.53	0.88	1.09	1.16	0.77
	Avg. $k_{b,all}$	0.21	0.44	0.63	0.73	0.78	0.56

The calculation of the bond dependent coefficient for the #6 bars using the stress-level approach yielded k_b values that were higher than the #5 bars. The recommended k_b values from the manufacturers were also reached at lower service stresses (approximately 20% of ultimate) than the #5 bars as shown in Tables 5.11 and 5.12. Based on these results, the bond performance of the larger bars is inferior to the smaller diameter bars and therefore, they require different k_b values in design. The slope approach was also used to calculate k_b and the values found were higher than the stress-level approach. However, specimens BV6 and BA6 had similar average k_b values on the first loading cycle using this method at 1.94 and 1.89. Following cycling, nearly all of this variability was reduced with the k_b values decreasing to 1.25 and 1.26, respectively.

Table 5.11 - k_b values calculated using stress-level approach for BV6

	Level	$0.2f_u$	$0.225f_u$	$0.25f_u$	$0.275f_u$	$0.30f_u$	Average
	Stress (MPa)	131.2	147.6	164	180.4	196.8	Average
BV6	k_{b1}	0.73	0.85	0.97	1.07	1.13	0.95
	k_{b2}	0.86	1.00	1.08	1.18	1.30	1.08
	Avg. $k_{b,side}$	0.79	0.93	1.03	1.12	1.21	1.01
	k_{b3}	0.81	1.03	1.09	1.15	1.22	1.06
	Avg. $k_{b,all}$	0.80	0.96	1.05	1.13	1.22	1.03

Table 5.12 - k_b values calculated using stress-level approach for BA6

	Level	$0.2f_u$	$0.225f_u$	$0.25f_u$	$0.275f_u$	$0.30f_u$	Average
	Stress (MPa)	138	155.25	172.5	189.75	207	Average
BA6	k_{b1}	0.75	0.89	1.09	1.08	1.02	0.97
	k_{b2}	1.16	1.28	1.38	1.44	1.53	1.36
	Avg. $k_{b,side}$	0.95	1.09	1.23	1.26	1.28	1.16
	k_{b3}	0.80	0.95	1.09	1.17	1.25	1.05
	Avg. $k_{b,all}$	0.90	1.04	1.19	1.23	1.27	1.13

5.3 PHASE IIB

As shown in Table 5.13, the k_b values calculated using a stress-level approach are variable for a given crack depending on the stress-level chosen for analysis. However, for both specimens, this variability is significantly reduced when analyzing the first crack to form in the specimen (crack 1). Over the service stress range of $20 - 30\%$ of the ultimate tensile strength of the bars, k_b for crack 1 remains essentially constant using this method of interpretation.

Table 5.13 - k_b values using stress-level approach for Phase IIB

	Level	$0.2f_u$	$0.225f_u$	$0.25f_u$	$0.275f_u$	$0.30f_u$	Average
	Stress (MPa)	137	154	171	188	205	
B38	k_{b1}	1.27	1.27	1.27	1.28	1.29	1.29
	k_{b3}	0.55	0.56	0.59	0.64	0.69	0.53
	Avg. $k_{b,side}$	0.91	0.92	0.93	0.96	0.99	0.91
	k_{b2}	0.51	0.61	0.70	0.77	0.83	0.59
	Avg. $k_{b,all}$	0.78	0.81	0.85	0.90	0.93	0.80
B50	k_{b1}	1.14	1.16	1.19	1.20	1.20	1.17
	k_{b3}	0.42	0.51	0.69	0.86	0.95	0.60
	Avg. $k_{b,side}$	0.78	0.84	0.94	1.03	1.07	0.88
	k_{b2}	0.50	0.61	0.69	0.75	0.79	0.57
	Avg. $k_{b,all}$	0.69	0.76	0.85	0.93	0.98	0.78

The k_b values calculated using a slope approach are shown in Table 5.14 and are higher than those calculated using a stress-level approach. This is especially true for crack 2, which is located on the tension face of the specimen. The average k_b values for this crack calculated using a stress-level approach are 0.59 and 0.57 for specimens B38 and B50. As shown in Table 5.14, the k_b values calculated for this crack using a slope are 1.85 and 1.99 respectively, which are more than double those calculated using a stress-level approach. The manufacturer, Pultrall Inc., recommends a k_b value of 0.8 for these bars which would be sufficient for the majority of the cracks monitored using the stress-level approach; however, this value would greatly underestimate the crack widths if analyzed using the slope approach.

Table 5.14 - k_b values calculated using slope approach for Phase IIB

	Crack 1	Crack 3	Avg. 1,3	Crack 2
B38	1.33	1.07	1.22	1.85
B50	1.37	1.27	1.30	1.99

5.3.1 Comparison with Phase IIA

The #5 V-Rod bars used in Phases IIA and IIB are identical in material and physical properties as they were produced by Pultrall Inc. in the same lot. The specimen cross sections were varied for this phase, where the depth of the section was decreased from 300 to 250 mm. In addition, two different bottom covers were investigated (38 and 50 mm) but the side cover of 38 mm was maintained in all specimens. As k_b is a material property of the bar, these specimens should exhibit similar k_b values to those from Phase IIA when the differences in their geometric properties are taken into account using the modified Frosch equation (Equation [2.7])

As the bars used in both phases are from the same lot, the k_b values calculated from the five identical specimens in Phase IIA can be used as a predictive tool for specimens B38 and B50. For this comparison, three different k_b values were considered from two different calculation approaches:

- k_b calculated using the stress-level approach at 30% of the guaranteed ultimate tensile strength ($0.30f_u$) of the bars, as this is defined at the upper limit of the service stress range.
- An average k_b value calculated using the stress-level approach between 20 and 30% of the guaranteed ultimate tensile strength of the bars ($0.20 - 0.30f_u$).
- k_b calculated using the slope approach over the entire range of calculated data once the crack gauges are installed.

These k_b values are shown in Table 5.15 and were calculated from the initial loading cycle. Different k_b values were applied depending on the location of formation of the crack (side of bottom face).

Table 5.15 - k_b values from Phase IIA used as a predictive tool for Phase IIB

	k_b (0.30f_u)		k_b (0.20-0.30f_u)		k_b (slope)	
	Avg. side	Bottom	Avg. side	Bottom	Avg. side	Bottom
B1V5	0.95	0.81	0.59	0.55	2.08	2.04
B2V5	1.07	1.14	0.73	0.77	2.28	2.04
B3V5	1.13	0.61	0.84	0.50	2.43	1.01
B4V5	0.97	1.14	0.72	0.89	1.85	1.40
B5V5	0.85	0.73	0.60	0.56	1.49	1.10
Avg.	**0.99**	**0.89**	**0.70**	**0.65**	**2.02**	**1.52**

Shown in Figure 5.8 are the aforementioned k_b values plotted in conjunction with the initial loading behaviour for specimens B38 and B50. As can be seen in Figure 5.8(a), the k_b value of 0.99, calculated using the stress-level approach at 0.30f_u, is a relatively good fit to the data and best predicts the crack widths observed in testing for specimen B38. It should be noted that B38 represents a specimen reinforced with #5 bars and the recommended cover of 38 mm. The k_b value of 0.70 (stress-level approach) underestimates the crack widths for the entire range of data, while the k_b value of 2.02 calculated using the slope approach significantly over predicts crack widths. Considering cracks on the tension face of the specimen, Figure 5.8(b), both k_b values calculated using the stress-level approach are conservative up to approximately 25-30% of the guaranteed ultimate tensile strength of the bars (175- 200 MPa) at which point they begin to under predict the crack widths observed in testing. For cracks on the tension face, the slope approach greatly over predicts the crack widths.
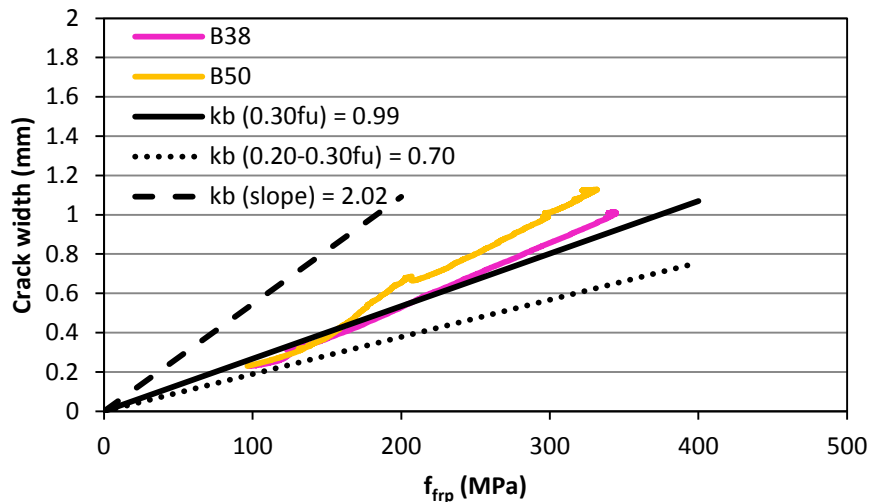
(a)
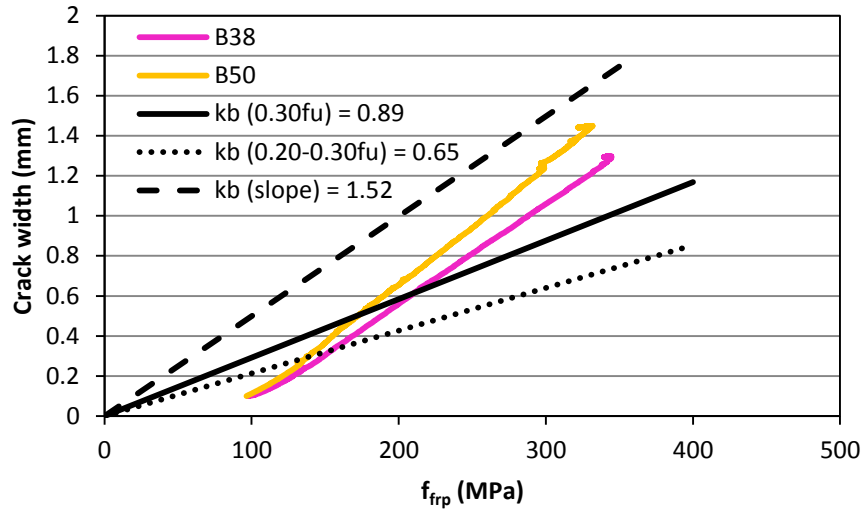
(b)

Figure 5.8 - Initial loading behaviour for Phase IIB specimens with k_b values from Phase IIA for: (a) average side crack width; and (b) tension face crack width

Based on the previous plots, the k_b values calculated using the stress-level approach are the best overall predictors, in particular the values calculated at $0.30f_u$. However, in both specimens, the k_b values calculated using the slope approach are very conservative. To further investigate the slope approach, the k_b values calculated using this method for the 25th loading cycle from Phase IIA, *[k_b (slope)]*, were plotted in conjunction with the data from specimens B38 and B50 on the 25th cycle of loading. As can be seen in Figure 5.9, in both cases (side and bottom crack widths) the k_b values of 1.17 and 0.93 are unconservative and therefore under predict the crack widths observed in experimental testing at equivalent stresses. In addition, average slopes and intercepts were determined from Phase IIA for the 25th loading cycle, as shown in Table 5.8, and the average equations, *[Phase IIA]*, are plotted in Figure 5.9(a) and (b). As the y-intercepts following cycling are small, the average equations have good agreement with k_b calculated using the slope approach where the y-intercept is neglected.

89
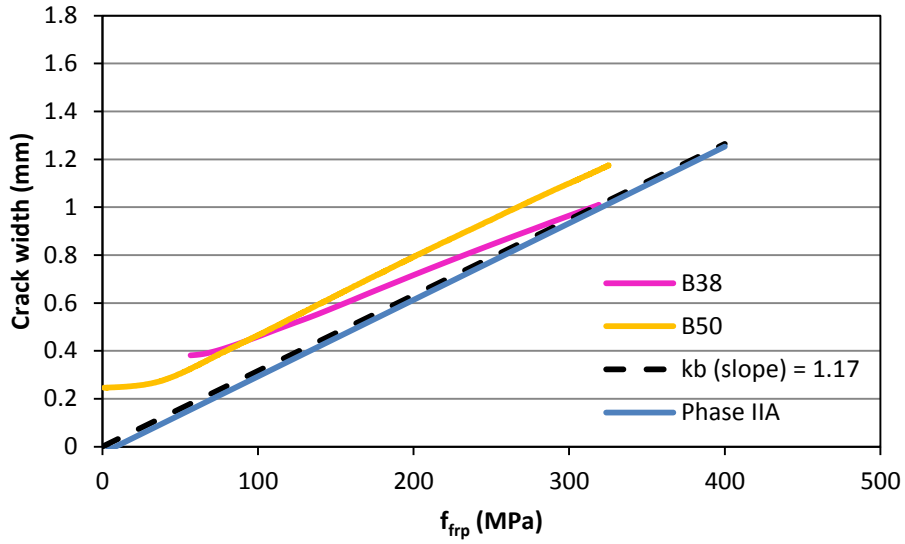
(a)
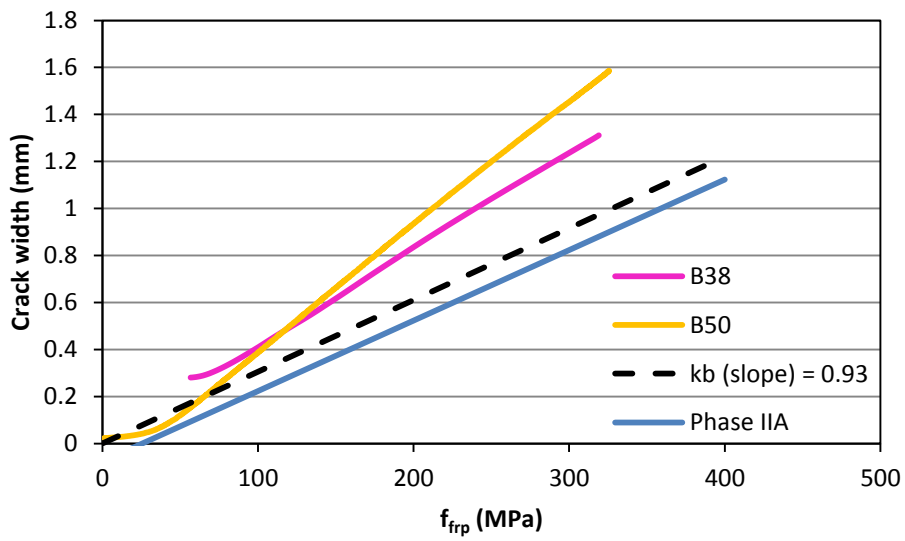
(b)

Figure 5.9 - Loading behaviour (25th cycle) for Phase IIB specimens with slope k$_b$ values from Phase IIA for: (a) average side crack width; and (b) tension face crack width

90

CHAPTER 6 : RECOMMENDATIONS AND CONCLUSIONS

For this thesis, the recommendations are broken down into three sub-sections relating to the test procedure, the calculation and interpretation of the bond dependent coefficient and recommendations for future testing in the field. Lastly, overall conclusions from the study are presented.

6.1 TEST PROCEDURE

The test procedure provided by ACI Committee 440 was modified as required during testing. The following recommendations are suggested for future testing using this procedure:

- As observed during testing, the first cracks to form are not necessarily the largest at the end of the test. It is therefore recommended that a digital image analysis system be used to measure all cracks that form within the constant moment region of the specimen.

- The test procedure also mentioned that this procedure was only applicable for typical (or normal strength) concrete mixes. Further testing is required to determine if this procedure would be able to accurately calculate k_b for self-consolidating concrete (SCC), FRC and high performance concrete (HPC) mixes.

- The specimen was to be loaded until the two cracks being monitored reached 1 mm; however, this was difficult to achieve prior to failure in some specimens, especially for the FRC mixes. As the maximum crack width guidelines are 0.5 and 0.7 mm for exterior and interior exposure criteria, the specimen need not be loaded significantly beyond this point.

- Crack gauges were to be installed one by one upon the immediate formation of the crack. However, when the gauges were being anchored this was not possible as the specimen required unloading to complete installation. In addition, for Phases IIA and IIB, the adhesive setting time was approximately 10 – 30 minutes and the sustained loading during this period of time would result in growth of the crack and therefore, the three gauges were installed simultaneously to minimize this effect.

- An important addition to the test procedure would be to further investigate cyclic behaviour as there is a drastic change in behaviour between the first and subsequent loading cycles.

6.2 CALCULATION AND INTERPRETATION OF k_B

As discussed in Sections 3.1 and 3.2, the most likely cause of variation for k_b is based on calculation and interpretation approaches. In order to achieve consistency in this calculation, the following recommendations are suggested:

- As there are two approaches cited most commonly in literature, (Bakis *et al.*, 2006; Lee *et al.*, 2010), there needs to be clear definition on whether the stress-level or slope approach be used for the calculation of k_b to increase consistency.

- If it is the intention that the stress-level approach be used for the calculation of k_b, the service stress at which it should take place needs to be clearly defined in current codes. In addition, there should be clarification for what is meant by maximum crack width.

- Although the slope approach is best able to represent a large range of data, the current design equation cannot accommodate the intercept and therefore, the predictions provided by a k_b calculated in this manner are typically conservative. However, based on the plot linearity for the specimens, it makes the most sense to adopt a slope approach with a non-zero intercept which can accurately represent all the data and provide reliable predictions.

- Based on the results from Phases IIA and IIB, the k_b value calculated using a stress-level approach at 30% of ultimate best predicts crack widths. This value of k_b is also typically similar to the values provided by the manufacturers.

- Reloading behaviour needs to be considered and addressed in current codes as the behaviour of the specimen is significantly affected. Structures in the field are subject to continual loading and unloading and therefore, this should be integrated into experimental testing to expand the current database of results. In addition, testing should be completed to determine if the maximum load (or crack width) influences the reloading path of the specimen and therefore impacts the calculation of k_b following cyclic loading.

6.3 FUTURE TESTING

Based on the recommendations to the test procedure and the calculation and interpretation of the bond dependent coefficient, the following experimental testing is recommended:

- Further investigative testing is required to determine if the modified Frosch equation is best suited and most accurate for FRP crack width prediction. The results from Phase IIB indicate that k_b is not the same for bars produced from the same lot despite the fact that k_b is defined as a material property of the bar. The equation is meant to account for changes in geometric properties; however, based on the differences in mechanical and physical properties between steel and FRP, the parameters affecting crack width may also be different.

- The role of concrete needs to be examined with experimental testing. The results from Phase IIA and IIB testing indicate that the initial cracking phase of the specimen is likely influenced by the mechanics of the concrete mix, as well as concrete consolidation and quality which influences the calculation of k_b.

- The dependence of the reloading curve on maximum load (or crack width) needs to be further investigated using specimens where the tests are stopped at varying locations.

- The correlation between measured and calculation strains for the FRP reinforcement needs to be further verified with experimental testing to make conclusive statements.

6.4 OVERALL CONCLUSIONS

After completion of this study, the following conclusions can be made:

- The variability of k_b can be explained and linked to interpretation methods and lack of clear definitions in codes and guidelines.

- Beam to beam consistency can be achieved in terms of cracking behaviour but significant variability is introduced by the calculation and interpretation approach used for the bond dependent coefficient. For the identical specimens in this study, COV's for the calculated k_b values range from $11 - 21\%$ at level of reinforcement

and increase to 21 – 29% for cracks on the tension face when analyzing one specific stress-level. For each specimen across 20 – 30% of ultimate, the COV's are increased and range from 40 – 58% at the level of reinforcement and 36 – 58% on the tension face.

- Based on current design guidelines, a k_b calculated at 30% of ultimate is best for prediction of crack widths at the level of reinforcement.

- The approximately linear behaviour of crack growth demonstrates that k_b is basically unchanged during testing. A slope approach can better represent the range of behaviour but requires a change in format of the current design equations. With the current format, predictions using the slope approach are very conservative as the non-zero intercept is neglected.

- The major flaw to the slope approach is the fact that it cannot take into account the non-zero intercept. Some parameter is required to modify Equation [2.7] that relates to initiation of cracking. For example, Lee *et al.* (2010) used the experimental cracking moment; however, a value is required that can be used for design without experimental testing.

- The first cracking cycle is more variable than subsequent loading cycles as it is primarily about concrete mechanics at this stage due to inelastic phenomena.

- The k_b value calculated using the slope approach is a better fit following cycling, as the intercepts begin to approach the origin and thus, a nearly zero-intercept.

- Although a consistent test method has been proposed, there will still be variability in the determination of k_b unless the interpretation of this coefficient is clearly defined.

- Despite the fact that a beam test is currently the standard for determination of k_b, the majority of FRP applications are likely to be slab specimens. Based on the results from this study, the beam test may not be the most appropriate for determination of k_b.

- The bottom crack width is more variable than those at the level of reinforcement based on the COV. It is therefore better to use cracks at the level of reinforcement for the calculation of k_b. This is also beneficial as the stress in the reinforcement is known at this location.

REFERENCES

ACI Committee 318. (1971). *Building Code Requirements for Reinforced Concrete (ACI 318-71).* Detroit, Michigan: American Concrete Institute.

ACI Committee 318. (1999). *Building Code Requirements for Structural Concrete (ACI 318-99).* Farmington Hills, Michigan: American Concrete Institute.

ACI Committee 440. (2001). *Guide for the Design and Construction of Concrete Reinforced with FRP Bars (ACI 440.1R-01).* Farmington Hills, Michigan, USA: American Concrete Institute.

ACI Committee 440. (2003). *Guide for the Design and Construction of Concrete Reinforced with FRP Bars (ACI 440.1R-03).* Farmington Hills, Michigan, USA: American Concrete Institute.

ACI Committee 440. (2006). *Guide for the Design and Construction of Structural Concrete Reinforced with FRP Bars (ACI 440.1R-06).* Farmington Hills, Michigan, USA: American Concrete Institute.

Alves, J., El-Ragaby, A., & El-Salakawy, E. (2011). Durability of GFRP Bars' Bond to Concrete Under Different Loading and Environmental Conditions. *Journal of Composites for Construction, 15*(3), 249-262.

ASTM C78-10. (2010). *Standard Test Method for Flexural Strength of Concrete (Using Simple Beam with Third-Point Loading).* West Conshohocken: American Society for Testing and Materials.

Bakis, C. E., Ospina, C. E., Bradberry, T. E., Benmokrane, B., Gross, S. P., Newhook, J. P., et al. (2006). Evaluation of Crack Widths in Concrete Flexural Members Reinforced With FRP Bars. *Third International Conference on FRP Composites in Civil Engineering*, (pp. 307-310). Miami.

Benmokrane, B. (2010). *Test Method for Determining the Bond-Dependent Coefficient of Fibre-Reinforced Polymer (FRP) Rods (Second Draft).* ACI 440-K Subcommittee.

Benmokrane, B., Eisa, M., El-Gamal, S., El-Salakaway, E., & Thebeau, D. (n.d.). First Use of GFRP Bars as Reinforcement for Continuous Reinforced Concrete Pavement. *Fourth International Conference on FRP Composites in Civil Engineering, CICE 2008.* Zurich, Switzerland.

Benmokrane, B., El-Salakaway, E., El-Ragaby, E., Desgagne, G., & Lackey, T. (2004). Design, Construction and Monitoring of Innovative Bridge Decks using FRP Composite Bars. *Proceedings of the 2004 Concrete Bridge Conference, CBC-04*, (pp. 1-19). Charlotte, North Carolina.

Broms, B. B. (1965). Crack Width and Crack Spacing in Reinforced Concrete Members. *ACI Journal, 62*(10), 1237-1256.

Campbell, F. C. (2010). *Structural Composite Materials.* Materials Park: ASM International.

Canadian Standards Association. (2006). *Canadian Highway Bridge Design Code (CAN/CS- S6-06).* Toronto: CSA International.

Canadian Standards Association. (2009). *Carbon Steel Bars for Concrete Reinforcement (CSA G30.18-09).* CSA International.

Canadian Standards Association. (2010). *Specification for fibre-reinforced polymers (S807-10).* Missisauga: CSA International.

Cheng, J. R., & Van Zwol, T. (2005, April 14). Steel Free Bridge Deck: Field Performance at Evaluation. 2005, Edmonton, Alberta, Canada.

Comité Euro-International du Béton (CEB). (1985). *Design Manual on Cracking and Deformations.* Lausanne.

Esfandeh, M., Sabet, A. R., Resadoust, A. M., & Alavi, M. B. (2008). *Bond Performance of FRP Rebars With Various Surface Deformations in Reinforced Concrete.* Wiley Interscience.

Eswari, S., Raghunath, P. N., & Suguna, K. (2008). Ductility Performance of Hybrid Fibre Reinforced Concrete. *American Journal of Applied Sciences*, 1257-1262.

Frosch, R. J. (1999). Another Look at Cracking and Crack Control in Reinforced Concrete. *ACI Structural Journal*, 438-442.

Galati, N., Nanni, A., Dharani, L. R., Focacci, F., & Aiello, M. A. (2006). Thermal Effects of Bond Between FRP Rebars and Concrete. *Composites Part A: Applied Science & Manufacturing, 37*(8), 1223-1230.

Galati, N., Rizzo, A., & Nanni, A. (2006). Structural Rehabilitation of an Off-System Bridge Using Externally Bonded CFRP Laminates. *Third International Conference on FRP Composites in Civil Engineering, CICE 2006*, (pp. 103-106). Miami, Florida.

Gergely, P., & Lutz, L. (1968). Maximum Crack Width in Reinforced Concrete Flexural Members. *Causes, Mechanism and Control of Cracking in Concrete* (pp. 87-117). Farmington Hills: American Concrete Institute.

Giernacky, R. (2002). *Durability of E-Glass FRP Reinforced Concrete Beams.* B.S. Thesis, Penn State University, Department of Engineering Science & Mathematics, University Park.

Hughes Brothers Inc. (2011). *Product Guide Specification.* Retrieved 06 20, 2012, from http://aslanfrp.com/Aslan100/Aslan100fiberglassrebar.html

Illinois Tool Works. (2013). *Epcon A7 Acrylic Adhesive.* Retrieved 02 04, 2013, from Red Head Concrete Anchoring Solutions: http://www.itwredhead.com

ISIS Canada Corporation. (2001). *Reinforcing Concrete Structures with Fibre Reinforced Polymers - Design Manual No. 3.* Winnipeg, Manitoba.

Kassem, C. (2004). *Cracking and Load-Deflection Behaviour of One-Way Concrete Elements Reinforced with FRP Bars Under Flexure.* Department of Civil Engineering. Sherbrooke: Universite de Sherbrooke.

Kassem, C., Farghaly, A. S., & Benmokrane, B. (2011). Evaluation of Flexural Behaviour and Serviceability Performance of Concrete Beams Reinforced with FRP Bars. *Journal of Composites for Construction*, 682-695.

Lee, W. K., Jansen, D. C., Berlin, K. B., & Cohen, I. E. (2010). Flexural Cracks in Fiber-Reinforced Concrete Beams With Fiber-Reinforced Polymer Reinforcing Bars. *ACI Structural Journal*, 321-329.

Masmoudi, R., Benmokrane, B., & Chaallal, O. (1996). Cracking of Concrete Beams Reinforced with Fiber Reinforced Plastic Bars. *Canadian Journal of Civil Engineering, 23*, 1172-1179.

Masmoudi, R., Theriault, M., & Benmokrane, B. (1998). Flexural Behaviour of Concrete Beams Reinforced with Deformed Fiber Reinforced Plastic Reinforcing Rods. *ACI Structural Journal, 95*(6), 665-675.

Newhook, J. (2000). The Use of Fibre Reinforced Concrete to Reduce Crack Widths in GFRP Reinforced Concrete Beams. In J. Humar, & A. Razaqpur (Ed.), *Proceedings of the 3rd International Conference on Advanced Composite Materials in Bridges and Structures, ACMBS III* (pp. 145-152). Montreal, Quebec: Canadian Society of Civil Engineering.

Newhook, J. P. (2006, June). Glass FRP Reinforcement in Rehabilitation of Concrete Marine Infrastructure. *The Arabian Journal for Science and Engineering*, 53-75.

Ospina, C., & Bakis, C. (2007). Indirect Flexural Crack Control of Concrete Beams and One-Way Slabs Reinforced with FRP Bars. *8th International Symposium on Fiber Reinforced Polymer Reinforcement for Concrete Structures*, (pp. 1-9). Patras.

Owens Corning Composite Materials. (2011). *Filament Winding*. Retrieved September 1, 2011, from http://www.owenscorning.com/composites/processes/Filament_Winding.asp

Pultrall Inc. (2007). *Pultrusion Manufacturing Process*. Retrieved June 15, 2011, from http://www.pultrall.com/Site2008/eng/proprietes-pultrusion.htm

Sheikh, S. A., & Homam, S. M. (2004). A Decade of Performance of FRP-Reinforced Concrete Structures. *Proceedings of ISIS-SHM Workshop.* Winnipeg, Manitoba.

Theisz, P. (2004). *Properties of High Performance Concrete Beams Reinforced with Carbon Fiber Reinforced Polymer Bars.* M.S. Thesis, Villanova University, Department of Civil Engineering, Villanova.

Theriault, M., & Benmokrane, B. (1998). Effects of FRP Reinforcement Ratio and Concrete Strength on Flexural Behaviour of Concrete Beams. *Journal of Composites for Construction, 2*(1), 7-16.

Thiagarajan, G. (2003). Experimental and Analytical Behaviour of Carbon Fiber-Based Rods as Flexural Reinforcement. *Journal of Composites for Construction, 7*(1), 64-72.

Tighouart, B., Benmokrane, B., & Gao, D. (1998). Investigation of Bond in Concrete Member with Fibre Reinforced Polymer (FRP) Bars. *Journal of Construction and Building Materials*, 453-462.

Tokyo Sokki Kenkyujo Co. Ltd. (2011). *PI Pie-Shape Displacement Transducer*. Retrieved July 21, 2011, from http://www.tml.jp/e/product/transducers/general/displacement/pi.html

Toutanji, H., & Deng, Y. (2003). Deflection and Crack-Width Prediction of Concrete Beams Reinforced with Glass FRP Rods. *Construction and Building Materials, 17*, 69-74.

Treece, R., & Jirsa, J. (1989). Bond Strength of Epoxy-Coated Reinforcing Bars. *ACI Materials Journal, 86*(2), 167-174.

Wang, H., & Belarbi, A. (2005). Flexural Performance of Fibre-Reinforced-Concrete Beams Reinforced with FRP Bars. *Seventh International Symposium on Fibre Reinforced Polymer Reinforcement for Concrete Structures*, (pp. 895-914). Kansas City.

Wight, J. K., & MacGregor, J. G. (2009). *Reinforced Concrete: Mechanics & Design.* Upper Saddle River: Pearson Education Inc.

Yang, J.-M., Min, K.-H., Shin, H.-O., & Yoon, Y.-S. (2012). Effect of Steel and Synthetic Fibers on Flexural Behaviour of High-Strength Concrete Beams Reinforced with FRP Bars. *Composites: Part B*.

APPENDIX A :   CASE STUDIES

Measurements from all graphs taken using 1:25 scale.

A1   CASE STUDY 1

All specimens were 125 x 250 mm (width x height) and tested in four point bending with a clear span of 1830 mm between supports.

Table A.1 - Bar properties for Case Study 1 (adapted from Lee et al., 2010)

Bar type	Bar size	Nominal diameter (mm)	Elastic modulus (GPa)	Tensile strength (MPa)
GFRP	#2	6.4	37.8	507
GFRP	#3	9.5	43.3	769
GFRP	#4	12.7	45.6	690
CFRP	#2	6.4	137.8	2068
CFRP	#3	9.5	132.3	2068
CFRP	#4	12.7	132.3	2068

Table A.2 - Specimen details for Case Study 1 (adapted from Lee et al., 2010)

Specimen	Bar type	Bar size	Concrete type	f'_c (MPa)	MOR (MPa)	ρ_{frp} (%)	ρ_b (%)
G2N0	GFRP	2 - #2	Plain	43	5.6	0.25	0.96
G2P1	GFRP	2 - #2	FRC	31	5.2	0.25	0.78
G4N0	GFRP	2 - #4	Plain	39	5.4	0.98	0.61
G4P1	GFRP	2 - #4	FRC	30	5.0	0.98	0.51
C2N0	CFRP	2 - #2	Plain	39	5.5	0.25	0.43
C2P1	CFRP	2 - #2	FRC	35	5.2	0.25	0.39
C4N0	CFRP	2 - #4	Plain	42	5.7	0.98	0.45
C4P1	CFRP	2 - #4	FRC	33	5.0	0.98	0.39

Table A.3 - Calculation of geometric constant for Case Study 1

Specimen	d_b (mm)	ρ_{frp}	f_c (MPa)	MOR (MPa)	E_c (MPa)	E_{frp} (MPa)	n_{frp}	A_{frp} (mm²)	c or y_{cr} (mm)	I_{cr} (10^6 mm⁴)	s* (mm)	Constant
G2N0	6.4	0.0025	43	5.6	29508	37800	1.28	64.34	15.38	2.96	69.85	2.58E-07
G3N0	9.5	0.0055	39	6.1	28102	43300	1.54	141.76	24.40	7.34	66.675	1.02E-07
G4N0	12.7	0.0098	39	5.4	28102	45600	1.62	253.35	32.63	12.96	63.5	5.44E-08
G2P1	6.4	0.0025	31	5.2	25055	37800	1.51	64.34	16.63	3.46	69.85	2.58E-07
G3P1	9.5	0.0055	33	5.2	25851	43300	1.68	141.76	25.37	7.92	66.675	1.02E-07
G4P1	12.7	0.0098	30	5	24648	45600	1.85	253.35	34.63	14.55	63.5	5.46E-08
C2N0	6.4	0.0025	39	5.5	28102	137800	4.90	64.34	28.96	10.24	69.85	7.25E-08
C3N0	9.5	0.0055	43	5.5	29508	132300	4.48	141.76	39.76	18.94	66.675	3.45E-08
C4N0	12.7	0.0098	42	5.7	29163	132300	4.54	253.35	51.41	31.04	63.5	1.94E-08
C2P1	6.4	0.0025	35	5.2	26622	137800	5.18	64.34	29.69	10.75	69.85	7.26E-08
C3P1	9.5	0.0055	31	5.2	25055	132300	5.28	141.76	42.74	21.77	66.675	3.47E-08
C4P1	12.7	0.0098	33	5	25851	132300	5.12	253.35	54.10	34.20	63.5	1.95E-08

d = 200 mm
b = 125 mm
d_c = 50 mm
d_s = 76.2 mm

*spacing was assumed to be 3 in (76.2 mm) from center to center of bars $\rightarrow$ side cover = 1 in

100

A1.1 #2 Bars

Horizontal axis (crack width)
0.2 mm = 40 units

Vertical axis (moment)
1 kNm = 19 units

Table A.4 - Calculation of slope and k_b for specimen G2N0

Crack 1			
$V_1 = 39.5$	$V_2 = 113.5$	Slope = 2.68 x 10^{-7}	$k_b = 1.04$
$H_1 = 0$	$H_2 = 209$		
Crack 2			
$V_1 = 69.5$	$V_2 = 113.5$	Slope = 4.94 x 10^{-7}	$k_b = 1.48$
$H_1 = 0$	$H_2 = 229$		
			Avg. $k_b = 1.26$

Table A.5 - Calculation of slope and k_b for specimen G2P1

Crack 1			
$V_1 = 74.5$	$V_2 = 132$	Slope = 2.90 x 10^{-7}	$k_b = 1.12$
$H_1 = 0$	$H_2 = 175.5$		
Crack 2			
$V_1 = 69.5$	$V_2 = 113.5$	Slope = 3.11 x 10^{-7}	$k_b = 1.2$
$H_1 = 0$	$H_2 = 229$		
			Avg. $k_b = 1.16$
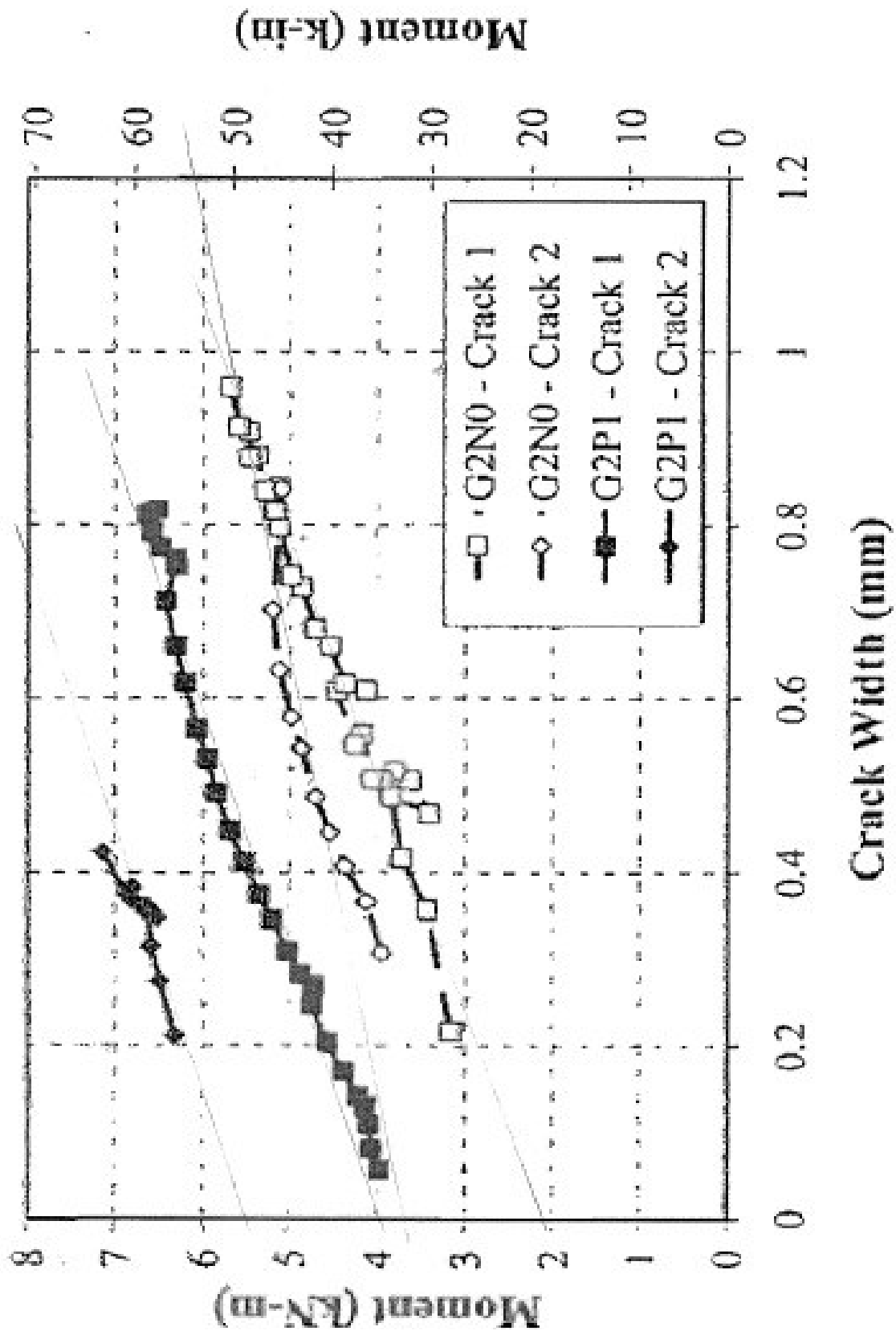
Horizontal axis (crack width)
0.4 mm = 45 units

Vertical axis (moment)
4 kNm = 26 units

Table A.6 - Calculation of slope and k_b for specimen C2N0

Crack 1			
$V_1 = 15.5$	$V_2 = 104$	Slope = 1.42 x 10^{-7}	$k_b = 1.96$
$H_1 = 0$	$H_2 = 218$		
Crack 2			
$V_1 = 23.5$	$V_2 = 104$	Slope = 1.40 x 10^{-7}	$k_b = 1.93$
$H_1 = 0$	$H_2 = 195$		
			Avg. $k_b = 1.95$

Table A.7 - Calculation of slope and k_b for specimen C2P1

Crack 1			
$V_1 = 26$	$V_2 = 130$	Slope = 9.31 x 10^{-8}	$k_b = 1.28$
$H_1 = 0$	$H_2 = 167.5$		
Crack 2			
$V_1 = 27$	$V_2 = 130$	Slope = 7.41 x 10^{-8}	$k_b = 1.02$
$H_1 = 0$	$H_2 = 132$		
Crack 3			
$V_1 = 102.5$	$V_2 = 156$	Slope = 8.37 x 10^{-8}	$k_b = 1.15$
$H_1 = 0$	$H_2 = 77.5$		
			Avg. $k_b = 1.15$
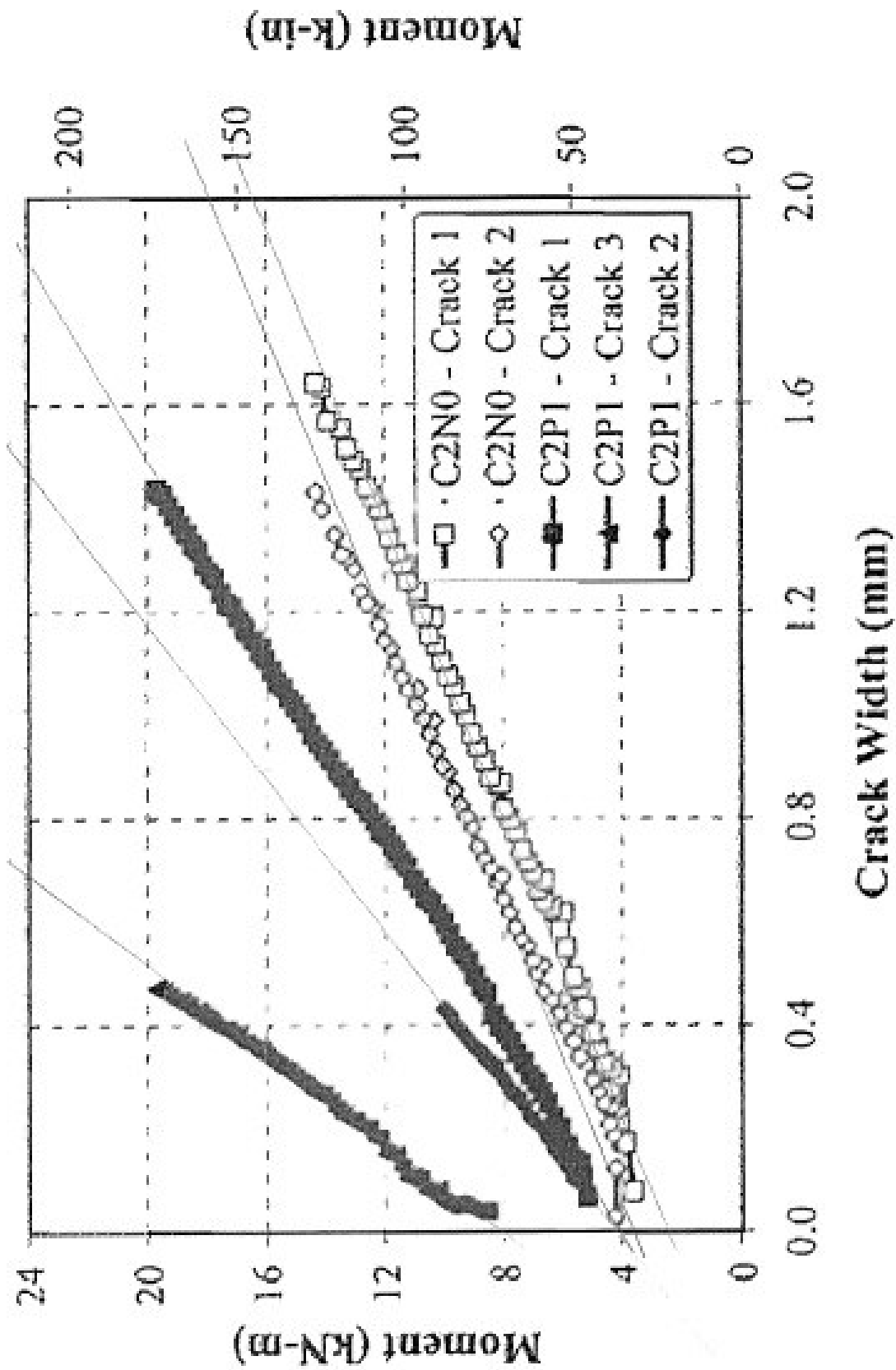
A1.2 #4 Bars

Horizontal axis (crack width)
0.1 mm = 28.5 units

Vertical axis (moment)
2 kNm = 16 units

Table A.8 - Calculation of slope and k_b for specimen G4N0

Crack 1			
$V_1 = 27.5$	$V_2 = 113$	Slope = 7.45×10^{-8}	$k_b = 1.37$
$H_1 = 0$	$H_2 = 227$		
Crack 2			
$V_1 = 30$	$V_2 = 80$	Slope = 7.21×10^{-8}	$k_b = 1.33$
$H_1 = 0$	$H_2 = 128.5$		
Crack 3			
$V_1 = 27.5$	$V_2 = 97$	Slope = 5.90×10^{-8}	$k_b = 1.08$
$H_1 = 0$	$H_2 = 146$		
			Avg. $k_b = 1.26$

Table A.9 - Calculation of slope and k_b for specimen G4P1

Crack 1			
$V_1 = 29$	$V_2 = 112.5$	Slope = 4.39×10^{-8}	$k_b = 0.8$
$H_1 = 0$	$H_2 = 130.5$		
Crack 2			
$V_1 = 24$	$V_2 = 145$	Slope = 2.29×10^{-8}	$k_b = 0.42$
$H_1 = 0$	$H_2 = 98.5$		
Crack 3			
$V_1 = 15.5$	$V_2 = 145$	Slope = 2.83×10^{-8}	$k_b = 0.52$
$H_1 = 0$	$H_2 = 159$		
Crack 4			
$V_1 = 32.5$	$V_2 = 145$	Slope = 2.99×10^{-8}	$k_b = 0.55$
$H_1 = 0$	$H_2 = 120$		
Crack 5			
$V_1 = 24$	$V_2 = 145$	Slope = 9.05×10^{-9}	$k_b = 0.17$
$H_1 = 0$	$H_2 = 39$		
Crack 6			
$V_1 = 42$	$V_2 = 145$	Slope = 2.53×10^{-8}	$k_b = 0.46$
$H_1 = 0$	$H_2 = 93$		
			Avg. $k_b = 0.49$
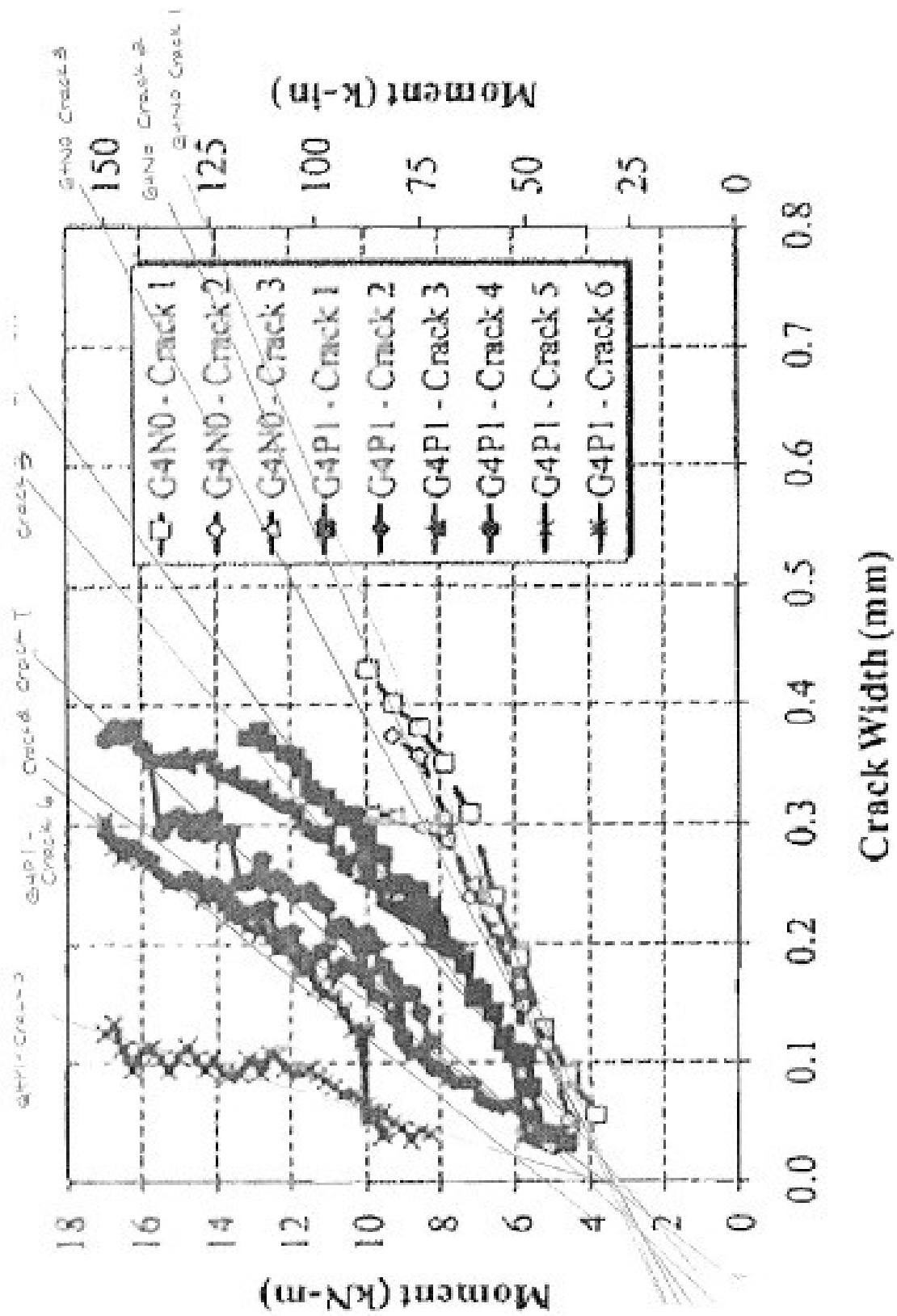
Horizontal axis (crack width)
0.4 mm = 34.5 units

Vertical axis (moment)
5 kNm = 21 units

Table A.10 - Calculation of slope and k_b for specimen C4N0

Crack 1			
$V_1 = 12.5$	$V_2 = 125.5$	Slope = 8.58 x 10^{-8}	$k_b = 4.4$
$H_1 = 0$	$H_2 = 199$		
Crack 2			
$V_1 = 4.5$	$V_2 = 125.5$	Slope = 6.20 x 10^{-6}	$k_b = 3.19$
$H_1 = 0$	$H_2 = 154$		
Crack 3			
$V_1 = 10.5$	$V_2 = 167.5$	Slope = 6.42 x 10^{-8}	$k_b = 3.3$
$H_1 = 0$	$H_2 = 207$		
			Avg. $k_b = 3.63$

Table A.11 - Calculation of slope and k_b for specimen C4P1

Crack 1			
$V_1 = 12.5$	$V_2 = 167.5$	Slope = 2.28 x 10^{-8}	$k_b = 1.17$
$H_1 = 0$	$H_2 = 72.5$		
Crack 2			
$V_1 = 12.5$	$V_2 = 167.5$	Slope = 1.70 x 10^{-8}	$k_b = 0.87$
$H_1 = 0$	$H_2 = 54$		
Crack 3			
$V_1 = -20$	$V_2 = 167.5$	Slope = 8.44 x 10^{-9}	$k_b = 0.43$
$H_1 = 0$	$H_2 = 32.5$		
Crack 4			
$V_1 = 45$	$V_2 = 167.5$	Slope = 1.25 x 10^{-8}	$k_b = 0.64$
$H_1 = 0$	$H_2 = 31.5$		
			Avg. $k_b = 0.78$
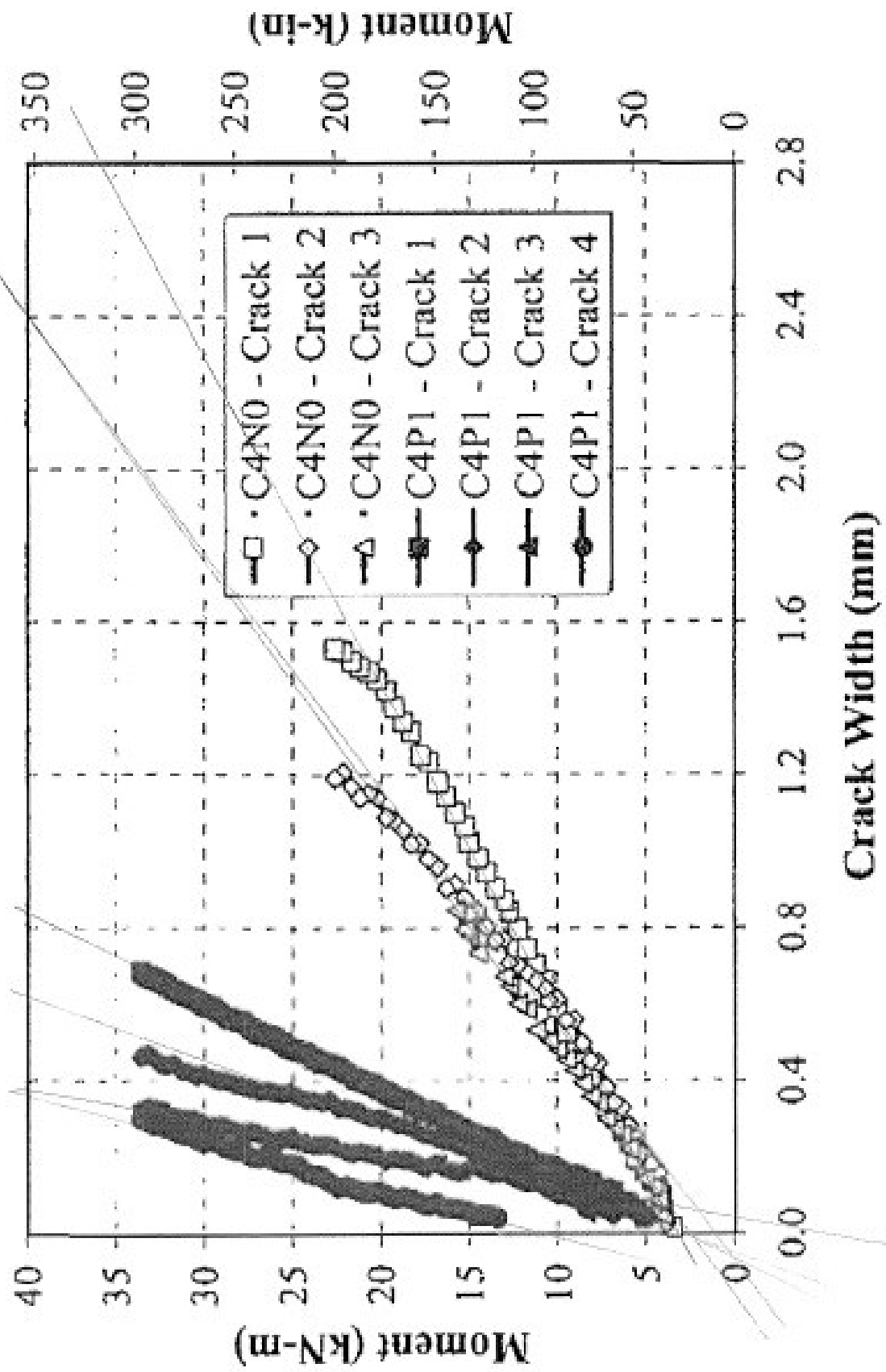
A2   CASE STUDY 2

All specimens were 200 x 300 x 3000 mm (width x length x height) and tested in four point bending over a simply supported clear span of 2750 mm and a shear span of 875 mm.

Table A.12 - Bar properties for Case Study 2 (adapted from Kassem et al., 2011)

Type	d_b (mm)	A_f (mm^2)	E_f (GPa)	f_{fu} (MPa)	ε_{fu} (%)	Surface texture
CFRP1	9.50	71	114 ± 11	1506 ± 99	1.2 ± 0.12	Sand-coated
CFRP2	9.00	64	122 ± 5	1988 ± 22	1.7 ± 0.04	Ribbed-deformed
GFRP1	12.70	129	40 ± 1	617 ± 16	1.5 ± 0.06	Sand-coated
GFRP2	12.00	113	36 ± 1	747 ± 34	1.8 ± 0.11	Ribbed-deformed
AFRP	9.50	71	52 ± 2	1800 ± 36	3.3 ± 0.03	Sand-coated

Table A.13 - Specimen details for Case Study 2 (adapted from Kassem et al., 2011)

Series	Beam	f'_c (MPa)	E_c (GPa)	ρ_f (%)	ρ_f/ρ_{fb}	E_fA_f (kN)
CFRP1	C1-4	40.4	31.6	0.6	1.2	32276
	C1-6	39.3	29.8	0.9	1.9	48564
	C1-8	39.3	29.8	1.2	2.5	64752
CFRP2	C2-4	39.9	29.8	0.5	1.7	31232
	C2-6	40.8	30.2	0.8	2.5	46848
	C2-8	40.8	30.2	1.1	3.3	62464
GFRP1	G1-6	39.1	29.3	1.6	1.5	30960
	G1-8	39.1	29.3	2.2	2.0	41280
GFRP2	G2-6	39.1	29.3	1.4	1.9	24408
	G2-8	39.1	29.3	1.9	2.5	32544
AFRP	AR-6	39.1	29.3	0.9	3.9	22152
	AR-8	39.1	29.3	1.2	5.2	29536
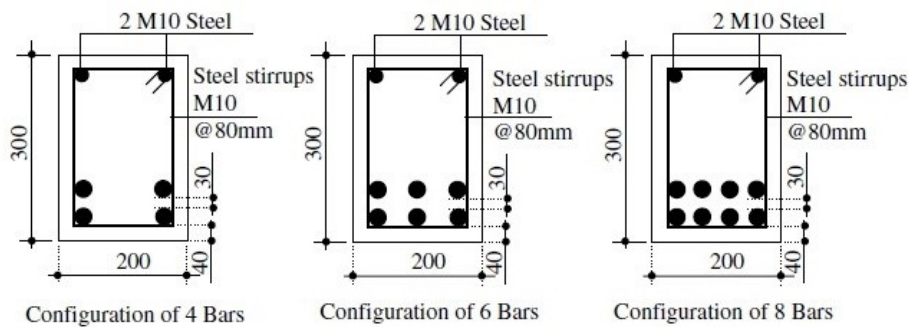
Figure A.1 - Bar configurations for Case Study 2 (Kassem et al., 2011)

Table A.14 - Calculation of geometric constant for Case Study 2

Specimen	A_f (MPa)	E_f (MPa)	ρ_f	c (mm)	I_{cr} (10^6 mm^4)	f_f (MPa)	M_n (kNm)	d_c* (mm)	s* (mm)	Constant
C1-4	284	114000	0.006	44.39	43.71	1223	73.4	44.75	121	2.10E-08
C1-6	426	114000	0.009	54.49	64.87	954	83.8	44.75	56	9.94E-09
C1-8	568	114000	0.012	61.67	82.18	805	92.5	44.75	34	6.84E-09
C2-4	256	122000	0.005	46.82	52.70	1388	81.7	44.5	122	2.01E-08
C2-6	384	122000	0.008	53.75	64.16	1072	86.5	44.5	57	1.01E-08
C2-8	512	122000	0.011	59.80	76.11	888	90.9	44.5	35	7.19E-09
G1-6	774	40000	0.016	45.55	47.03	438	73.3	46.35	51	1.51E-08
G1-8	1032	40000	0.022	50.87	56.31	365	77.6	46.35	30	1.08E-08
G2-6	678	36000	0.014	40.94	38.30	451	67.0	46	52	1.89E-08
G2-8	904	36000	0.019	46.15	47.39	380	72.8	46	31	1.34E-08
AR-6	426	52000	0.009	38.69	33.49	680	62.2	44.75	56	2.13E-08
AR-8	568	52000	0.012	44.06	43.10	578	69.5	44.75	34	1.46E-08

*Values assumed → not clear if 40 mm is to stirrup or bottom of bar; assumed cover of 30 mm on sides including stirrups

A2.1 Beams C1

Horizontal axis (crack width)
1 mm = 99.5 units

Vertical axis (moment)
20 kNm = 36 units

Table A.15 - Calculation of slope and k_b for Beams C1

Specimen C1-8			
$V_1 = 4$	$V_2 = 108$	Slope = 1.11 x 10^{-8}	$k_b = 1.63$
$H_1 = 0$	$H_2 = 64$		
Specimen C1-6			
$V_1 = 8$	$V_2 = 108$	Slope = 1.63 x 10^{-8}	$k_b = 1.64$
$H_1 = 0$	$H_2 = 90$		
Specimen C1-4			
$V_1 = 36$	$V_2 = 108$	Slope = 2.27 x 10^{-8}	$k_b = 1.09$
$H_1 = 49.5$	$H_2 = 140$		
			Avg. $k_b = 1.45$

Figure showing Moment (kN.m) versus Crack width (mm) for Beams C1, with curves labelled C1-8, C1-6, C1-4, and C1-4b.

112
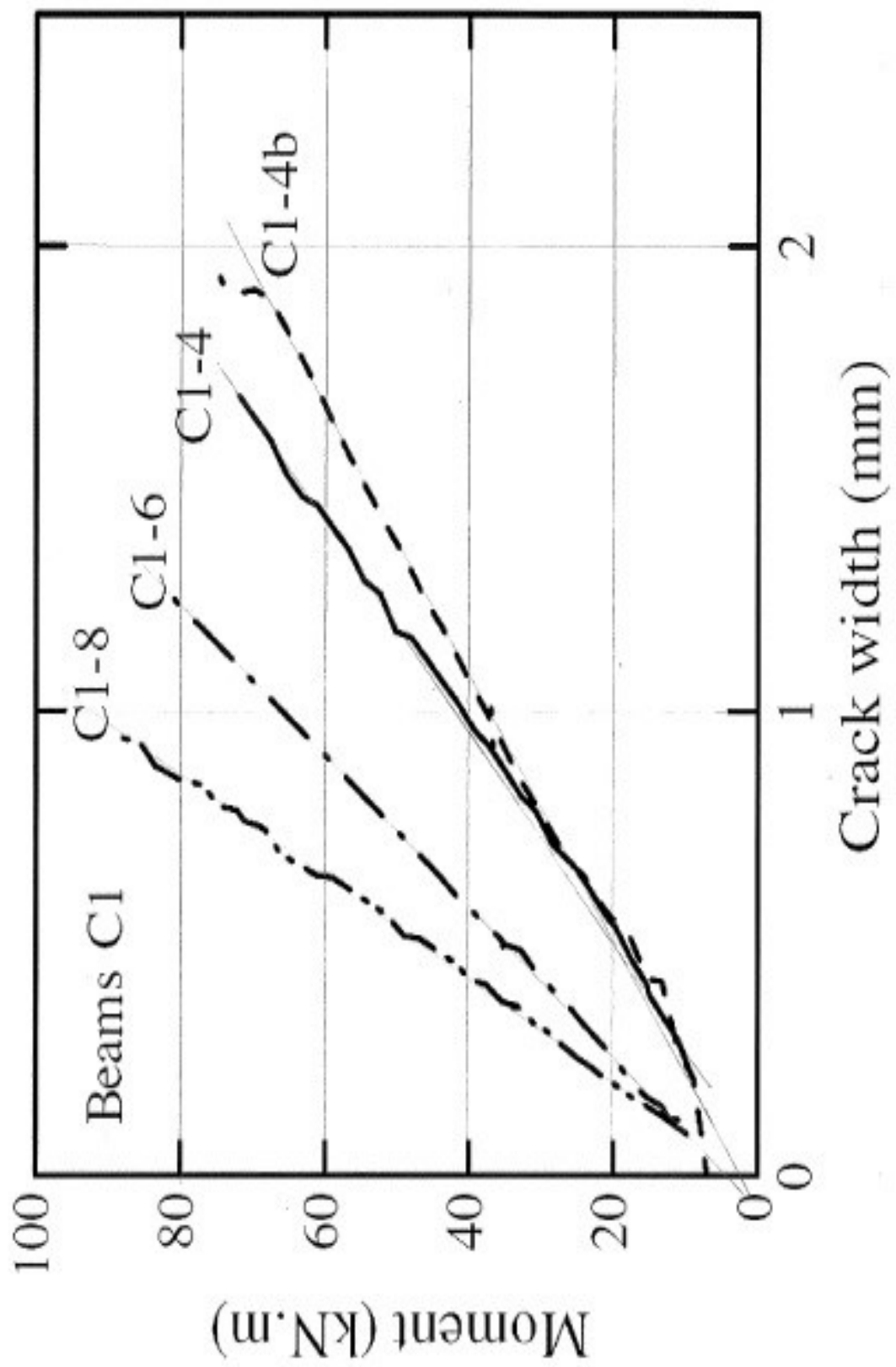
A2.2 Beams C2

Horizontal axis (crack width)
1 mm = 101 units

Vertical axis (moment)
20 kNm = 36 units

Table A.16 - Calculation of slope and k_b for Beams C2

Specimen C2-8			
$V_1 = 0$	$V_2 = 108$	Slope = 9.16×10^{-9}	$k_b = 1.27$
$H_1 = 0$	$H_2 = 55.5$		
Specimen C2-6			
$V_1 = 9$	$V_2 = 108$	Slope = 1.58×10^{-8}	$k_b = 1.56$
$H_1 = 0$	$H_2 = 88$		
Specimen C2-4			
$V_1 = 36$	$V_2 = 108$	Slope = 2.35×10^{-8}	$k_b = 1.17$
$H_1 = 56$	$H_2 = 151$		
			Avg. $k_b = 1.33$
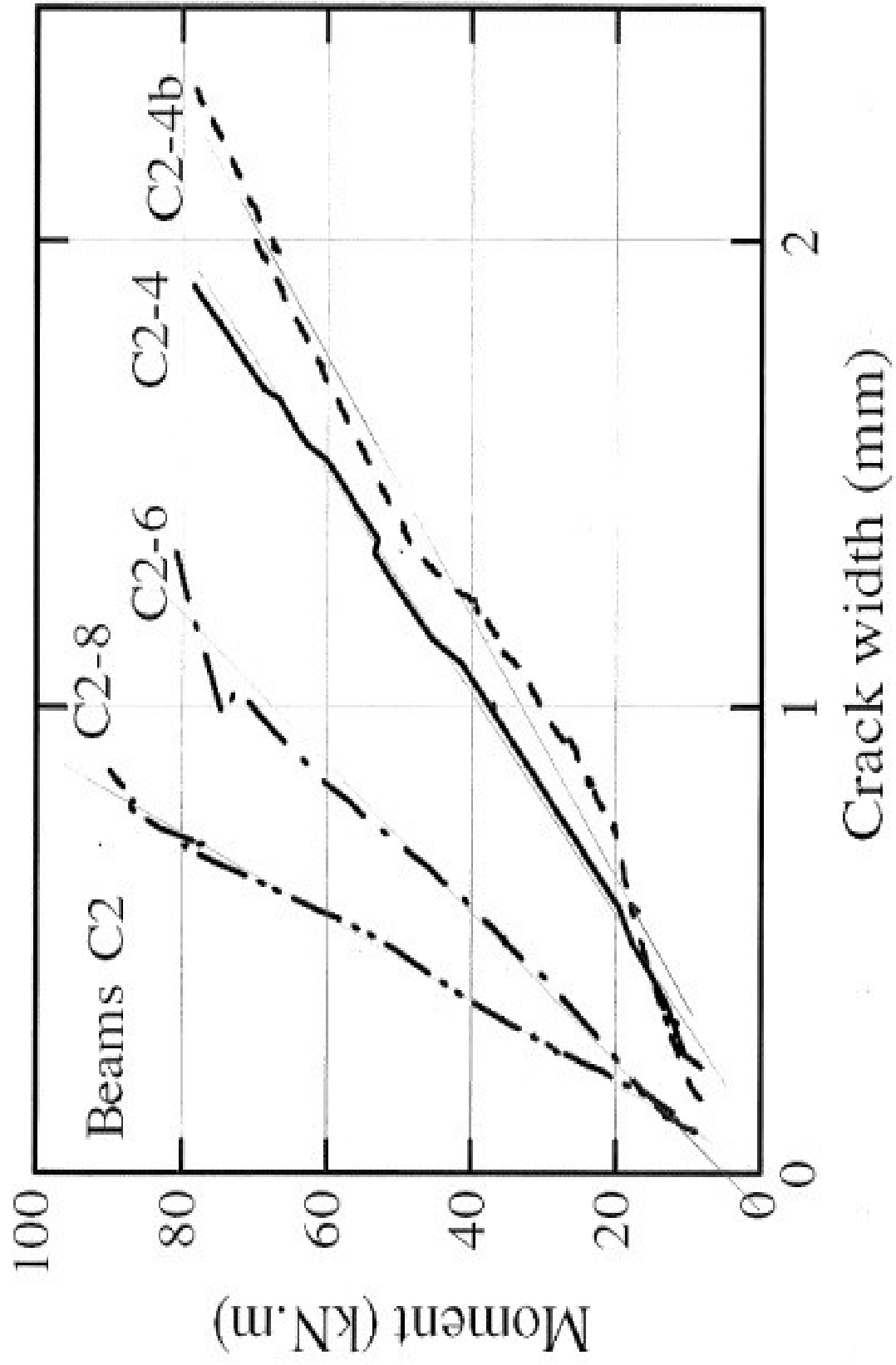
A2.3 Beams G1 and G2

Horizontal axis (crack width)
1 mm = 99 units

Vertical axis (moment)
20 kNm = 36 units

Table A.17 - Calculation of slope and k_b for Beams G1 and G2

Specimen G1-8			
$V_1 = 36$	$V_2 = 108$	Slope = 1.23 x 10^{-8}	$k_b = 1.13$
$H_1 = 34$	$H_2 = 82.5$		
Specimen G2-8			
$V_1 = 36$	$V_2 = 108$	Slope = 1.14 x 10^{-8}	$k_b = 0.85$
$H_1 = 43$	$H_2 = 88$		
Specimen G1-6			
$V_1 = 36$	$V_2 = 108$	Slope = 2.77 x 10^{-8}	$k_b = 1.83$
$H_1 = 74$	$H_2 = 183.5$		
Specimen G2-6			
$V_1 = 36$	$V_2 = 108$	Slope = 2.49 x 10^{-8}	$k_b = 1.31$
$H_1 = 42.5$	$H_2 = 141$		
			Avg. $k_b = 1.28$

Beams G1 and G2

G1-6

G2-6

G1-8

G2-8

Moment (kN.m)
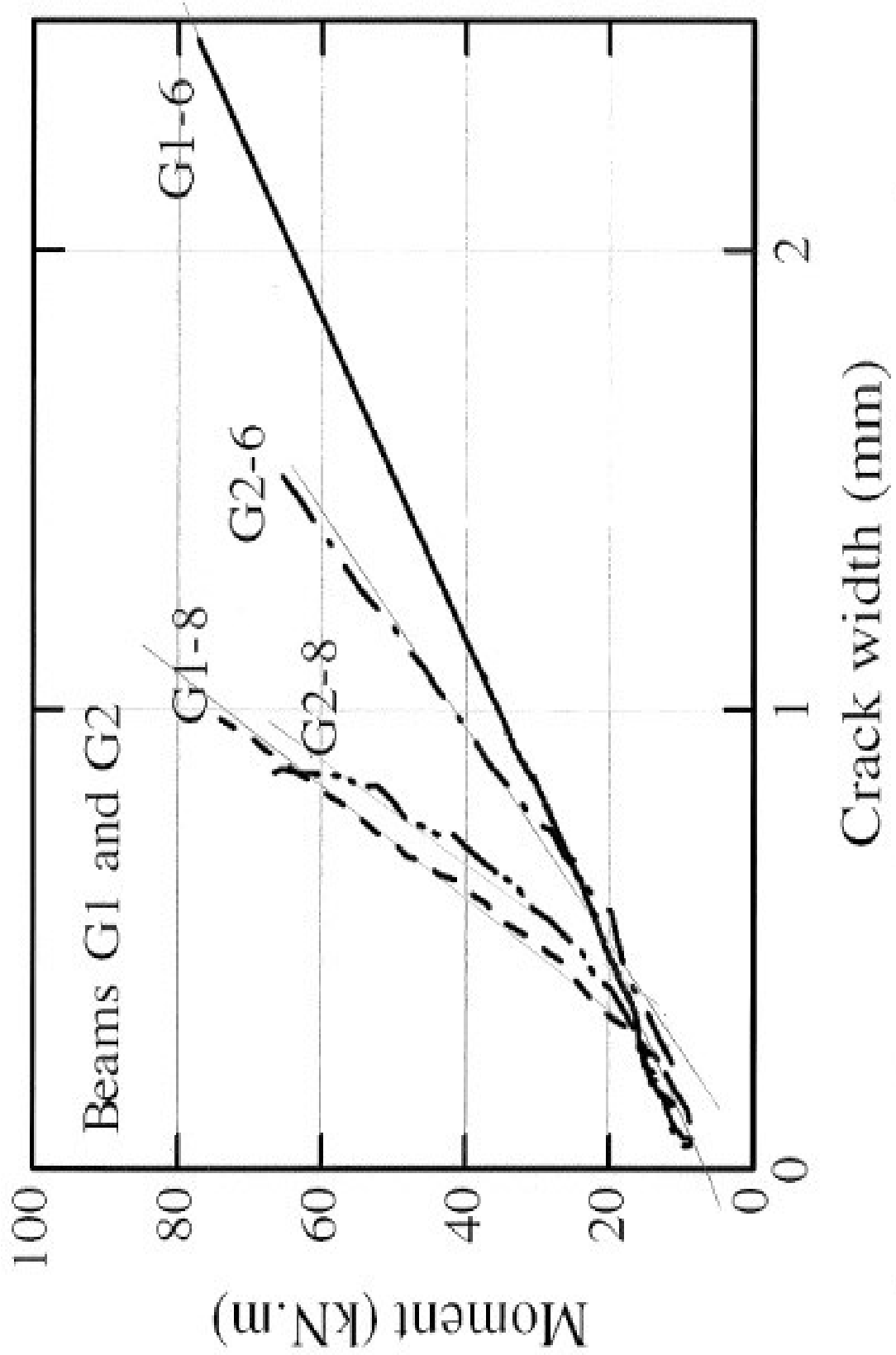
Crack width (mm)

A2.4 Beams AR

Horizontal axis (crack width)
1 mm = 96.5 units

Vertical axis (moment)
20 kNm = 35 units

Table A.18 - Calculation of slope and k_b for Beams AR

Specimen AR-8			
$V_1 = 35$	$V_2 = 70$	Slope = 3.26 x 10^{-8}	$k_b = 2.24$
$H_1 = 63$	$H_2 = 126$		
Specimen AR-6			
$V_1 = 35$	$V_2 = 70$	Slope = 3.19 x 10^{-8}	$k_b = 1.5$
$H_1 = 81$	$H_2 = 142.5$		
			Avg. $k_b = 1.87$

Figure: Moment vs. Crack width (mm) for Beams AR, showing curves AR-6 and AR-8.
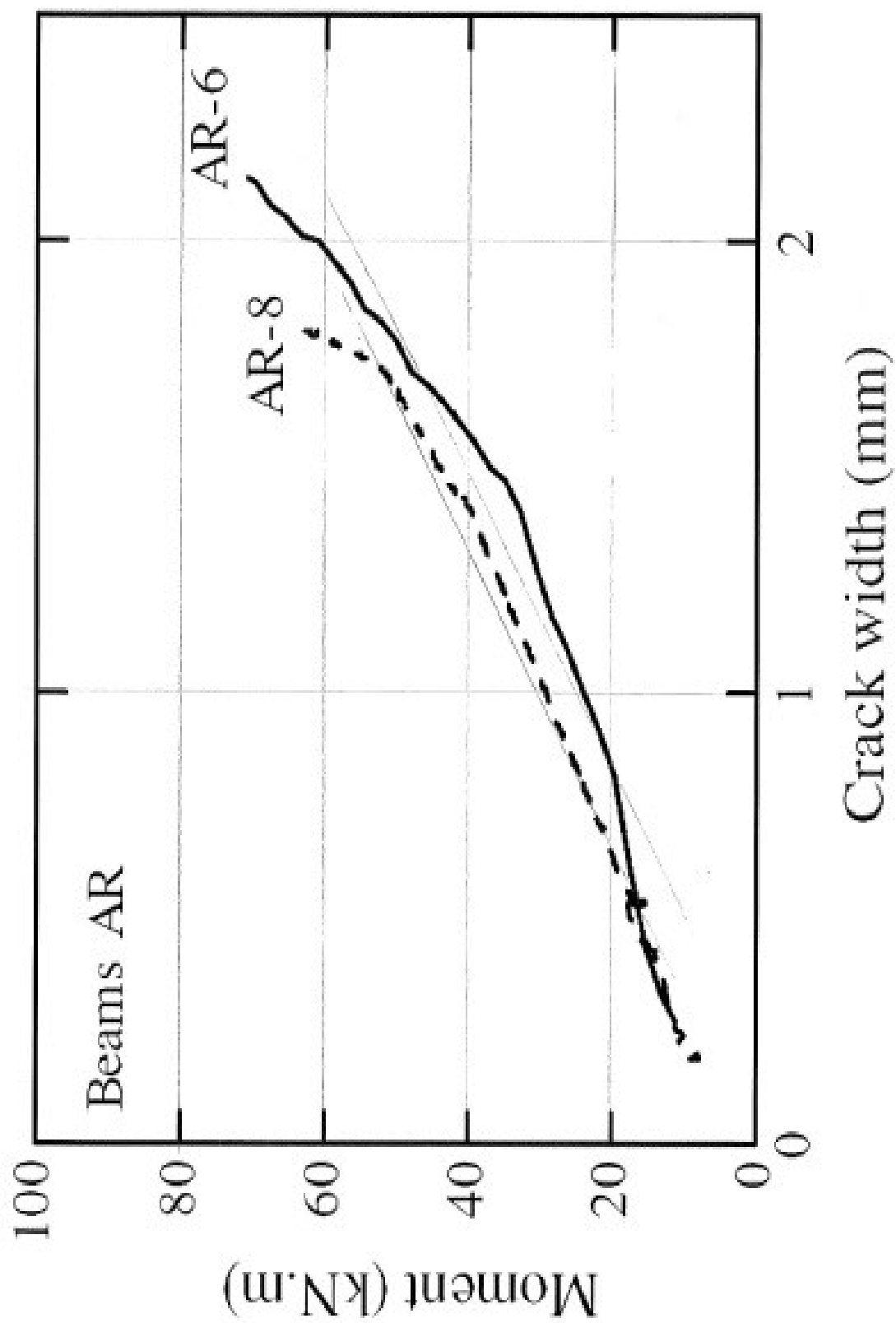
APPENDIX B :   ACI 440 TEST METHOD

Test Method for Determining the Bond-Dependent Coefficient of Fibre-Reinforced Polymer (FRP) Rods (*Second Draft*)

Brahim Benmokrane, ACI 440 member
University of Sherbrooke, Sherbrooke (Qc), Canada

Submitted to:
ACI 440-K subcommittee

March 16th, 2010

1─Scope

1.1 This test method specifies the test requirements for determining the bond-dependent coefficient (k_b) of the FRP rods used as flexural tension reinforcement in concrete members subjected to bending.

1.2 This test method is intended to determine the effects of surface treatment on the bond- dependent coefficient (k_b) of FRP rods. It can be used to test GFRP rods ranging in size from No. 3 to No. 8 and CFRP rods ranging in size from No. 3 to No. 5, using a beam with minimum concrete strength of 28MPa.

2─Referenced Documents

2.1 *ASTM Standards*

C 39 – 94   Standard Test Method for Compressive Strength of Cylindrical Concrete Specimens

C 143 – 90a Standard Test Method for Slump of Hydraulic Cement Concrete

C 192 – 95 Standard Practice for Making and Curing Concrete Test Specimens in the Laboratory

C 234 – 91a Standard Test Method for Comparing Concrete on the Basis of the Bond Developed with Reinforcing Steel

C 617 – 87 Standard Practice for Capping Cylindrical Concrete Specimens

D 5229/D 5229M–92 Standard Test Method for Moisture Absorption Properties and Equilibrium Conditioning of Polymer Matrix Composite Materials

E 4-01 Standard Practices for Force Verification of Testing Machines

D7205 / D7205M –06. Standard Test Method for Tensile Properties of Fiber Reinforced Polymer Matrix Composite Bars.

3─Significance and Use

3.1 This test method is used to determine the bond-dependent coefficient (k_b) of FRP reinforcing rods to be used in flexural members. Thus, this test procedure is based upon beam testing in two points loading.

3.2 This test method is designated to provide bond behavior and strength for material specifications, research and development, quality assurance, and structural design and analysis.

3.3 The beams specimens dimensions and reinforcement are designed so that they will not fail in shear prior to concrete crushing, or having bar slip.

3.4 This test method may also be used to determine the conformance of a product or a treatment to a requirement relating to its effect on the bond developed between FRP rod and concrete.

4─Terminology

4.1 Bond-dependent coefficient (k_b): factor that accounts for the bond between a bar and concrete.

4.2 Development length: length of embedded reinforcement required to develop the tensile capacity.

5─Test Equipment and Requirements

5.1 A schematic of a suitable testing system is shown in

5.2 Figure .

5.3 Beams dimensions should be close to L = 3000 *mm*, b = 200 *mm*, h = 300 *mm*, to be representative of real structural member.

5.4 Shear span «*a*» should be at least equal to ℓ /3, or 3 times the height of the beam. Bigger shear span is suitable to reduce shear but the maximum moment region «*x*» should not be smaller than 500 *mm*.

5.5 Bar length from the loading point to the bar end must exceed the development length to avoid any bar slip.

5.6 Clear concrete cover for FRP bars is 1½ inch for bars #2, #3, #4, #5 and 2 inches for bars #6, #7 and #8.

5.7 The loading system shall be capable of measuring the forces to an accuracy within ±2% of the applied load, when calibrated in accordance with ASTM Practices E 4. The load should be applied quasi-statically to the beam at a displacement rate close to 1.2 mm/min.

5.7 The hydraulic jack should be fixed between two hinges to ensure that the applied load remains vertical along the test.

5.8 Initial crack width of the two first flexural cracks should be measured with hand optical or digital microscope, as shown in Figu .

5.9 The opening of the two first flexural cracks should be monitored with one displacement meter each.

5.10 Initial crack width of the two first flexural cracks should be added in the analysis to the readings of the displacement meters to have the real opening.

5.11 The displacement meters should be LVDTs or similar apparatuses.

5.12 Mid-span deflection should be measured with minimum of two displacement meters.

5.13   FRP bars strain at mid-span should be measured with a minimum of two electrical strain gages. It is suitable to put strain gages 10 mm apart from the center line of the beam.

6─Specimen Preparation

6.1 FRP rods to be embedded into the specimen should be representative of the lot production being tested.

6.2 For each type of bars, the set of specimens should be casted in the same batch.

6.3 Transverse reinforcement may be placed over the entire length of the beam at a uniform spacing to avoid a shear failure. However maximum moment region «x» can be transverse reinforcement free to avoid confinement effect.

6.4 FRP rods used in a given series of tests need to be of the same type and size, and have the same pattern of any deformations or other means of mechanical and frictional interlock with the concrete. The length of the individual rods over the loading point should be such as to meet the requirements of the test specimens and the expected development lengths.

6.5 The concrete should be a standard mix, and a minimum of five standard 150 by 300-mm control cylinders should be made for determining compressive strength from each batch of concrete. These cylinders and control tests should follow ASTM C39. The concrete mix should be batched and mixed in accordance with the applicable portions of ASTM C192. The slump should conform to the measurements of ASTM C143, and have a value of 10 ± 2 cm.

6.6 The concrete should be cast in approximately equal layers, not exceeding 250mm in depth. Each layer shall be adequately consolidated with an internal vibrator to ensure removal of entrapped air. The specimen may be cast on its side, or upside down to control the amount of concrete under the bar during the cast.

6.7 The test specimen shall be cured in the forms using a curing compound or a plastic membrane, or both, to prevent rapid evaporation of water for at least 48 hours.

6.8 Molds should not be removed from the specimens earlier than 20 hours after casting. Immediately after removing the molds, specimens should be cured in accordance with ASTM C511 until the time of test. Specimens should be tested at an age of 28 ± 3 days.

6.3 Two specimens constitute a set of test specimens. If a specimen is found to have failed prematurely, an additional test should be performed on a separate specimen using FRP rods taken from the same lot as the failed specimen.

7─Test Conditions

7.1 Unless a different testing environment is specified as part of the experiment, the tests should be conducted at the standard laboratory atmosphere (23 ± 3 $^{\circ}$C and 50 ± 10 % relative humidity).

8─Test Method

8.1 Beams should be simply supported and tested in two points loading.

8.2 Load is applied until the first flexural crack appears. At that stage loading is held constant to measure initial crack width with a microscope as shown in Figu.

8.3 Displacement meter is installed at the level of reinforcing bars to monitor the crack width until the end of testing (see Figure).

8.4 Resume loading until having a 2nd flexural crack, and the same steps as for the first crack are repeated.

8.5 Resume loading until having crack width exceeding 1 *mm* or until beam failure if the ultimate performance is needed.

9─Calculations

9.1 The bond-dependent coefficient k_b should be determined from the measured crack widths and strains in the FRP bars (at service stage) during testing and using Eq. 1 (ACI 440.1R-06) if strain readings are poor or bad, stress calculated with elastic crack theory can be used:

$$w = 2\frac{f_f}{E_f}\beta \times k_b \ \times \sqrt{d_c^2 + \left(\frac{s}{2}\right)^2}$$ (1)

Where

w : maximum crack width (mm)

E_f: modulus of elasticity of FRP bar (MPa)

f_f : stress in FRP reinforcement in tension (MPa)

k_b : bond-dependent coefficient

β : ratio of distance from neutral axis to extreme tension fiber to distance from neutral axis to centre of tensile reinforcement

d_c : thickness of concrete cover measured from extreme tension fiber to centre of bar (mm)

s : longitudinal FRP bar spacing (mm)

9.2 In Eq. 1, the w is measured experimentally using displacement meter. All other terms in the equation are known values except the k_b which can be then calculated (mean value). The crack width values, w, for calculating k_b should not exceed 0.7 mm.

10─Report

The test report should include the following items:

10.1 Properties of the concrete

10.1.1 The mix proportions of cement, fine aggregate, coarse aggregate, admixture (if any used), and the water cement ratio

10.1.2 Slump of freshly mixed concrete as determined in accordance with ASTM C 143

10.1.3 Twenty-eight day strength of control cylinders as determined in accordance with ASTM C 39

10.1.4 Any deviation from the stipulated standards in such aspects as mixing, curing, dates of demolding and testing of control cylinders

10.2 Properties of the FRP rod

10.2.1 The trade name, shape and date of manufacture if available and lot number of product tested

10.2.2 Type of fiber and fiber binding material as reported by the manufacturer, fiber volume fraction, surface treatment and pre-conditioning of FRP rod

10.2.3 Designation, diameter, and cross-sectional area

10.2.4 Modulus of elasticity and ultimate tensile strength as determined in accordance with ASTM D7205 / D7205M – 06.

10.2.5 A close-up photograph of the rods showing surface deformations and characteristics

10.3 Numbers or identification marks of test specimens

10.4 Date of test, test temperature, loading rate

10.5 Dimensions of test specimens, bonded length of FRP rod, clear cover above the FRP test bar, and size, spacing, and type of transverse reinforcement .

10.6 Average bond-dependent coefficient k_b at service load and its standard deviation.
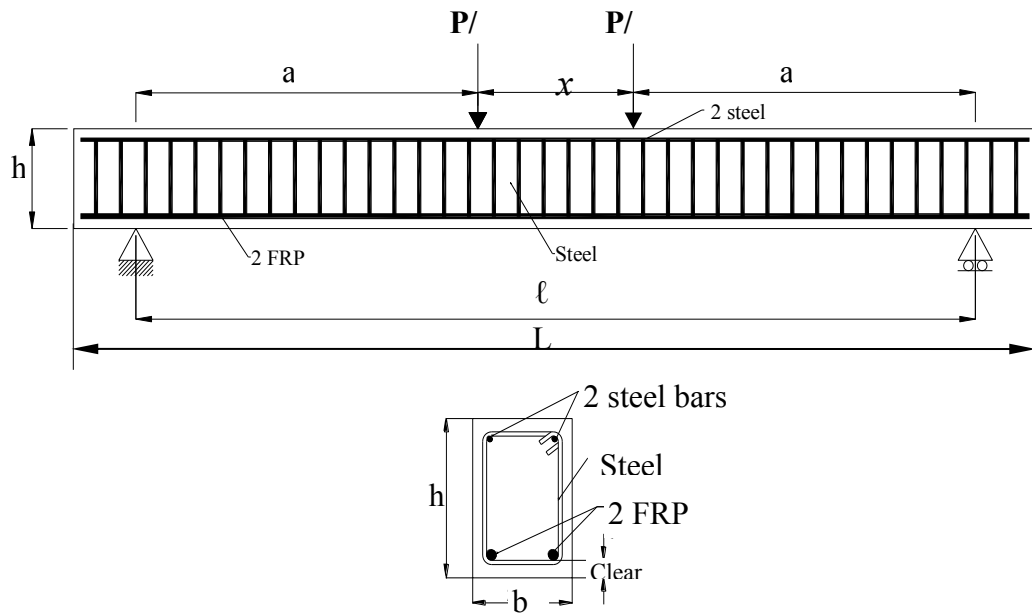
Figure 1: The dimensions and reinforcement details of the specimens
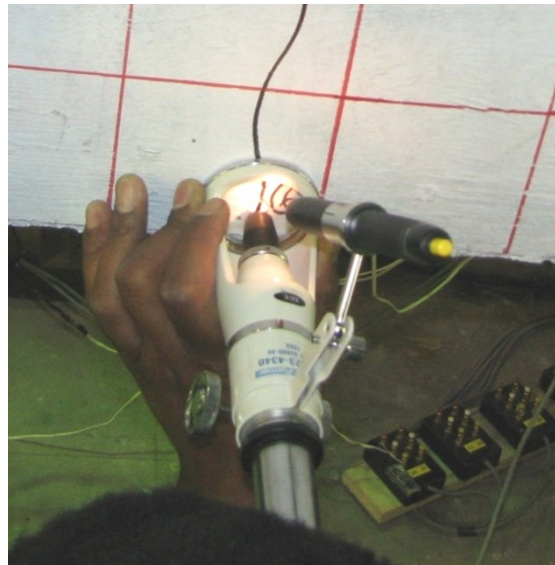
Figure 2: Hand optical microscope for measuring initial crack-width
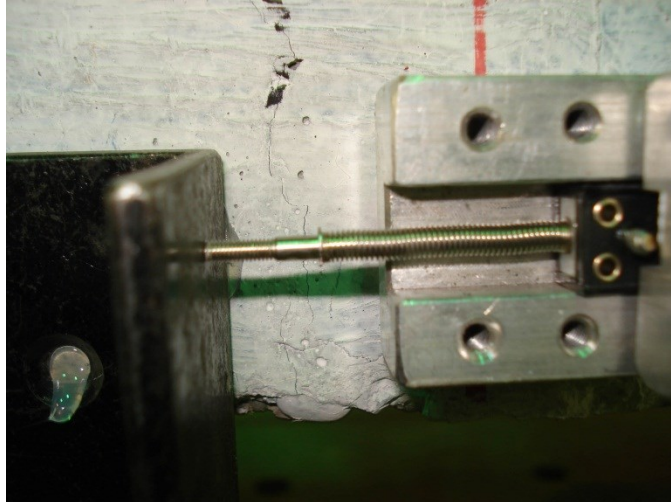
**Figure 3: monitoring crack –width with displacement meter
crack –width with displacement meter**

APPENDIX C : MANUFACTURER BAR CERTIFICATIONS

	PULLRALL	Validation de commande
		Order monitoring

Client / *Customer*: Uni Dalhousie

Projet / *Project*:

PO:

Couleur / *Tag colour*: Green and white   . Bar run:

pal.	Ø	longueur length	description	n° lot batch nr	qté comm. ord. qty	qté exp. ship. qty	qté ctrl ctrl. qty
P2	5	2800	Vrod	13 5006	10	10	
P3	6	2800	Vrod	135067	4	4	
		Utiliser meme	Lot par diametre				

échantillons
samples

validation sign off	production		date 1Y - 3 - 1d
	qualité / *quality*		19 - 03 - 12
	expédition / *shipping*		

Certificate of Compliance

Materials

bar diameter: #5
type of resin: vinylester
fibre type: E-glass

grade: standard

project: Uni Dalhousie

Production

manufacturing process: pultrusion
lot number: 125005   total length: 10582 m
production started on: 24-02-2012
production ended on: 27-02-2012

a production lot is defined by a change of the lot number of the resin and/or a change of setup (diameter)

Product characterisation

Cross sectional area:
test method ACI 440.3R B1

sample	mm²
1	221,8
2	220,9
3	231,9
4	222,9
5	229,2
average	225,4
std deviation	4,4

Longitudinal tensile properties:
test method CSA S806 Annex C

sample	load at break (kN)	strength (MPa)	modulus (MPa)	elongation (m/m)
1	284	1434,3	52512	2,7%
2	277	1400,0	52950	2,6%
3	283	1430,1	52697	2,7%
4	260	1313,5	53297	2,5%
5	281	1419,0	51986	2,7%
average	277,0	1399,4	52689	2,7%
std deviation	8,8	44,6	439	0,1%
minimum	254,0	1283,5		

Fibre content (per weight):
test method ASTM D2584 (temp 650°C, sand coating discarded from result)

sample	%
1	82,8%
2	82,8%
3	82,9%
4	82,8%
5	82,8%
average	82,8%
std deviation	0,0%

LAB03 F02 rev 1

Void content:
test method ASTM D5117

sample	wicking
1	ok
2	ok
3	ok
4	ok
5	ok

Water absorption:
test method ASTM D570 (24h at 50 °C)

sample	weight variation
1	0,10%
2	0,07%
3	0,07%
4	0,07%
5	0,06%
average	0,08%
std deviation	0,01%

Cure ratio and glass transition temperature:
test method ASTM D3418 and CSA S807 Annex A

sample	cure ratio (%)	Tg (°C)
1	99,91	123
2	98,08	115
3	98,67	126
4	99,91	118
5	99,37	121
average	99,19	120,6
std deviation	0,72	3,9

Notes:
Water absorption: long term test conditions make it impossible to provide test results at the time of shipping. This test is currently not done on V-Rod bars.
Every reported test result was validated by a satisfying mode of rupture of the sample.

Test setup
All tensile tests are done on a Satec-Baldwin UTM, with a 400000 lbfs load cell calibrated on February 23rd 2011 and with an Epsilon 200mm extensometer calibrated on Oct 14th 2011.
Length of samples for tensile tests: 1735mm
Length of anchors for tensile tests: 550mm

The values reported in this document meet the specification requirements where applicable.

Date: March 20 2012

QC representative: _____

PULTRALL

Certificate of Compliance

V-ROD

Materials
bar diameter: #6   grade: standard   project: Uni Dalhousie
type of resin: vinylester
fibre type: E-glass

Production
manufacturing process: pultrusion

lot number:	125007	total length:	19680 m
		production started on:	12-03-2012
		production ended on:	20-03-2012

a production lot is defined by a change of the lot number of the resin and/or a change of setup (diameter)

Product characterisation
Cross sectional area:
test method ACI 440.3R B1

sample	mm²
1	320,7
2	298,4
3	305,5
4	306,3
5	322,4
average	310,7
std deviation	9,3

Longitudinal tensile properties:
test method CSA S806 Annex C

sample	load at break (kN)	strength (MPa)	modulus (MPa)	elongation (m/m)
1	384	1348,6	53707	2,5%
2	351	1232,5	52773	2,3%
3	368	1290,4	53695	2,4%
4	374	1310,5	53738	2,4%
5	370	1298,8	52788	2,5%
average	369,4	1296,2	53340	2,4%
std deviation	10,7	37,5	457	0,1%
minimum	341,6	1196,5		

Fibre content (per weight):
test method ASTM D2584 (temp 650°C, sand coating discarded from result)

sample	%
1	84,6%
2	84,6%
3	84,6%
4	84,6%
5	84,6%
average	84,6%
std deviation	0,0%

Void content:

test method ASTM D5117

sample	wicking
1	ok
2	ok
3	ok
4	ok
5	ok

Water absorption:

test method ASTM D570 (24h at 50°C)

sample	weight variation
1	0,05%
2	0,09%
3	0,08%
4	0,08%
5	0,08%
average	0,08%
std deviation	0,01%

Cure ratio and glass transition temperature:

test method ASTM D3418 and CSA S807 Annex A
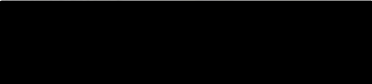
sample	cure ratio (%)	Tg (°C)
1	99,68	127
2	98,37	115
3	98,07	105
4	99,84	131
5	99,48	129
average	99,09	121,4
std deviation	0,72	9,7

Notes:

Water absorption: long term test conditions make it impossible to provide test results at the time of shipping. This test is currently not done on V-Rod bars.

Every reported test result was validated by a satisfying mode of rupture of the sample.

Test setup

All tensile tests are done on a Satec-Baldwin UTM, with a 400000 lbfs load cell calibrated on February 21st 2012 and with an Epsilon 200mm extensometer calibrated on February 24th 2012.

Length of samples for tensile tests: 2112mm

Length of anchors for tensile tests: 675mm

The values reported in this document meet the specification requirements where applicable.

Date: March 20 2012

QC representative: _____

LAB03-F02 rev 1

Tensile Testing of GFRP Rebar

AslanFRP
Hughes Brothers

TEST MACHINE
Baldwin Model 120 CS S/N: 1005
Electromechanical
120,000 lbs Capacity Tension/Compression
Certification Number 148081511124011
By Instron   15-August-2011
Operating System - MTEST Windows
Grip V Style

☉ Production
○ Experimental **Tested By**
○ Durability

Field	Value	Field	Value
Rebar Size	RB5	Lot Type	
Stock Order	154148	Test Date	1/31/2012
Work Order	1	Reinforcement	ECR-Glass
Date Produced	1/24/2012	Filament Diameter	23 Micron
Lot Color Code		Sizing	Silane
Matrix	VE	Yield	113
Formulation	RBVEIP2567-22 FA	# of Ends	68
Test Temp	75.4°F	Sample Length	48.00"
Test R/H	18%	Free Length	27.500"
Load Rate	0.50"/min	Anchor Length	10.00"
		Potting Material	M-183

Sample #	Load @ Failure (lbs)	Tensile Strength (psi)	Tensile Strength (MPa)	Ultimate Strain (in/in)	Modulus of Elasticity (psi)	Modulus of Elasticity (GPa)
1	36,205.7	118,010.8	813.7	0.0161	7,316,310	50.4
2	34,969.9	113,982.7	785.9	0.0157	7,264,115	50.1
3	35,842.1	116,825.6	805.5	0.0160	7,292,634	50.3
4	35,873.1	116,926.7	806.2	0.0160	7,296,727	50.3
5	37,030.6	120,699.5	832.2	0.0164	7,338,367	50.6
6	36,828.1	120,039.4	827.7	0.0164	7,301,209	50.3
7	35,426.0	115,469.4	796.2	0.0159	7,242,892	49.9
8	34,634.1	112,888.2	778.4	0.0156	7,222,509	49.8
Averages				0.0160	7,284,345	50.2

Tensile Strength	PSI	MPa	Strain
Average	116,855.3	805.7	
Sigma	2,553.6	17.6	0.0003
3 Sigma	7,660.9	52.8	0.0008
σ -3 Sigma	109,194.4	752.9	0.0152

Extensometer Epsilon Model 3543

Distance from Anchors	10.750"
LBS of Load at Removal	14,573
Percent of Load at Removal	50%
Span	6.0"

Lot Comments

Surface: Undulated Externally Wrapped
Spacing of Wrap .75 - 1.0"
Silica Sand applied to Surface During Process
* Samples cut using Diamond Blade Cutoff Saw
** Anchorages are cut to length and wheel abrated
Schedule 40 Pipe

Sample	Mode of Failure
1	Split Center
2	Delam Center
3	Delam Center
4	Split Center
5	Delam Center
6	Delam Center
7	Delam Center
8	Split Center

Additional Lab Test Data

% Glass to Matrix	74.92 / 25.08	ASTM D2584 By Weight
Barcol Hardness	60.0	ASTM D2583
Wicking	Not Continuous	ASTM D5117
Transverse Shear	29,975.7 psi	ASTM D7617-11
Apparent Shear	8,674.4 psi	ASTM D4475
Water Absorption Average 24 Hour	0.0987 %	ASTM D570 P7.7

	Actual Ø (in)	Actual CSA A, (in)
	0.6421	0.3239

Rebar Size	Required Tensile Strength psi / MPa	Load Cell Min (lbs / N)	Standard Ø (in / mm)	Standard CSA A, (in / mm)
5	105,000	32,214	0.6250	0.3068
16	724.0	143,298	15.88	197.9

Metric References

Hughes Brothers, Inc.   Seward, NE   Per ASTM D7205-06

Tensile Testing of GFRP Rebar

Aslan FRP
Hughes Brothers

TEST MACHINE
Baldwin Model 120 CS S/N: 1005
Electromechanical
120,000 lbs Capacity Tension/Compression
Certification Number 148081511124011
By Instron 15-August-2011
Operating System - MTEST Windows
Grip V Style

○ Production
○ Experimental **Tested By** R Colberg
○ Durability **Test Date** 7/22/2011
Lot Type

Field	Value	Field	Value
Rebar Size	RB6		
Stock Order	8352-8381	Reinforcement	ECR-Glass
Work Order	1	Filament Diameter	23 Micron
Date Produced	7/11/2011	Sizing	Silane
Lot Color Code		Yield	113
Matrix	VE	# of Ends	97
Formulation	RBVEIP2567-25 FA	Sample Length	48.00"
Test Temp	77.4°F	Free Length	33.500"
Test R/H	37%	Anchor Length	
Load Rate	0.50"/min	Potting Material	Swaged

Sample #	Load @ Failure (lbs)	Tensile Strength (psi)	Tensile Strength (MPa)	Ultimate Strain (in/in)	Modulus of Elasticity (psi)	Modulus of Elasticity (GPa)
1	54,274.6	122,848.8	847.0	0.0174	7,073,989	48.8
2	52,132.5	118,000.2	813.6	0.0167	7,076,815	48.8
3	51,427.7	116,404.9	802.6	0.0165	7,068,717	48.7
4	52,391.1	118,585.6	817.6	0.0167	7,088,834	48.9
5	52,731.2	119,355.4	823.0	0.0170	7,002,432	48.3
6	51,887.3	117,445.2	809.8	0.0168	6,994,243	48.2
7	50,553.7	114,426.7	789.0	0.0160	7,149,662	49.3
8	51,447.2	116,449.1	802.9	0.0160	7,268,263	50.1
Averages				0.0166	7,090,369	48.9

Tensile Strength	PSI	MPa	Strain
Average	117,939.5	813.2	
Sigma	2,336.9	16.1	0.0004
3 Sigma	7,010.6	48.3	0.0013
σ -3 Sigma	110,928.9	764.9	0.0153

Extensometer Epsilon Model 3543

Distance from Anchors	13.750"
LBS of Load at Removal	19,881
Percent of Load at Removal	50%
Span	6.0"

Lot Comments

Sample	Mode of Failure
1	Delam Center
2	Delam Center
3	Split Top
4	Delam Bottom
5	Delam Bottom
6	Delam Top
7	Delam Bottom
8	Delam Top

Surface: Undulated Externally Wrapped
Spacing of Wrap .75 - 1.0"
Silica Sand applied to Surface During Process
* Samples cut using Diamond Blade Cutoff Saw
** Anchorages are cut to length and wheel abrated
Schedule 40 Pipe

Additional Lab Test Data

% Glass to Matrix	75.49 / 24.51	ASTM D2584 By Weight
Barcol Hardness	60.8	ASTM D2583
Wicking	Not Continuous	ASTM D5117
Transverse Shear	22,312.5 psi	ASTM D7617-11
Apparent Shear	7,592.6 psi	ASTM D4475
Water Absorption Average 24 Hour	0.0793 %	ASTM D570 P7.7

Metric References

Rebar Size	Required Tensile Strength psi / MPa	Load Cell Min (lbs / N)	Actual Ø (in)	Actual CSA A, (in)
			0.7859	0.4850
			Standard Ø (in / mm)	Standard CSA A, (in / mm)
6	100,000	44,180	0.7500	0.4418
19	689.5	196,523	19.05	285.0

Hughes Brothers, Inc.   Seward, NE

Per ASTM D7205-06

APPENDIX D : CONCRETE PROPERTIES

Concrete compressive strength testing was completed on 101.6 x 203.2 mm (diameter x length) cylinders at 28 days unless otherwise noted. Modulus of rupture testing was completed on 152.4 x 152.4 x 538 mm (width x height x length) concrete blocks.

D1 PHASE I

Table D.1 - Pour #1 Compressive Strength (Cast June 23, 2010)

	Strength		Average strength (MPa)	Fibre content (kg/m^3)
	(lbs)	(MPa)		
Plain	57000	31.2	31.2	0
	57000	31.2		
FRC	66000	36.1	36.2	1.8
	66150	36.2		
	67000	36.7		
	65250	35.7		

Table D.2 - Pour #2 Compressive Strength (Cast June 29, 2010)

	Strength		Average strength (MPa)	Fibre content (kg/m^3)
	(lbs)	(MPa)		
Plain	67000	36.7	35.9	0
	64000	35.1		
FRC	58300	31.9	31.5	2.4
	57000	31.2		
	57250	31.4		
	57500	31.5		

Table D.3 - Pour #3 Compressive Strength (Cast July 7, 2010)

	Strength		Average strength (MPa)	Fibre content (kg/m^3)
	(lbs)	(MPa)		
Plain	54000	29.6	30.3	0
	56500	30.9		
FRC	58000	31.8	32.2	3.0
	60750	33.3		
	58000	31.8		
	58500	32.0		

Table D.4 - Pour #4 Compressive Strength (Cast August 23, 2010)

	Strength		Average strength (MPa)	Fibre content (kg/m^3)
	(lbs)	(MPa)		
Plain	51000	27.9	28.5	0
	52000	29		
FRC	52250	28.6	27.9	4.6
	51500	28.2		
	49500	27.1		
	50750	27.8		

Table D.5 - Pour #5 Compressive Strength (Cast August 29, 2010)

	Strength		Average strength (MPa)	Fibre content (kg/m^3)
	(lbs)	(MPa)		
Plain	45000	24.6	25.3	0
	47500	26.0		
FRC	48000	26.3	28.1	6.9
	52000	28.5		
	53000	29.0		
	52500	28.8		

D2 PHASE IIA

Table D.6 - Pour #6 Compressive Strength (Cast June 5, 2012)

Age at testing (days)	Curing	Strength		Average (MPa)
		(lbs)	(MPa)	
7	Room temp.	47500	26.0	28.5
28	Room temp.	51000	28.0	
28	Room temp.	57500	31.5	
28	Moist-cured	57500	31.5	33.8
28	Moist-cured	63000	34.5	
28	Moist-cured	64500	35.3	

Table D.7 - Pour #6 MOR Testing (Tested July 20, 2012)

	Peak load (kN)	M_{cr} (kNm)	P_{cr} (kN)	MOR (MPa)
B1	33.07	15.57	17.89	5.17
B2	32.17	15.15	17.41	5.03
B3	35.57	16.75	19.25	5.56
B4	39.98	18.83	21.64	6.25
B5	30.48	14.35	16.50	4.76
Average	34.25	16.13	18.54	5.35

Table D.8 - Pour #7 Compressive Strength (Cast June 12, 2012)

Age at testing (days)	Curing	Strength		Average (MPa)
		(lbs)	(MPa)	
7	Room temp.	53000	29.0	31.7
28	Room temp.	60000	32.9	
28	Room temp.	60500	33.1	
28	Moist-cured	67500	37.0	37.1
28	Moist-cured	70000	38.3	
28	Moist-cured	66000	36.1	

Table D.9 - Pour #7 MOR Testing (Tested July 20, 2012)

	Peak load (kN)	MOR (MPa)
B6	38.01	5.94
B7	40.61	6.35
B8	41.42	6.47
B9	38.90	6.08
B10	38.71	6.05
Average	39.53	6.18

Table D.10 - Pour #7 M_{cr} and P_{cr} based on average MOR

	M_{cr} (kNm)	P_{cr} (kN)
B5V5	18.61	21.39
BV6	18.63	21.41
BA5	18.60	21.38
BA6	18.62	21.41
Average	18.62	21.40

D3   PHASE IIB

Table D.11 - Pour #8 Compressive Strength (Cast November 7, 2012)

Age at testing (days)	Curing	Strength		Average (MPa)
		(lbs)	(MPa)	
7	Room temp.	53500	29.3	35.2
28	Room temp.	62500	34.2	
28	Room temp.	66000	36.1	
14	Moist-cured	57500	31.5	38.7
28	Moist-cured	71000	38.9	
28	Moist-cured	68500	37.5	
28	Moist-cured	72500	39.7	

Table D.12 - Pour #8 MOR Testing (Tested January 29, 2013)

	Peak load (kN)	MOR (MPa)
B1	38.38	6.00
B2	36.50	5.70
B3	36.69	5.73
B4	42.17	6.59
B5	38.81	6.06
B6	35.70	5.58
Average	38.04	5.94

Table D.13 - Pour #8 M_{cr} and P_{cr} based on average MOR

	M_{cr} (kNm)	P_{cr} (kN)
B38	11.68	13.42
B50	11.67	13.41
Average	11.68	13.42

APPENDIX E :   MANUAL CRACK WIDTH MEASUREMENTS

This section presents a summary of manual crack width measurements taken during testing. All crack widths within the constant moment region are reported in the tables below and the cracks monitored with gauges are represented as *1*, *2* and *3*.

E1   PHASE I

E1.1 Beam Specimens

Table E.1 - Beam B1 manual crack width measurements

	Load (kN)	Crack width (mm)
Initial measurements	19	*1* - 0.06; *2* - 0.08
After 100 cycles at level of reinforcement (front face)	60	*1* - 0.6; *2* - 0.8
After 100 cycles at level of reinforcement (back face)	60	*1* - 1; 0.8; 0.43; 0.81; *2* - 1.25
After 100 cycles on tension face (back to front face)	60	*1* - 1, 1, 0.8; *2* - 0.8, 0.8, 1.25

Table E.2 - Beam B2 manual crack width measurements

	Load (kN)	Crack width (mm)
Initial measurements	23	*1* - 0.09; *2* - 0.06
After 100 cycles on tension face (back to front face)	123	*1* - 1.25, 1.5, 1.5; *2* - 1, 1.25, 1.25

Table E.3 - Beam B3 manual crack width measurements

	Load (kN)	Crack width (mm)
Initial measurements	20	*1* - 0.08; 0.06; *2* - 0.09
Initial loading at level of reinforcement (front face)	88	*2* - 1.25; 1; 0.8; 1; *1* - 0.8; 0.9; 0.42
Initial loading at level of reinforcement (back face)	88	0.6; 0.4; *1* - 1; 0.5; 0.5; 0.8; *2* - 1
Initial loading on tension face (back to front face)	88	*2* - 0.8, 1, 1.25; 1.25, 1.25, 1; 1.5, 1.25, 1; 1, 1.25, 1; *1* - 1, 1, 0.8; 0.8, 0.6, 0.6; 0.4, 0.4, 0.25
After 100 cycles at level of reinforcement (front face)	88	*2* - 1.4; 1.2; 1.1; 1.1; *1* - 1.1; 1; 0.5
After 100 cycles at level of reinforcement (back face)	88	0.5; 0.4; *1* - 0.8; 0.4; 0.5; 0.8; *2* - 0.7
After 100 cycles on tension face (back to front face)	88	*2* - 0.8, 0.8, 1; 1.5, 1.25, 1; 1.5, 1.25,1; 0.8, 0.8, 1; *1* - 1.25, 1.25, 1; 1, 1, 1.5; 0.8, 0.6, 0.4

Table E.4 - Beam B4 manual crack width measurements

	Load (kN)	Crack width (mm)
Initial measurements	20	*1* - 0.12; 0.05; *2* - 0.04
Initial loading at level of reinforcement (front face)	100	*2* - 0.32; 1.25; 0.87; 0.95; 0.6; *1* - 0.95
Initial loading at level of reinforcement (back face)	100	*1*; 0.8; 1; 1.25; 1; *2*
Initial loading on tension face (back to front face)	100	*2* - 1, 1, 1.25; >1.5, >1.5, 1.25; 1.25, 1.25, 1.5; 1, 0.8, 1.5; 0.6, 0.6, 0.8; *1* - 0.8, 0.8, 1
After 100 cycles at level of reinforcement (front face)	100	*2* - 0.4; 1.25; 0.9; 0.95; 0.8; *1* - 1
After 100 cycles at level of reinforcement (back face)	100	*1* - 1; 1; 1.25; 1.25; 1; *2* - 1.1
After 100 cycles on tension face (back to front face)	100	*2* - 1, 1.25, 1.25; >1.5, >1.5, 1.25; 1.5, 1.5, 1.5; 1, 1, 1.5; 0.8, 0.8, 1; *1* - 1.25, 1.25, 1.25

Table E.5 - Beam B5 manual crack width measurements

	Load (kN)	Crack width (mm)
Initial measurements	18	*1* - 0.04; *2* - 0.03
Initial loading at level of reinforcement (front face)	65	0.29; 0.57; *2* - 1.1; 0.32; 0.4; *1* - 1.05; 0.14; 1.3
Initial loading at level of reinforcement (back face)	65	1.1; 0.27; *1*; 0.3; 0.4; *2*; 0.45; 0.35
Initial loading on tension face (back to front face)	65	0.4, 0.5, 0.35; 0.8, 0.6, 0.6; *2* - 1.5, 1.5, 1.5; 0.4, 0.3, 0.6; 1, 0.8, 0.8; *1* - 1.25, 1, 0.8; 0.4, 0.5, 0.3; 1.5, 1.25, 1.25
After 100 cycles at level of reinforcement (front face)	65	0.3; 0.5; *2* - 1.2; 0.36; 0.52; *1* - 1.3; 0.23; 1.6
After 100 cycles at level of reinforcement (back face)	65	0.95; 0.47; *1* - 0.85; 0.27; 0.38; *2* -1.1; 0.86; 0.37
After 100 cycles on tension face (back to front face)	65	0.5, 0.5, 0.5; 0.8, 0.8, 1; *2* - 1.5, 1.5, 1.5; 0.5, 0.4, 0.4; 1, 1, 0.8; *1* - 1.25, 0.8, 1; 0.5, 0.5, 0.4; 1.25, 1.25, 1.25

Table E.6 - Beam B6 manual crack width measurements

	Load (kN)	Crack width (mm)
Initial measurements	21	*1* - 0.06; 0.04; *2* - 0.05
Initial loading at level of reinforcement (front face)	100	*2* - 0.86; 0.9; 0.73; 0.15; 0.93; *1* - 1.7; 0.9
Initial loading at level of reinforcement (back face)	100	0.62; *1*; 0.25; 0.55; 0.47; 1.1; *2*
Initial loading on tension face (back to front face)	100	*2* - 0.8, 0.8, 0.8; 0.8, 1.25, 1.25; 0.8, 1, 0.8; 1, 1.25, 1.25; 0.5, 0.8, 1.25; *1* - 0.8, 0.8, 1.25; 0.8, 0.8, 1.25
After 100 cycles at level of reinforcement (front face)	100	*2* - 0.85; 0.65; 0.85; 0.15; 1.2; *1* - 1.3; 0.95
After 100 cycles at level of reinforcement (back face)	100	0.8; *1* - 0.65; 0.35; 0.67; 0.46; 1; *2* - 1.1
After 100 cycles on tension face (back to front face)	100	*2* - 1.25, 1, 1; 1, 1.25, 1.25; 0.8, 1, 0.5; 1.25, 1.5, 1.5; 0.8, 0.8, 1.25; *1* - 0.8, 0.8, 1.25; 0.8, 0.8, 1.25

Table E.7 - Beam B7 manual crack width measurements

	Load (kN)	Crack width (mm)
Initial measurements	20	0.05; *1* - 0.04; *2* - 0.04
Initial loading at level of reinforcement (front face)	65	*2* - 1; 0.14; 1; 0.23; 0.35; *1* - 0.95; 0.3; 0.75
Initial loading at level of reinforcement (back face)	65	0.5, 0.35; *1*; 0.5; 0.4; 0.4; 0.8; *2*
Initial loading on tension face (back to front face)	65	*2* - 1, 0.8, 0.4; 1, 0.6, 0.5; 0.4, 0.5, 0.3; 0.5, 0.6, 0.8; *1* - 0.4, 1, 1.25; 0.6, 0.4, 0.4; 0.6, 0.6, 0.4
After 100 cycles at level of reinforcement (front face)	65	*2* - 1.1; 0.22; 1; 0.27; 0.34; *1* - 1; 0.45; 1.1
After 100 cycles at level of reinforcement (back face)	65	0.7; 0.28; *1* - 1.2; 0.45; 0.4; 0.35; 0.87; *2* - 0.6
After 100 cycles on tension face (back to front face)	65	*2* - 0.8, 0.8, 0.4; 1, 0.6, 0.4; 0.3, 0.3, 0.5; 0.8, 0.6, 0.6; *1* - 1, 1.25, 0.5; 0.8, 0.4, 0.4; 0.6, 0.5, 0.3

Table E.8 - Beam B8 manual crack width measurements

	Load (kN)	Crack width (mm)
Initial measurements	20	*1* - 0.09; *2* - 0.04; 0.05
Initial loading at level of reinforcement (front face)	100	1.1; 0.37; *2* - 0.93; 0.76; 0.5; 0.88; 0.31; *1* - 0.48
Initial loading at level of reinforcement (back face)	100	*1*; 0.25; 0.26; 0.38; 0.25; 0.13; 0.1; *2*; 0.35; 0.65
Initial loading on tension face (back to front face)	100	1.25, 1.5, 1.25; 1, 1, 0.6; *2* - 1, 0.5, 0.5; 0.5, 0.3, 0.8; 1, 1, 1; 1.25, 1.25, 1; 0.35, 0.35, 0.3; *1* - 0.4, 1, 1.25
After 100 cycles at level of reinforcement (front face)	100	1.3; 0.25; *2* - 0.85; 0.88; 0.9; 0.58; 0.41; *1* - 0.38
After 100 cycles at level of reinforcement (back face)	100	*1* - 0.3; 0.2; 0.58; 0.38; 0.2; 0.4; 0.3; *2* - 0.35; 0.5; 0.65
After 100 cycles on tension face (back to front face)	100	1.5, 1.5, >1.5; 1.25, 1.25, 1; *2* - 0.5, 0.4, 1; 0.5, 0.5, 1; 1.25, 1.25, 1; 1.25, 1.25, 1; 0.4, 0.4, 0.5; *1* - 0.8, 0.4, 0.4

Table E.9 - Beam B9 manual crack width measurements

	Load (kN)	Crack width (mm)
Initial measurements	20	*1* - 0.07; *2* - 0.07; 0.09
Initial loading at level of reinforcement (front face)	71	*2* - 0.35; 0.5; 0.23; 0.55; 0.3; 0.12; *1* - 0.7; 0.15; 0.05
Initial loading at level of reinforcement (back face)	71	0.95; 0.25; *1*; 0.25; 0.3; 1.1; 0.95; *2*
Initial loading on tension face (back to front face)	71	*2* - 0.5, 0.5, 0.4; 0.2, 0.25, 0.35; 0.5, 0.8, 0.8; 0.5, 0.6, 0.4; 0.8, 0.8, 1; 0.35, 0.35, 0.2; *1* - 0.8, 1, 0.4; 0.6, 0.4, 0.4; 0.5, 0.6, 0.6
After 100 cycles at level of reinforcement (front face)	71	*2* - 0.65; 0.75; 0.68; 0.73; 0.24; 0.07; *1* - 0.68; 0.23; 0.93
After 100 cycles at level of reinforcement (back face)	71	0.95; 0.4; *1* - 0.3; 0.22; 0.35; 0.98; 0.85; *2* - 0.58
After 100 cycles on tension face (back to front face)	71	*2* - 0.5, 0.4, 0.3; 0.3, 0.3, 0.4; 0.8, 1, 0.8; 0.6, 0.6, 0.0.3; 1, 1, 1.25; 0.4, 0.4, 0.4; *1* - 0.5, 0.6, 0.3; 0.5, 0.5, 0.5; 0.35, 0.6, 0.8

Table E.10 - Beam B10 manual crack width measurements

	Load (kN)	Crack width (mm)
Initial measurements	19	0.05; *1* - 0.11; *2* - 0.06
Initial loading at level of reinforcement (front face)	93	0.18; *2* - 0.73; 0.37; 0.08; *1* - 2.1; 0.65; 0.32; 0.55
Initial loading at level of reinforcement (back face)	93	0.68; 0.26; 1.3; 0.2; *1*; 0.2; 0.2; *2*; 0.3
Initial loading on tension face (back to front face)	93	0.35, 0.35, 0.3; *2* - 1, 1.25, 1.25; 0.35, 0.4, 0.5; 0.1, 0.1, 0.1; *1* - 1.5, 1.5, 1.5; 0.8, 0.8, 0.6; 1.5, 1.25, 1.25; 0.35, 0.35, 0.2; 0.8, 1.25, 1.25
After 100 cycles at level of reinforcement (front face)	93	0.36; *2* - 0.73; 0.28; 0.2; *1* - 1.7; 0.62; 0.5; 0.58
After 100 cycles at level of reinforcement (back face)	93	0.7; 0.28; 1.4; 0.35; *1* - 1.5; 0.21; 0.32; *2* - 0.66; 0.35
After 100 cycles on tension face (back to front face)	93	0.35, 0.5, 0.5; *2* - 1, 1.25, 1; 0.4, 0.4, 0.6; 0.2, 0.2, 0.2; *1* - 0.8, 1.5, >1.5; 0.8, 0.8, 0.8; 1.5, 1.25, >1.5; 0.35, 0.35, 0.35; 1, 1.25, 1

Table E.11 - Beam B13 manual crack width measurements

	Load (kN)	Crack width (mm)
Initial measurements	14	*1* - 0.09; *2* - 0.08
Initial loading at level of reinforcement (front face)	65	*2* - 0.17; 0.12; 0.5; 0.13; 0.1; 0.25; 0.23; 0.5; 0.6; 0.65; *1* - 0.65
Initial loading at level of reinforcement (back face)	65	*1*; 0.48; 0.25; 0.4; 0.18; 0.23; 0.12; 0.09; 0.63; 0.43; *2*
Initial loading on tension face (back to front face)	65	*2* - 1, 1, 0.5; 0.25, 0.35, 0.1; 0.5, 0.5, 0.5; 0.1, 0.1, 0.1; 0.1, 0.1, 0.1; 0.6, 0.8, 0.8; 0.4, 0.4, 0.1; 0.3, -, -; 0.3, 0.5, 0.5; 1, 0.8, 0.5; *1*- 1, 0.8, 0.5;
After 100 cycles at level of reinforcement (front face)	65	*2* - 0.4; 0.2; 0.55; 0.25; 0.17; 0.45; 0.3; 0.6; 0.12; 0.55; *1* - 0.65
After 100 cycles at level of reinforcement (back face)	65	*1* - 1.05; 0.7; 0.26; 0.35; 0.19; 0.21; 0.24; 0.05; 0.6; 0.5 *2* - 0.7
After 100 cycles on tension face (back to front face)	65	*2* - 0.6, 1, 1; 0.2, 0.4, 0.2; 0.6, 0.6, 0.5; 0.2, 0.2, 0.2; 0.3, 0.3, 0.3; 0.6, 0.5, 0.8; 0.35, 0.35, 0.35; 0.2, -, -; 0.35, 0.6, 0.6; 0.1, 0.1, 0.1; 1.5, 0.8, 0.6; *1*- 1.5, 0.8, 0.6;

Table E.12 - Beam B14 manual crack width measurements

	Load (kN)	Crack width (mm)
Initial measurements	17	*1* - 0.08; *2* - 0.06
Initial loading at level of reinforcement (front face)	97	0.85; 0.5; 0.65; 0.5; 0.18; *2* - 0.28; 0.09; 0.12; *1* - 1.1; 0.95
Initial loading at level of reinforcement (back face)	97	0.75; *1*; 0.25; 0.13; *2*; 0.15; 0.38; 0.46; 0.23; 0.5
Initial loading on tension face (back to front face)	97	1.25, 1, 1; 0.4, 0.4, 0.4; 1, 0.8, 0.8; 0.8, 0.6, 0.8; 0.25, 0.25, 0.25; *2* - 1.25, 1.25, 1.25; 0.4, 0.45, 0.35; 0.5, 0.4, 0.4; *1*- 0.8, 0.6, 1; 0.6, 1, 0.5
After 100 cycles at level of reinforcement (front face)	97	0.95; 0.45; 0.8; 0.58; 0.19; *2* - 0.4; 0.2; 0.35; *1* - 0.65; 0.93
After 100 cycles at level of reinforcement (back face)	97	0.75; *1* - 0.65; 0.25; 0.3; *2* - 0.3; 0.1; 0.5; 0.45; 0.3; 0.6
After 100 cycles on tension face (back to front face)	97	1.25, 1.25, 1; 0.5, 0.5, 0.4; 0.6, 0.8, 0.8; 1, 1, 0.8; 0.35, 0.35, 0.35; *2* - 1.25, 1, 1; 0.35, 0.35, 0.5; 0.6, 0.5, 0.5; *1*- 1.25, 0.8, 0.8; 0.6, 1, 0.8

Table E.13 - Beam B15 manual crack width measurements

	Load (kN)	Crack width (mm)
Initial measurements	21	*1* - 0.13; *2* - 0.07
Initial loading at level of reinforcement (front face)	100	0.45; 0.6; 0.35; 0.43; 0.75; 0.3; 0.7; *2* - 0.72; 0.4; *1* - 0.5; 0.08
Initial loading at level of reinforcement (back face)	100	*1*; 0.58; *2*; 0.19; 0.53; 0.15; 0.77; 0.2; 1; 0.22; 0.95
Initial loading on tension face (back to front face)	100	0.8, 0.8, 1; *1* - 0.35, 0.5, 0.5; 0.8, 0.8, 0.5; *2* - 1.25, 1, 1; 1, 0.8, 0.5; 0.6, 0.6, 0.3; 0.3, 0.5, 0.5; 1.25, 0.5, 1; 0.2, 0.6, 0.6; 0.5, 1.25, 1; 0.3, 0.3, 0.3; 0.6, 0.6, 0.3
After 100 cycles at level of reinforcement (front face)	100	0.4; 0.63; 0.2; 0.45; 0.73; 0.35; 0.8; *2* - 0.8; 0.53; *1* - 0.65; 0.11
After 100 cycles at level of reinforcement (back face)	100	*1* - 0.75; 0.13; 0.65; *2* - 1.3; 0.15; 0.65; 0.18; 0.45; 0.2; 0.7; 0.32; 1.1
After 100 cycles on tension face (back to front face)	100	0.8, 1, 1; *1* - 0.4, 0.6, 0.6; 0.8, 0.8, 0.8; *2* - 1.25, 1, 1; 0.8, 1, 0.8; 0.8, 0.5, 0.5; 0.35, 0.4, 0.5; 1.5, 0.8, 1; 0.2, 0.6, 0.6; 0.8, 1.5, 1.5; 0.3, 0.4, 0.4; 0.4, 0.4, 0.4

Table E.14 - Beam B16 manual crack width measurements

	Load (kN)	Crack width (mm)
Initial measurements	24	*1* - 0.15; *2* - 0.06
Initial loading at level of reinforcement (front face)	100	0.76; 0.09; 0.23; *2* - 0.38; 0.35; 0.58; 0.23; 0.25; 0.61; *1* - 0.8; 0.58
Initial loading at level of reinforcement (back face)	100	0.45; *1*; 0.89; 0.25; 0.65; 0.51; *2*; 0.6; 0.18; 1.5
Initial loading on tension face (back to front face)	100	0.5, 1, 1.5; 0.3, 1, 1.5; 0.8, 0.8, 0.8; *2* - 0.4, 0.8, 0.8; 0.8, 0.8, 0.5; 0.2, 0.2, 0.2; 0.4, 0.4, 0.3; 0.6, 0.6, 0.3; *1* - 0.8, 0.6, 0.8; 1.5, 1, 1
After 100 cycles at level of reinforcement (front face)	100	0.55; 0.11; 0.15; *2* - 0.8; 0.4; 0.55; 0.25; 0.25; 0.65; *1* - 0.8; 0.65
After 100 cycles at level of reinforcement (back face)	100	0.5; *1* - 0.72; 0.85; 0.35; 0.65; 0.55; *2* - 0.9; 0.45; 0.35; 1.25
After 100 cycles on tension face (back to front face)	100	1, 1.5, 1.5; 0.5, 1.5, 1.5; 0.6, 0.6, 0.8; *2* - 0.35, 0.8, 0.8; 1, 0.8, 0.6; 0.6, 0.6, 0.3; 0.4, 0.4, 0.3; 0.2, 0.5, 0.5; 0.5, 0.5, 0.8; *1* - 0.5, 0.8, 0.8; 1.5, 1.25, 1

E1.2 Slab Specimens

Table E.15 - Slab S1 manual crack width measurements

	Load (kN)	Crack width (mm)
Initial measurements	17	*1* - 0.02; *2* - 0.03
Initial loading at level of reinforcement (front face)	65	0.48; 0.5; 0.19; 0.61; *2* - 0.63; 0.53; 0.32; 0.21; 0.42; *1* - 0.51; 0.34
Initial loading at level of reinforcement (back face)	65	0.8; *1*; 0.5; 0.26; 0.4; *2*; 0.19; 0.09; 0.31; 0.4; 0.45
Initial loading on tension face (back to front face)	65	1.5, 1.25, 1.25; 1.25, 0.4, 0.6; 1.25, 0.8, 0.8; 1.5, 0.8, 1.5; 0.5, 0.6, 1.5; 1.25, 0.6, 1.5; *2* - 0.35, 0.35, 1.5; 0.6, 1, 1; 0.5, 1, 1.25; 1.25, 0.6, 0.6; 0.8, 0.6, 0.6; *1* - 1, 1, 0.6; 1.25, 1.25, 0.6
After 100 cycles at level of reinforcement (front face)	65	0.56; 0.51; 0.21; 0.61; *2* - 0.76; 0.43; 0.33; 0.65; 0.49; *1* - 0.6; 0.35
After 100 cycles at level of reinforcement (back face)	65	0.8; *1* - 0.45; 0.51; 0.27; 0.65; *2* - 0.35; 0.6; 0.11; 0.18; 0.48; 0.83
After 100 cycles on tension face (back to front face)	65	1.5, 1.25, 1.25; 1.5, 0.6, 0.6; 1.5, 1, 0.8; 1.5, 1.5, >1.5; 0.5, 1.5, >1.5; 1.5, 0.8, 1.5; *2* - 0.5, 0.8, 1.5; 0.6, 1.25, 0.6; 0.6, 1, 1; 0.6, 1, 1; 1, 1, 0.8; *1* - 1.5, 1.25, 1; 1.25, 1.25, 0.8

Table E.16 - Slab S2 manual crack width measurements

	Load (kN)	Crack width (mm)
Initial measurements	17	*1* - 0.06; *2* - 0.06
Initial loading at level of reinforcement (front face)	65	0.46; 0.36; *2* - 0.39; 0.21; *1* - 0.29; 0.33; 0.23; 0.11; 0.25; 0.14
Initial loading at level of reinforcement (back face)	65	0.56; 0.21; 0.68; 0.88; 0.3; *1*; 0.29; *2*; 0.29; 0.24
Initial loading on tension face (back to front face)	65	1, 1, 1; 0.8, 0.6, 0.8; *2* - 0.5, 0.5, 0.8; 0.5, 0.5, 1; *1* - 1, 1, 1; 0.6, 0.6, 1; 0.5, 0.5, 0.8; 0.35, 0.35, 0.2; 1.5, 1.5, 1.5; 0.2, 0.2, -; 1, 1, 1.25
After 100 cycles at level of reinforcement (front face)	65	0.42; 0.51; *2* - 0.4; 0.38; *1* - 0.49; 0.29; 0.3; 0.18; 0.24; 0.31
After 100 cycles at level of reinforcement (back face)	65	0.45; 0.4; 0.63; 0.82; 0.45; *1* - 0.74; 0.26; *2* - 0.49; 0.29; 0.45
After 100 cycles on tension face (back to front face)	65	1, 1, 1.25; 0.8, 0.8, 1; *2* - 0.6, 0.8, 1; 0.6, 0.6, 1.25; *1* - 1, 1, 1.25; 0.8, 0.8, 1.25; 0.6, 0.8, 1; 0.5, 0.5, 0.3; >1.5, >1.5, >1.5; 0.3, 0.3, -; 1, 1.25, 1.25

Table E.17 - Slab S3 manual crack width measurements

	Load (kN)	Crack width (mm)
Initial measurements	17	*1* - 0.31; *2* - 0.28
Initial loading at level of reinforcement (front face)	60	0.29; 0.36; 0.21; 0.43; *2* - 0.35; *1* - 0.96; 0.45
Initial loading at level of reinforcement (back face)	60	0.83; *1*; 0.72; *2*; 0.25; 0.79; 0.42; 0.70
Initial loading on tension face (back to front face)	60	1, 1, 1; 0.6, 0.6, 1; 0.6, 0.8, 1; 1.25, 1, 1; *2* - 1.25, 1, 0.8; 0.5, 0.3, 0.2; *1* - 0.8, 1, 1.25; 1, >1.5, >1.5
After 100 cycles at level of reinforcement (front face)	60	0.31; 0.36; 0.41; 0.45; 0.17; *2* - 0.59; *1* - 1; 0.47
After 100 cycles at level of reinforcement (back face)	60	1.05; *1* - 0.76; 0.82; *2* - 0.86; 0.38; 0.84; 0.53; 0.67
After 100 cycles on tension face (back to front face)	60	1, 1, 1; 0.6, 0.8, 0.8; 1.25, 1, 1; 1.25, 1, 1; *2* - 1.5, 1.25, 1.25; 0.8, 0.5, 0.5; *1* - 1.5, 1.25, 1.25; >1.5, >1.5, >1.5

Table E.18 - Slab S4 manual crack width measurements

	Load (kN)	Crack width (mm)
Initial measurements	19	*1* - 0.07; *2* - 0.21
Initial loading at level of reinforcement (front face)	65	0.21; 0.71; *2* - 0.65; 0.59; *1* - 0.81; 0.93
Initial loading at level of reinforcement (back face)	65	0.47; 0.19; 0.36; *1*; 0.42; *2*; 0.49; 0.53; 0.63
Initial loading on tension face (back to front face)	65	0.8, 0.6, 0.8; 1, 0.8, 1; 0.8, 1, 0.5; *2* - 0.8, 1, 0.5; 1, 1, 1; *1* - 0.5, 0.6, 1.25; 0.8, 0.6, 1.25; 1.5, 1.25, 1.25; 0.2, 0.2, 0.5
After 100 cycles at level of reinforcement (front face)	65	0.42; 0.63; *2* - 0.65; 0.68; *1* - 0.82; 0.83
After 100 cycles at level of reinforcement (back face)	65	0.63; 0.31; 0.37; *1* - 0.45; 0.63; *2* - 0.69; 0.56; 0.75; 0.69
After 100 cycles on tension face (back to front face)	65	0.5, 1.25, 0.6; 1.25, 1, 1.25; 0.8, 0.8, 0.5; *2* - 0.8, 0.8, 0.5; 1, 1, 1.25; *1* - 0.6, 1, 1.5; 0.8, 1, 1.5; 1.5, 1.25, 1.25; 0.3, 0.3, 0.3

Table E.19 - Slab S5 manual crack width measurements

	Load (kN)	Crack width (mm)
Initial measurements	19	*1* - 0.08; *2* - 0.01
Initial loading at level of reinforcement (front face)	65	0.26; 0.47; 0.25; 0.21; *1* - 0.39; 0.24; 0.26; 0.3; 0.41
Initial loading at level of reinforcement (back face)	65	0.3; 0.32; 0.22; 0.18; 0.39; *1*; 0.19; 0.15; *2*; 0.2; 0.16
Initial loading on tension face (back to front face)	65	1.25, 1.25, 1; 0.5, 0.8, 1; 1, 1, 1; 0.6, 1, 0.3; *1* - 0.4, 0.5, 0.3; 0.2, 0.3, 0.4; 1, 0.8, 0.8; 0.6, 0.6, 0.2; 1.5, 1.5, 0.8; 1, 1.5, 0.8
After 100 cycles at level of reinforcement (front face)	65	0.29; 0.45; 0.28; 0.2; *1* - 0.41; 0.29; 0.3; 0.25; 0.45
After 100 cycles at level of reinforcement (back face)	65	0.27; 0.35; 0.34; 0.24; 0.4; *1* - 0.52; 0.21; 0.19; *2* - 0.07; 0.2; 0.25
After 100 cycles on tension face (back to front face)	65	1.25, 1.5, 1.5; 0.5, 0.8, 1.25; 1.25, 1.25, 1.25; 0.6, 1.25, 0.3; *1* - 0.4, 0.6, 0.6; 0.25, 0.4, 0.6; 1, 1, 1; 0.6, 0.6, 0.4; >1.5, >1.5, 1.5; 0.6, >1.5, 1.5

Table E.20 - Slab S6 manual crack width measurements

	Load (kN)	Crack width (mm)
Initial measurements	32	*1* - 0.02; *2* - 0.08
Initial loading at level of reinforcement (front face)	80	0.14; 0.4; 0.34; 0.12; 0.33; *2* - 0.45; 0.29; *1* - 0.46; 0.34
Initial loading at level of reinforcement (back face)	80	0.43; *1*; 0.41; *2*; 0.33; 0.17; 0.18; 0.07; 0.16
Initial loading on tension face (back to front face)	80	0.6, 0.8, 0.4; 0.35, 0.4, 0.5; 0.8, 1, 1; 0.2, 0.2, 0.2; 0.8, 0.3, 0.3; *2* - 0.8, 0.6, 0.5; 0.8, 0.4, 0.4; *1* - 0.8, 0.8, 1; 1, 1, 1
After 100 cycles at level of reinforcement (front face)	80	0.21; 0.45; 0.47; 0.24; 0.35; *2* - 0.41; 0.26; *1* - 0.38; 0.36
After 100 cycles at level of reinforcement (back face)	80	0.42; *1* - 0.35; 0.29; *2* - 0.38; 0.23; 0.13; 0.28; 0.19; 0.21
After 100 cycles on tension face (back to front face)	80	0.8, 0.8, 0.5; 0.4, 0.5, 0.8; 0.6, 0.8, 0.8; 0.3, 0.2, 0.2; 0.8, 0.8, 0.8; *2* - 0.6, 0.8, 0.6; 0.6, 0.8, 0.8; *1* - 0.8, 0.8, 0.8; 0.6, 0.6, 1

Table E.21 - Slab S7 manual crack width measurements

	Load (kN)	Crack width (mm)
Initial measurements	23	*1* - 0.16; *2* - 0.13
Initial loading at level of reinforcement (front face)	77	0.43; 0.58; *2* - 0.63; 0.51; 0.42; *1* - 0.71
Initial loading at level of reinforcement (back face)	77	*1*; 0.45; 0.46; *2*; 0.15; 0.53; 0.75
Initial loading on tension face (back to front face)	77	1.25, 0.8, 0.8; 0.8, 0.4, 0.8; 0.6, 0.6, 0.8; *2* - 0.6, 0.4, 0.4; 0.8, 0.6, 0.3; 0.5, 0.5, 1; *1* - 1.25, 0.6, 0.6
After 100 cycles at level of reinforcement (front face)	77	0.41; 0.63; *2* - 0.74; 0.53; 0.39; *1* - 0.78
After 100 cycles at level of reinforcement (back face)	77	*1* - 1.05; 0.59; 0.6; *2* - 0.64; 0.51; 0.72; 0.68
After 100 cycles on tension face (back to front face)	77	1.25, 1, 1; 1, 0.5, 1; 0.8, 0.8, 1; *2* - 0.6, 0.6, 1; 1, 1, 0.4; 0.8, 0.8, 1; *1* - 1, 0.8, 0.5

Table E.22 - Slab S8 manual crack width measurements

	Load (kN)	Crack width (mm)
Initial measurements	26	*1* - 0.06; *2* - 0.23
Initial loading at level of reinforcement (front face)	84	0.79; *2* - 0.86; 0.65; *1* - 0.44; 0.41; 0.98
Initial loading at level of reinforcement (back face)	84	1.05; 0.75; *1*; 0.25; *2*; 1.05
Initial loading on tension face (back to front face)	84	0.25, 0.25, 0.8; *2* - 1.25, 0.5, 1; 1.25, 0.8, 1; *1* - 1.25, 1, 0.8; 0.3, 0.5, 0.8; 0.5, 1, 1
After 100 cycles at level of reinforcement (front face)	84	0.96; *2* - 0.8; 0.73; *1* - 0.51; 0.46; 0.95
After 100 cycles at level of reinforcement (back face)	84	1.1; 0.83; *1* - 0.86; 0.27; *2* - 1.09; 0.78
After 100 cycles on tension face (back to front face)	84	1.5, 0.4, 1.25; *2* - 1.25, 0.6, 1; 1, 0.8, 1; *1* - 1.5, 1, 0.8; 0.4, 0.4, 0.8; 1, 0.5, >1.5

Table E.23 - Slab S9 manual crack width measurements

	Load (kN)	Crack width (mm)
Initial measurements	26	*1* - 0.10; *2* - 0.12
Initial loading at level of reinforcement (front face)	80	0.24; *2* - 0.35; 0.55; *1* - 0.85; 0.23
Initial loading at level of reinforcement (back face)	80	0.35; *1*; 0.52; *2*; 0.45
Initial loading on tension face (back to front face)	80	0.8, 0.6, 0.8; *2* - 0.4, 0.6, 0.4; 1, 1, 0.8; *1* - 0.8, 1, 0.8; 0.8, 0.8, 0.4
After 100 cycles at level of reinforcement (front face)	80	0.43; *2* - 0.65; 0.75; *1* - 0.85; 0.36
After 100 cycles at level of reinforcement (back face)	80	0.48; *1* - 0.69; 0.55; *2* - 0.52; 0.65
After 100 cycles on tension face (back to front face)	80	1, 1, 0.6; *2* - 0.8, 0.4, 0.8; 1, 1, 0.6; *1* - 0.8, 0.8, 1.25; 0.8, 1, 0.4

E2 PHASE IIA

Table E.24 - Beam B1V5 manual crack width measurements

	Load (kN)	Crack width (mm)
Initial measurements	27	*1* - 0.06; *2* - 0.09; *3* - 0.10
Initial loading at level of reinforcement (front face)	60	0.35; 0.95; 0.81; 0.88; 0.26
After 25 cycles at level of reinforcement (front face)	60	0.39; 0.98; 0.87; 0.31; 0.83; 0.39

Table E.25 - Beam B2V5 manual crack width measurements

	Load (kN)	Crack width (mm)
Initial measurements	25	*1* - 0.05; *2* - 0.11; *3* - 0.10
Initial loading at level of reinforcement (front face)	55	0.77; 0.35; 0.47; 0.54; 0.45; 0.66
After 25 cycles at level of reinforcement (front face)	55	0.82; 0.40; 0.51; 0.57; 0.65; 0.68

Table E.26 - Beam B3V5 manual crack width measurements

	Load (kN)	Crack width (mm)
Initial measurements	25	*1* - 0.13; *2* - 0.08; *3* - 0.10
Initial loading at level of reinforcement (front face)	65	0.75; 0.51; 0.65; 0.58; 0.89; 0.85
After 25 cycles at level of reinforcement (front face)	65	0.93; 0.53; 0.61; 0.6; 0.87; 0.78

Table E.27 - Beam B4V5 manual crack width measurements

	Load (kN)	Crack width (mm)
Initial measurements	25	*1* - 0.09; *2* - 0.06; *3* - 0.10
Initial loading at level of reinforcement (front face)	65	0.66; 0.76; 0.61; 0.8; 0.83; 0.98
After 25 cycles at level of reinforcement (front face)	65	1.05; 0.81; 0.63; 1.05; 0.83; 0.95

Table E.28 - Beam B5V5 manual crack width measurements

	Load (kN)	Crack width (mm)
Initial measurements	27	*1* - 0.12; *2* - 0.10; *3* - 0.10
Initial loading at level of reinforcement (front face)	85	0.90; 0.73; 0.68; 0.67; 0.12; 0.71; 0.53; 0.80
After 25 cycles at level of reinforcement (front face)	85	1.2; 0.88; 0.84; 0.90; 0.23; 0.72; 0.44; 0.81

Table E.29 - Beam BA5 manual crack width measurements

	Load (kN)	Crack width (mm)
Initial measurements	28	*1* - 0.13; *2* - 0.10; *3* - 0.05
Initial loading at level of reinforcement (front face)	90	1.2; 0.47; 0.35; 0.76; 1.3; 0.38; 1.05; 1.1
After 25 cycles at level of reinforcement (front face)	90	1.2; 0.63; 0.45; 0.78; 1.3; 0.49; 1.2; 1.2

Table E.30 - Beam BV6 manual crack width measurements

	Load (kN)	Crack width (mm)
Initial measurements	28	*1* - 0.13; *2* - 0.12; *3* - 0.10
Initial loading at level of reinforcement (front face)	85	0.99; 0.82; 0.55; 0.72; 0.28; 0.83
After 25 cycles at level of reinforcement (front face)	85	1; 0.86; 0.60; 0.75; 0.35; 0.93

Table E.31 - Beam BA6 manual crack width measurements

	Load (kN)	Crack width (mm)
Initial measurements	27	*1* - 0.11; *2* - 0.23; *3* - 0.10
Initial loading at level of reinforcement (front face)	80	1.02; 0.91; 0.55; 0.89; 0.19; 0.86
After 25 cycles at level of reinforcement (front face)	80	1.09; 0.93; 0.48; 0.35; 0.89; 0.45; 0.79

E3   PHASE IIB

Table E.32 - Beam B38 manual crack width measurements

	Load (kN)	Crack width (mm)
Initial measurements	18	*1* - 0.37; *2* - 0.10; *3* - 0.09
Initial loading at level of reinforcement (front face)	60	0.08; 0.59; 0.47; 0.77; 0.58; 0.69
Initial loading at level of reinforcement (back face)	60	0.63; 0.48; *1*; *2*; *3*; 0.52; 0.12
After 25 cycles at level of reinforcement (front face)	60	0.12; 0.61; 0.62; 1.1; 0.55; 0.73
After 25 cycles at level of reinforcement (back face)	60	1.05; 0.63; *1*; *2*; *3*; 0.72; 0.14

Table E.33 - Beam B50 manual crack width measurements

	Load (kN)	Crack width (mm)
Initial measurements	28	*1* - 0.35; *2* - 0.10; *3* - 0.11
Initial loading at level of reinforcement (front face)	85	0.80; 0.17; 0.93; 1.1; 0.26; 0.45; 0.93
Initial loading at level of reinforcement (back face)	85	*3*; 0.82; 0.41; *1*; *2*; 1.2; 0.25; 0.66
After 25 cycles at level of reinforcement (front face)	85	0.92; 0.27; 0.93; 1.2; 0.29; 0.46; 0.9; 0.06
After 25 cycles at level of reinforcement (back face)	85	*3*; 0.93; 0.45; *1*; *2*; 1.2; 0.27; 0.75

APPENDIX F : EXPERIMENTAL PLOTS

Reinforcement stress versus crack width plots for all specimens can be found in this section. Lines of best fit and the corresponding regression equations are also shown for all monitored cracks.
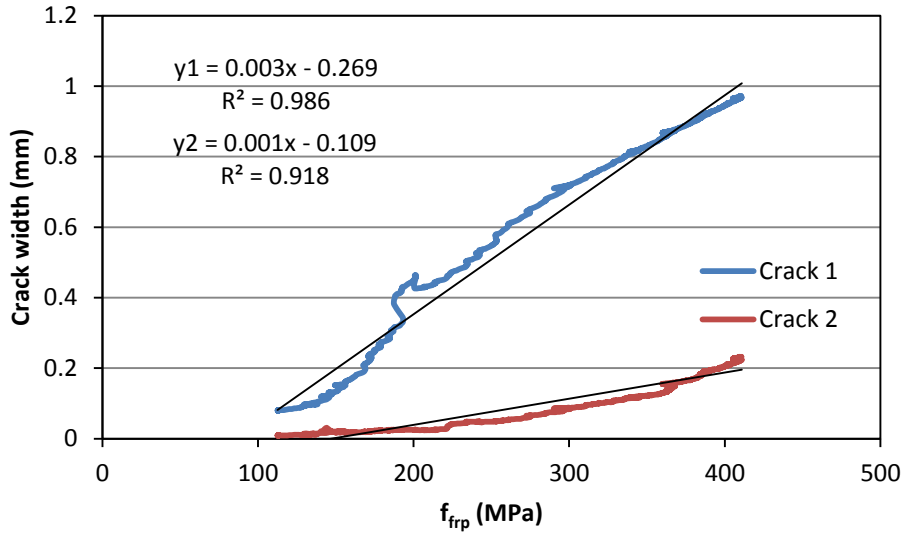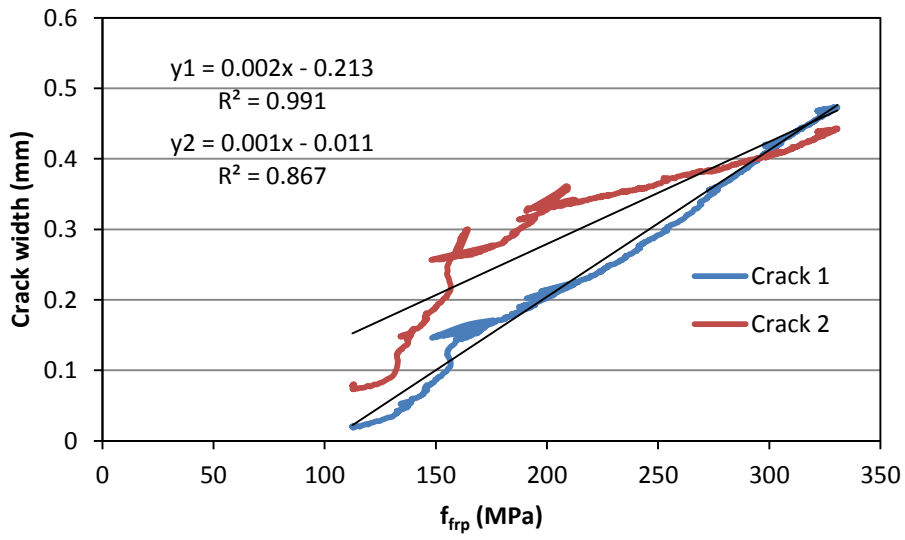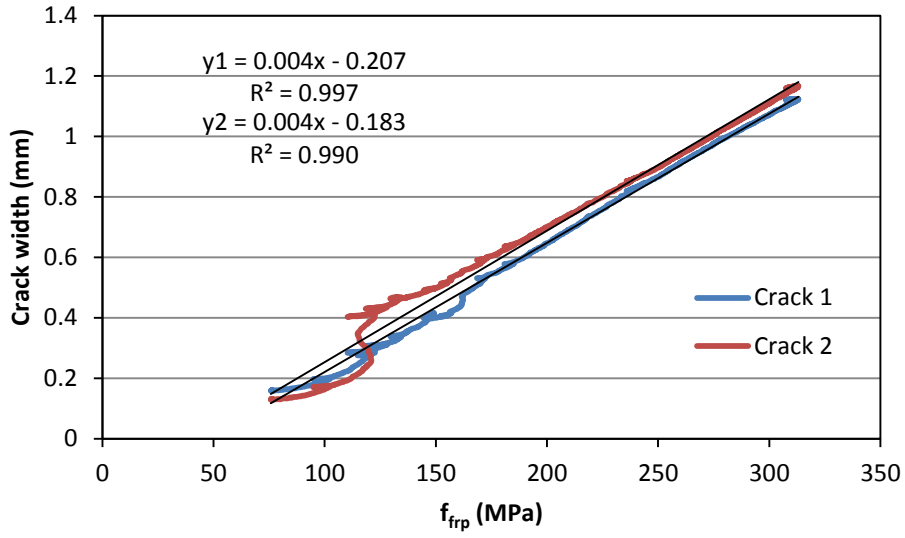
F1 PHASE I
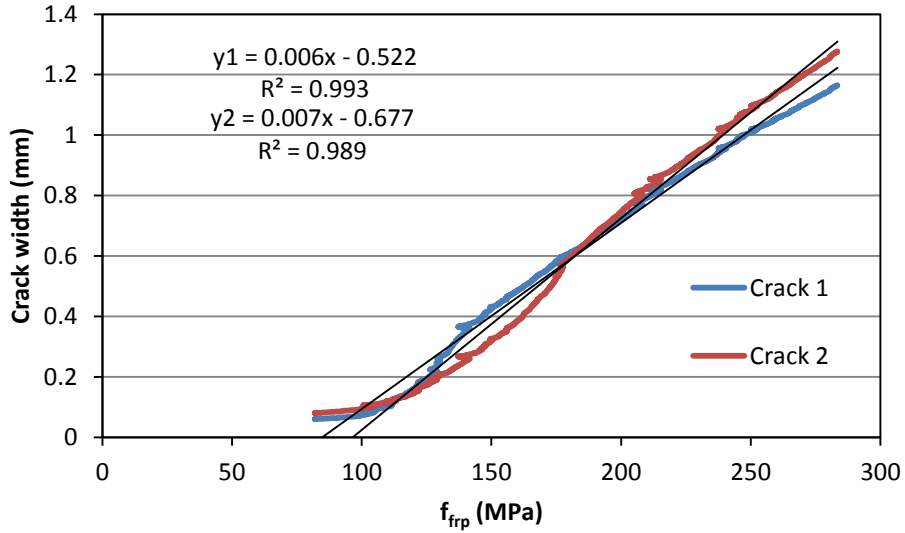
Figure F.1 - Typical cracking behaviour for B1
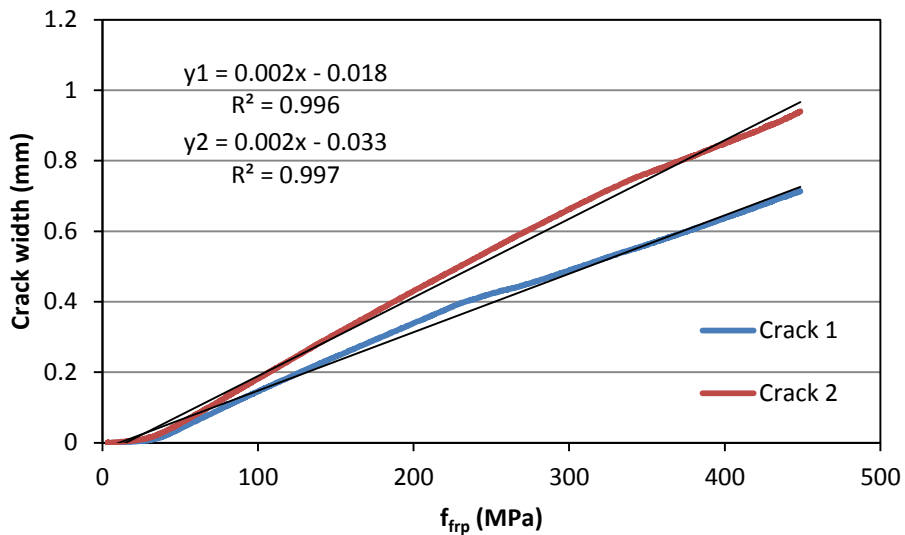
Figure F.2 - Typical cracking behaviour for B2
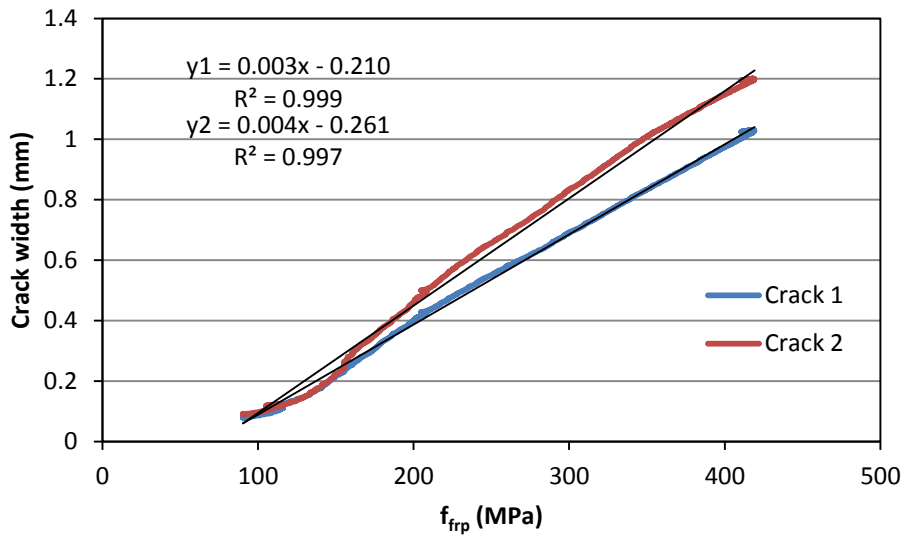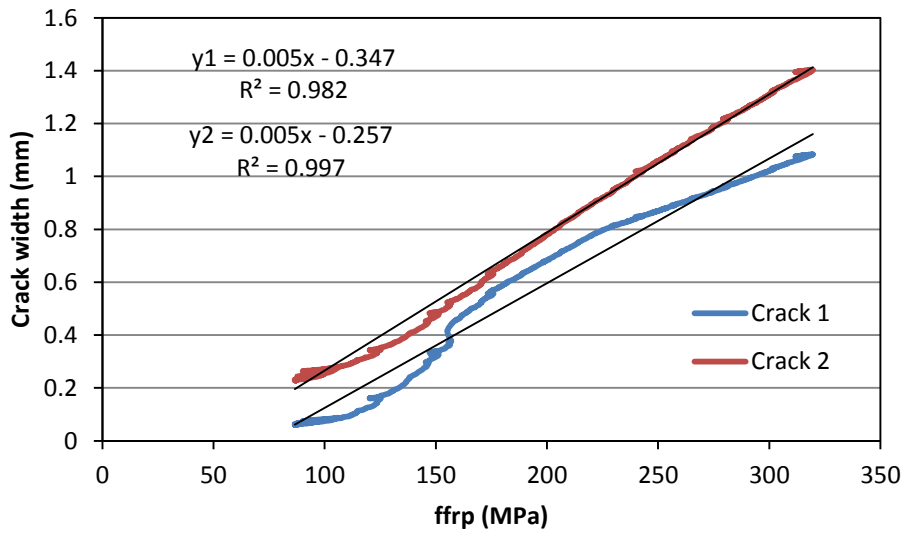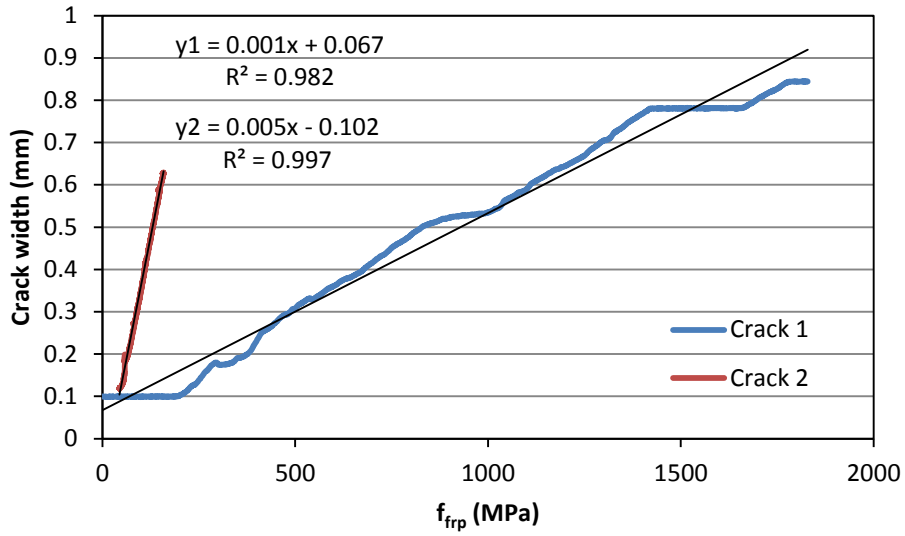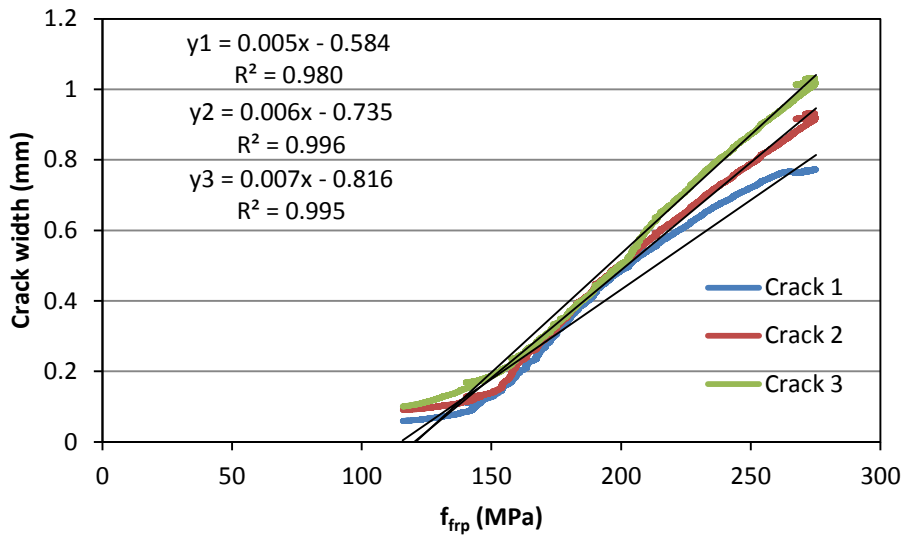
Figure F.3 - Typical cracking behaviour for B3
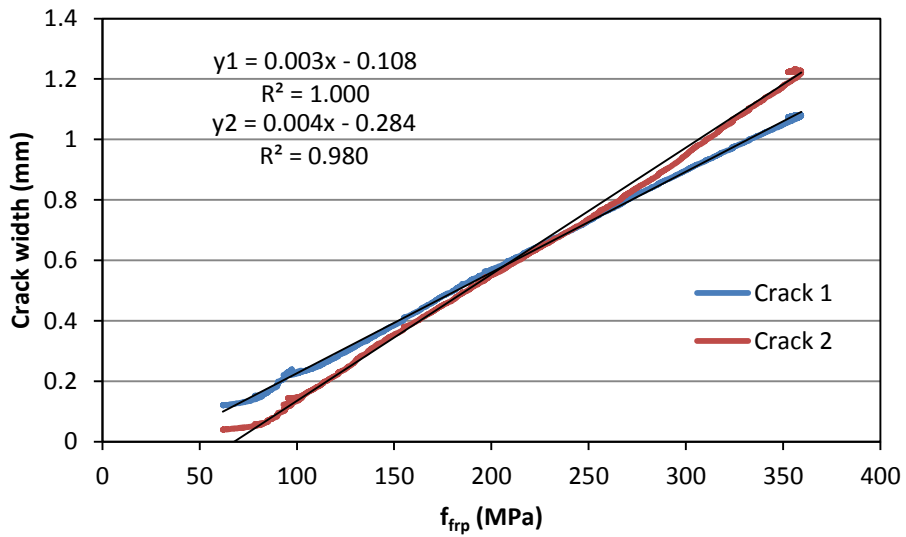
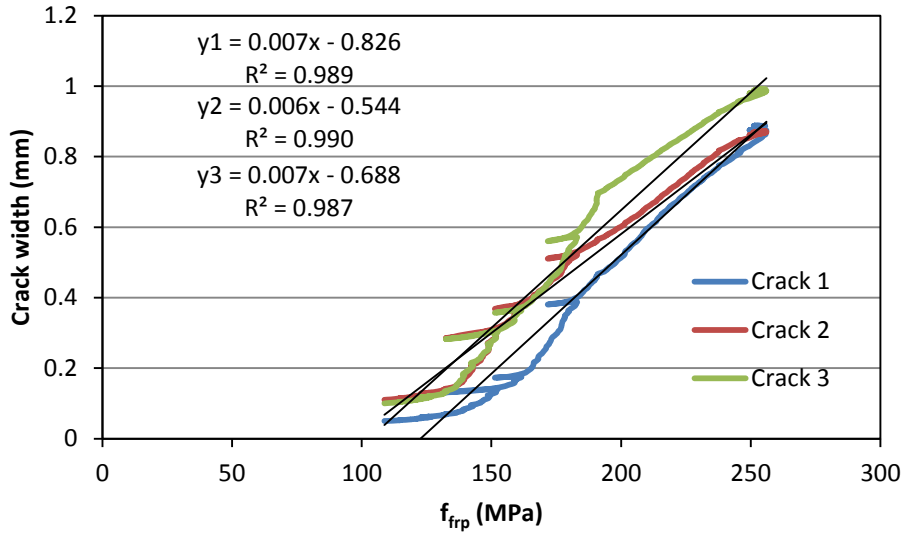**Figure F.4 - Typical cracking behaviour for B4**

165
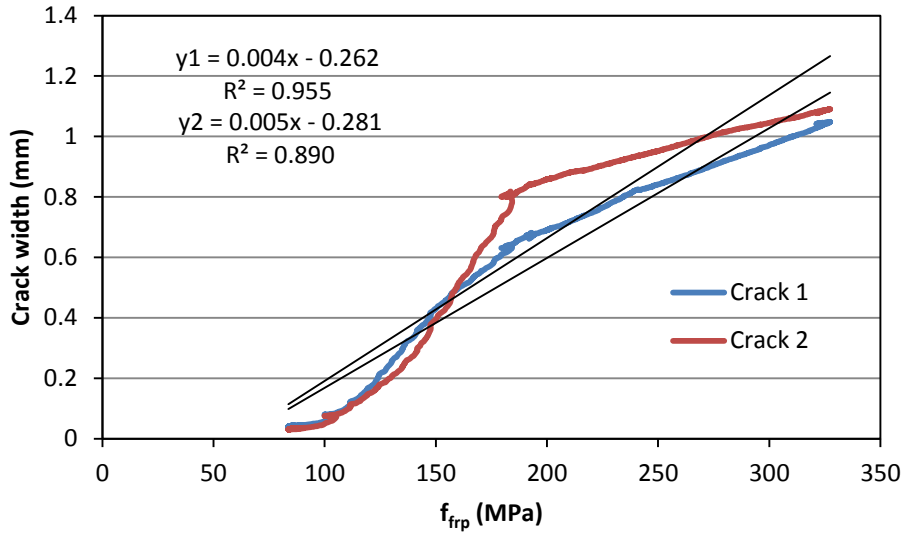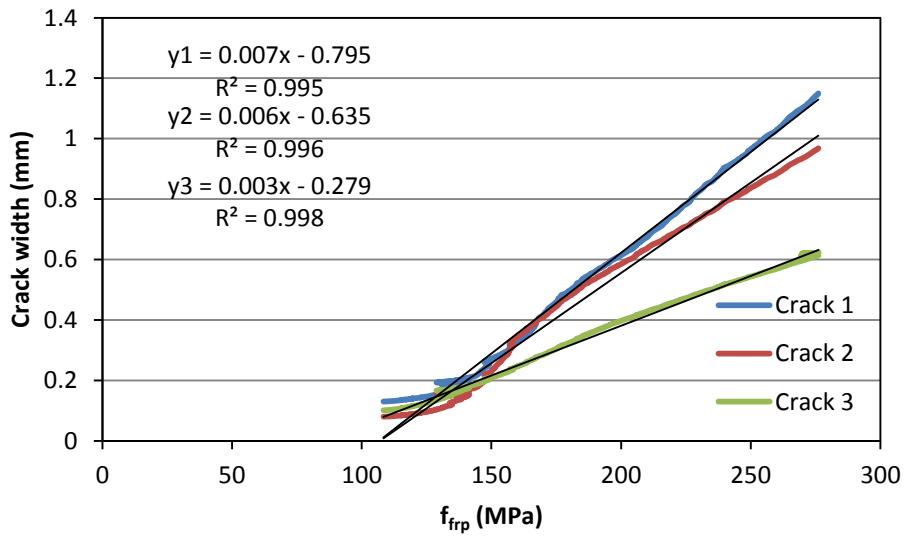
Figure F.5 - Typical cracking behaviour for B5
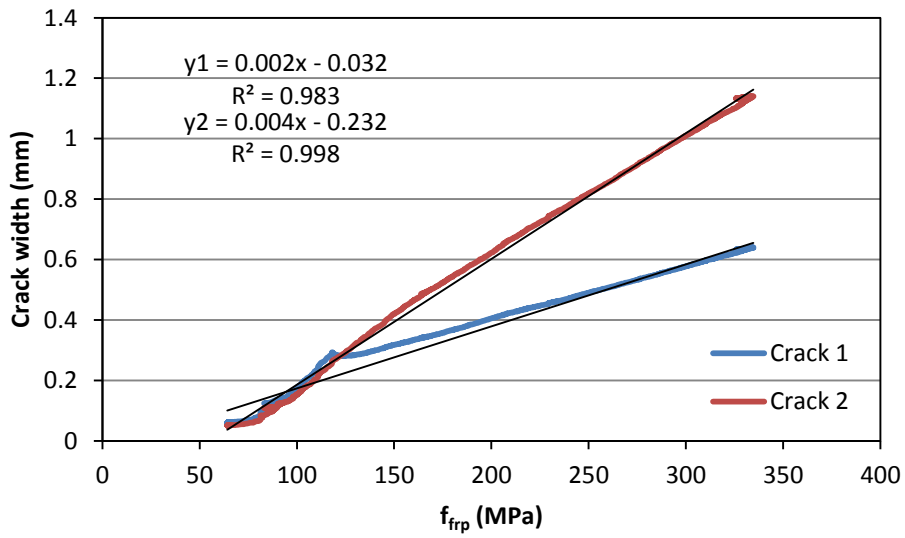
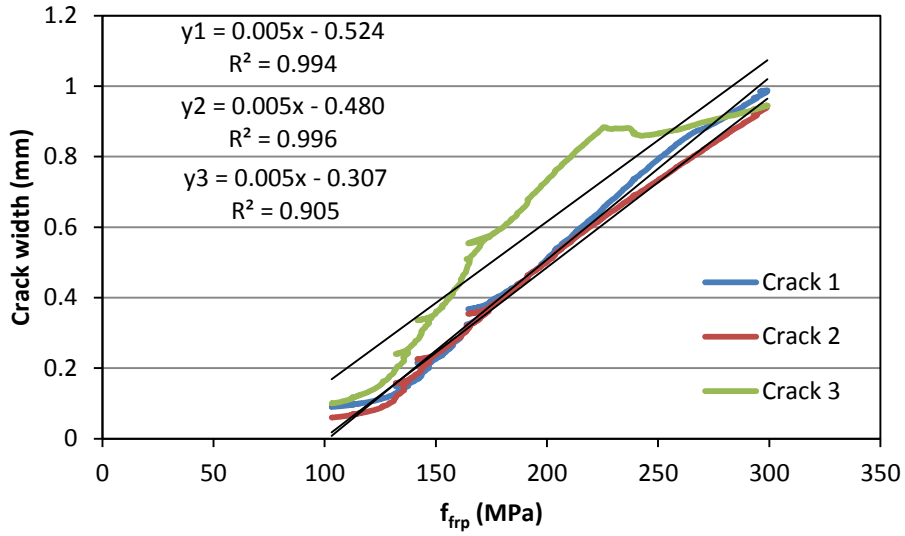

Figure F.6 - Typical cracking behaviour for B6
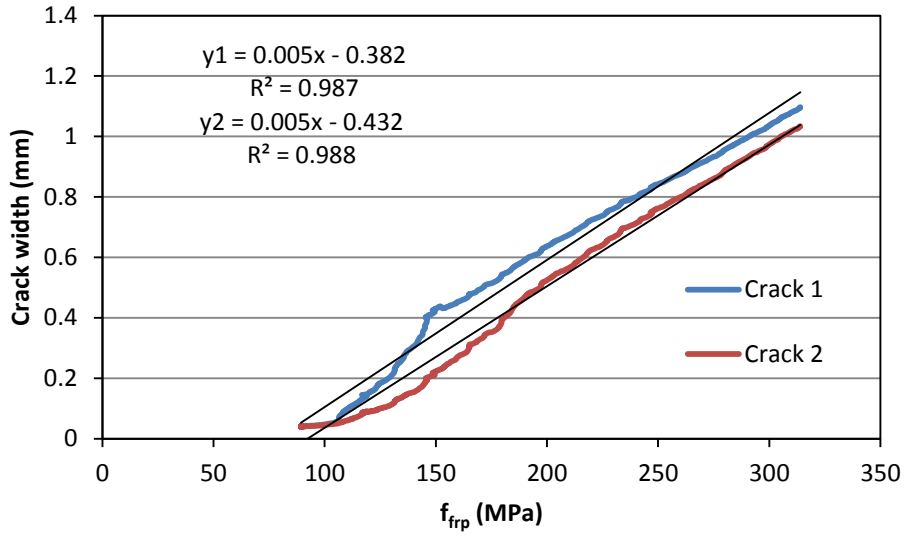
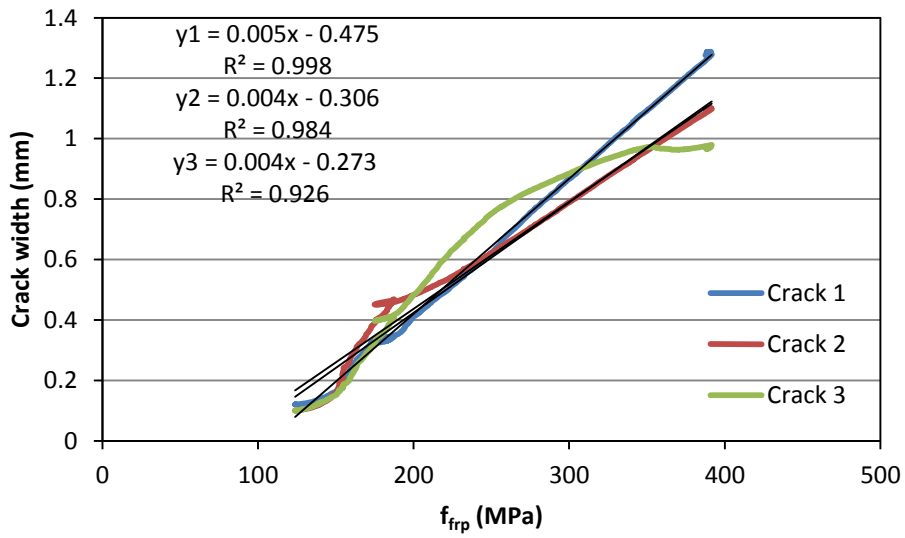**Figure F.7 - Typical cracking behaviour for B7**
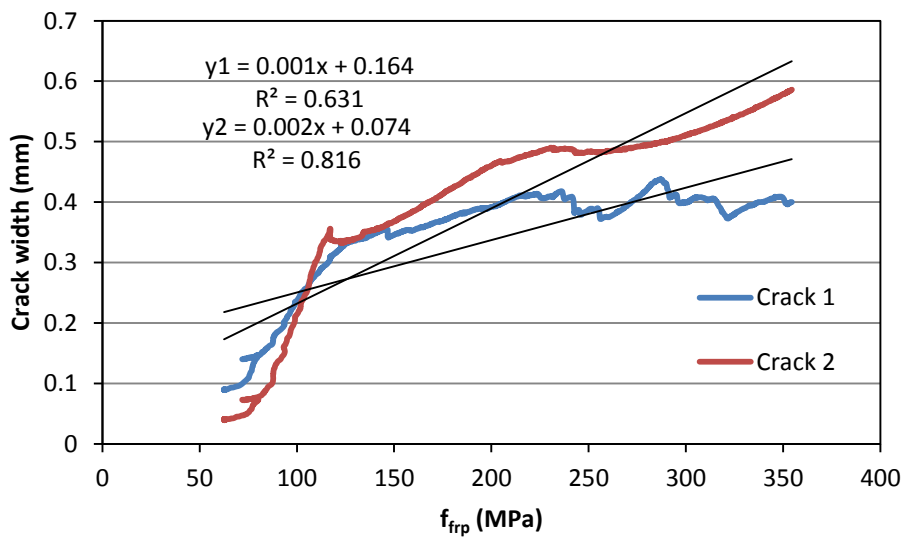
Figure F.8 - Typical cracking behaviour for B8
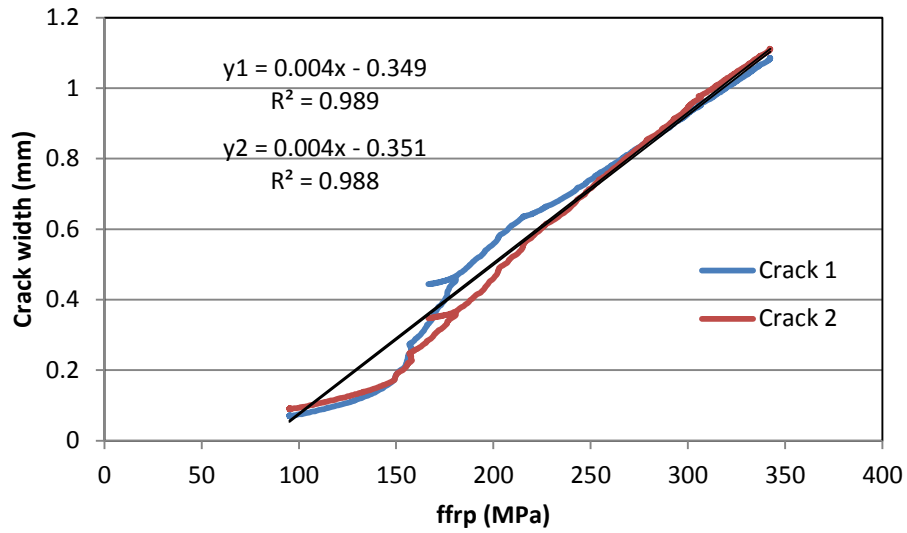
Figure F.9 - Typical cracking behaviour for B9
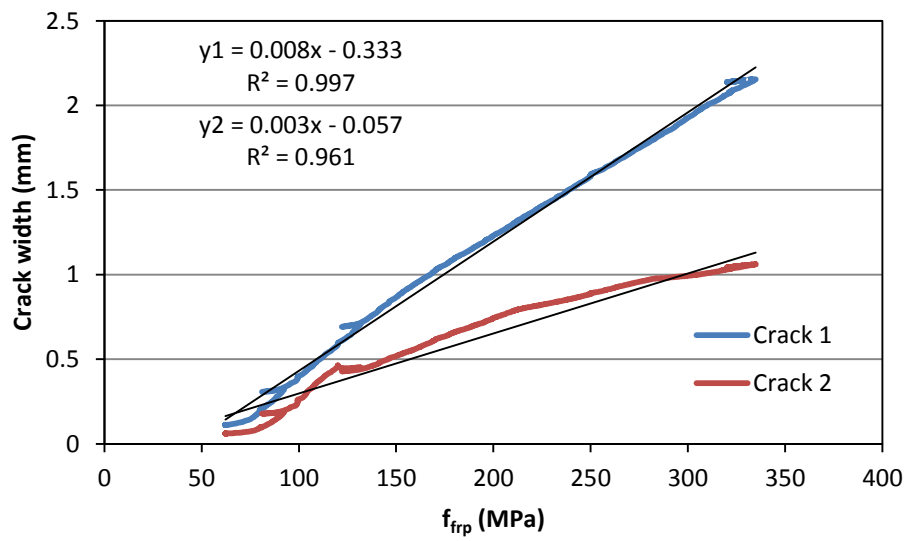
Figure F.10 - Typical cracking behaviour for B10
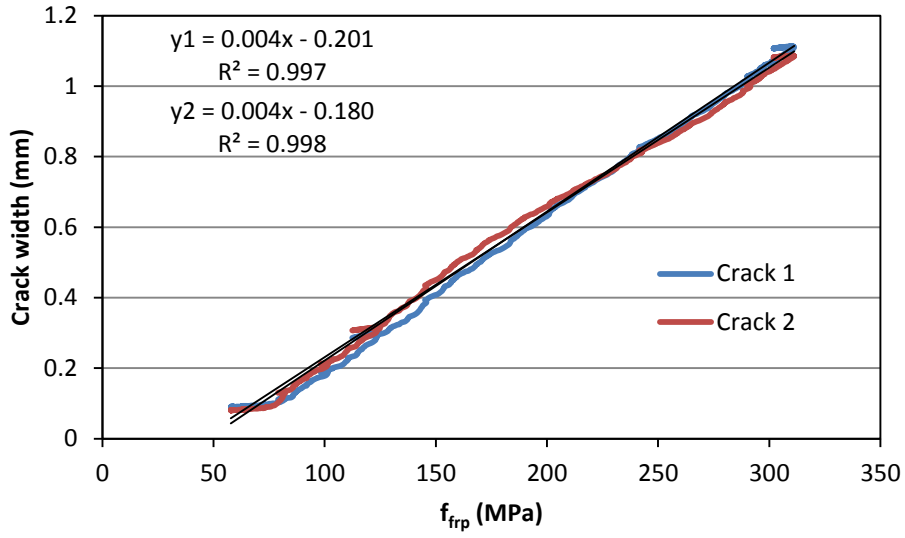
Figure F.11 - Typical cracking behaviour for B13
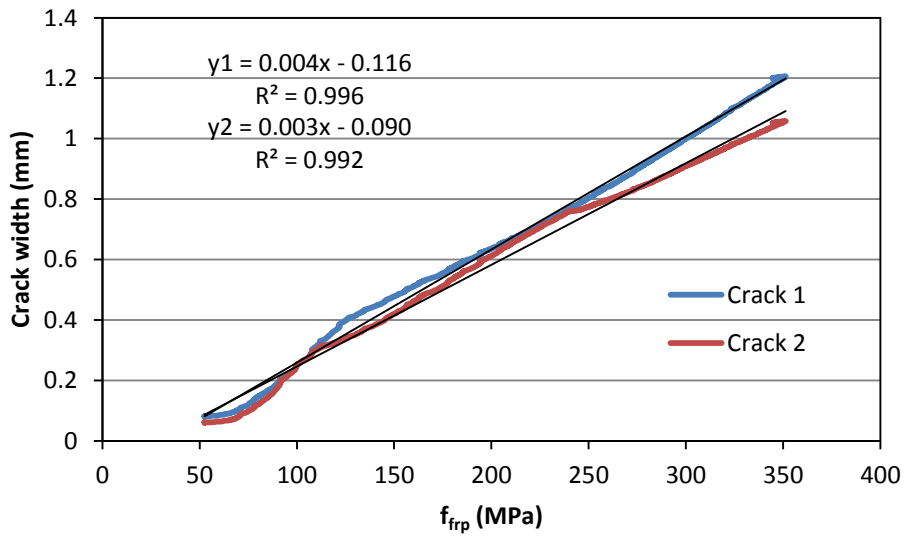
Figure F.12 - Typical cracking behaviour for B14

y1 = 0.003x - 0.013
R² = 0.936
y2 = 0.003x - 0.157
R² = 0.998
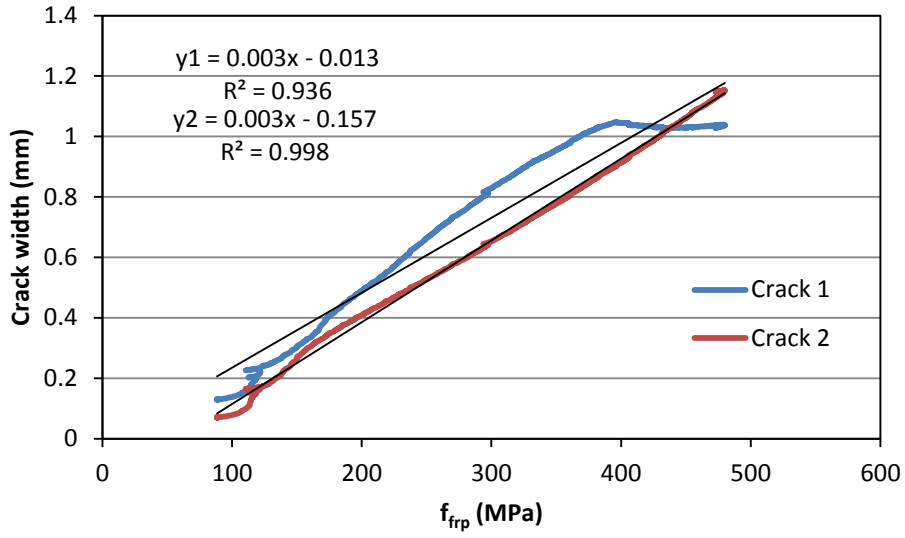
Figure F.13 - Typical cracking behaviour for B15

y1 = 0.003x - 0.083
R² = 0.999

y2 = 0.004x - 0.227
R² = 0.994
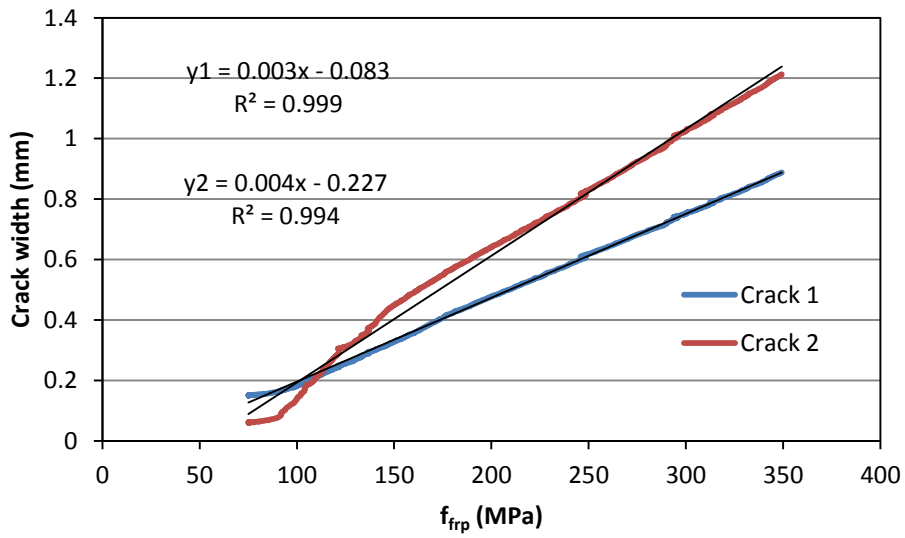
Figure F.14 - Typical cracking behaviour for B16

170
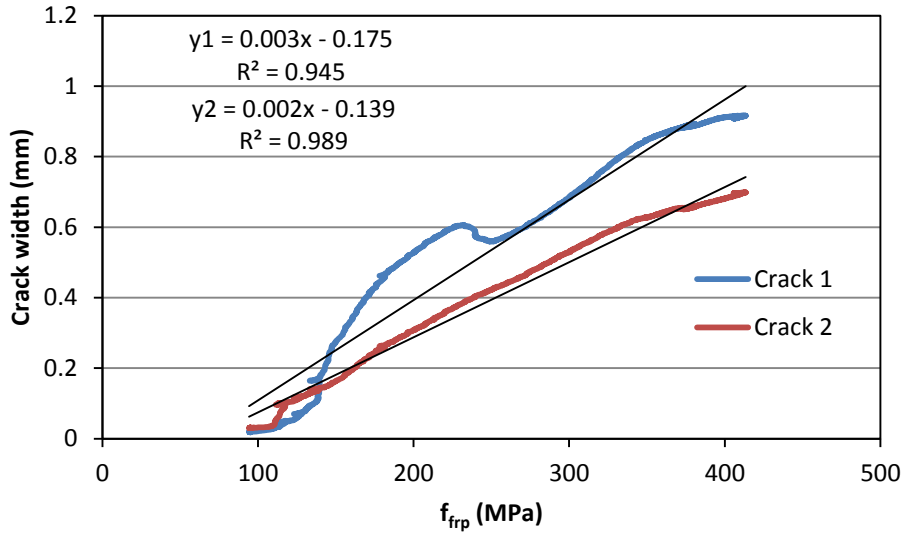
Figure F.15 - Typical cracking behaviour for S1
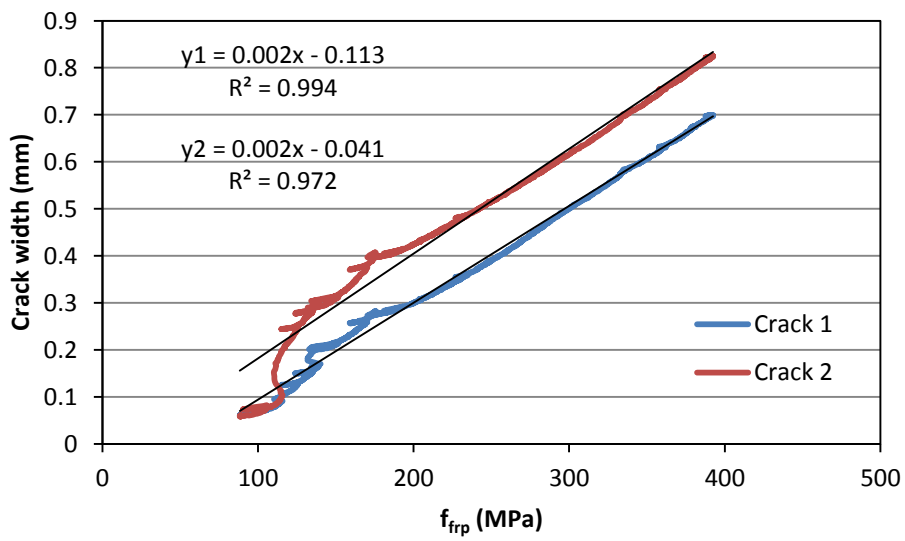
Figure F.16 - Typical cracking behaviour for S2
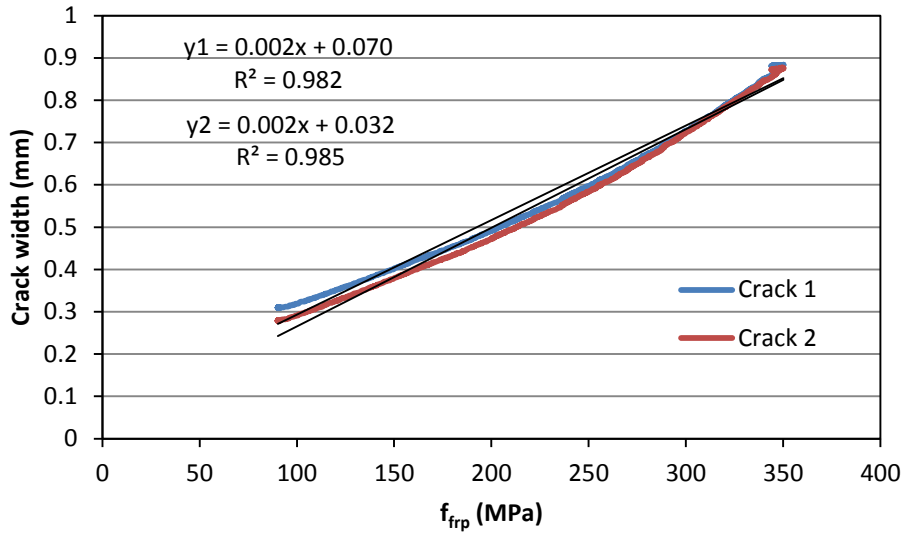
Figure F.17 - Typical cracking behaviour for S3
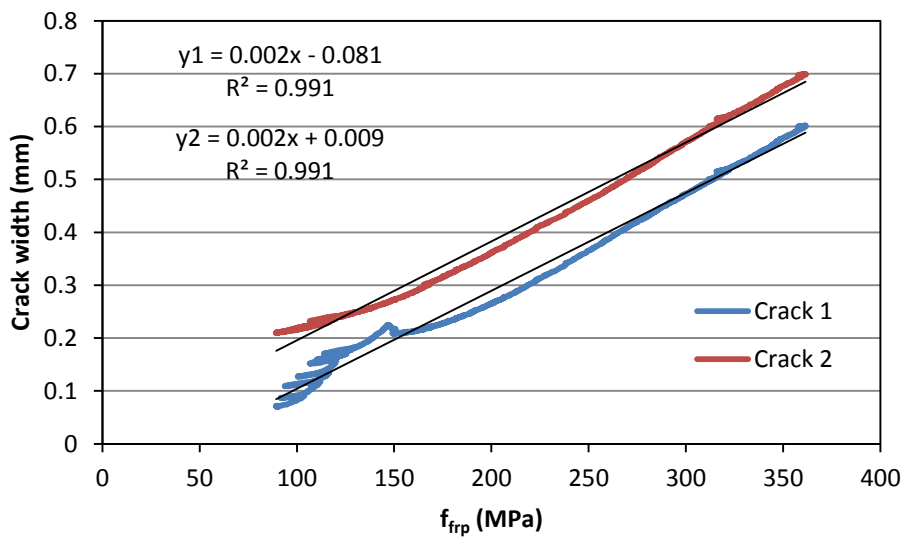
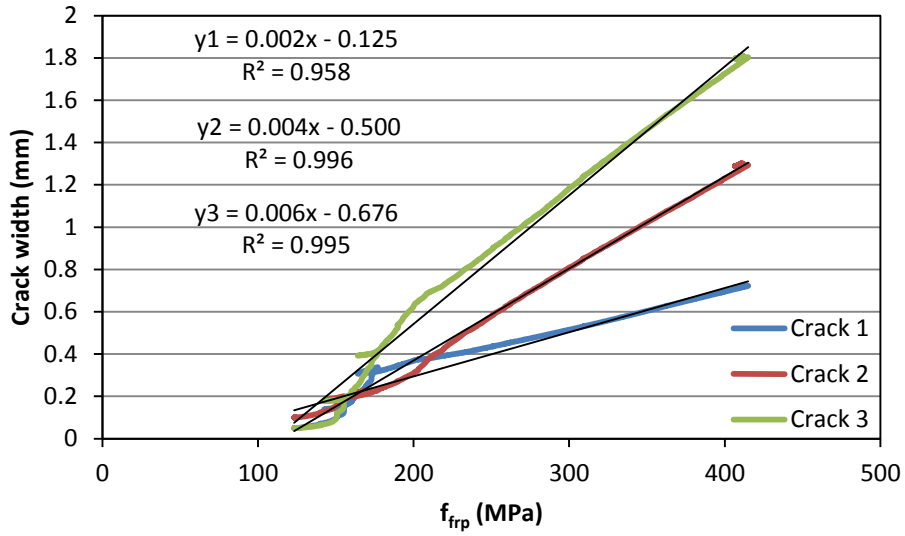**Figure F.18 - Typical cracking behaviour for S4**

Figure F.19 - Typical cracking behaviour for S5
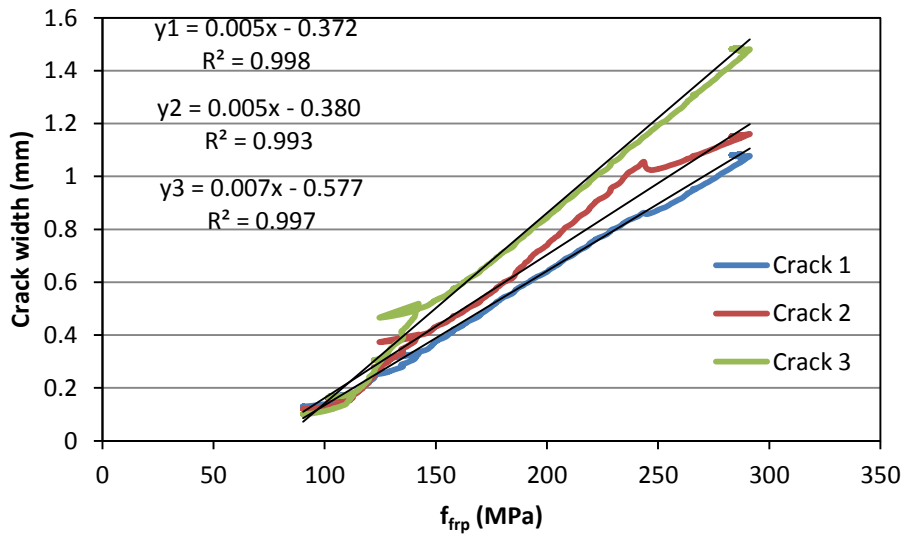

Figure F.20 - Typical cracking behaviour for S6

Figure F.21 - Typical cracking behaviour for S7

Figure F.22 - Typical cracking behaviour for S8

174

Figure F.23 - Typical cracking behaviour for S9

F2   PHASE IIA

Figure F.24 - Typical cracking behaviour for B1V5

Figure F.25 - Typical cracking behaviour for B2V5

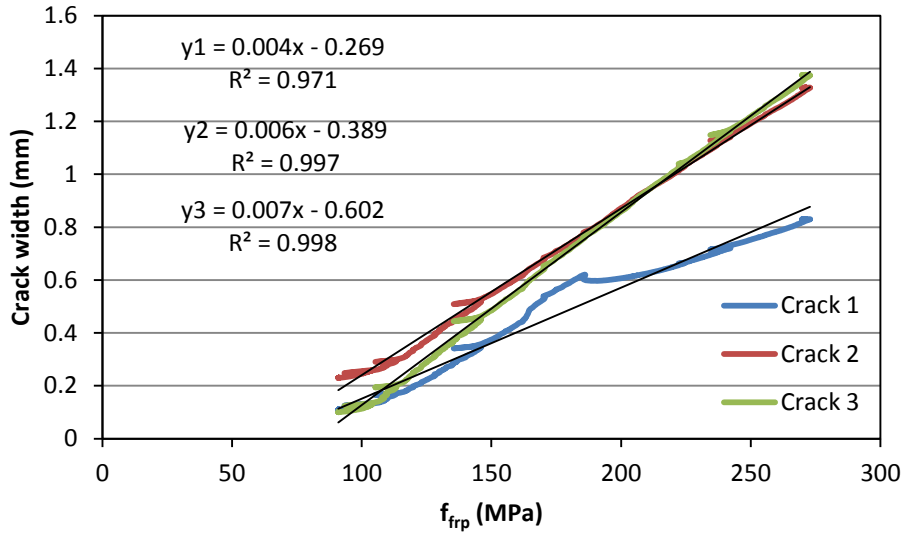**Figure F.26 - Typical cracking behaviour for B3V5**

Figure F.27 - Typical cracking behaviour for B4V5

Figure F.28 - Typical cracking behaviour for B5V5

Figure F.29 - Typical cracking behaviour for BA5

Figure F.30 - Typical cracking behaviour for BV6
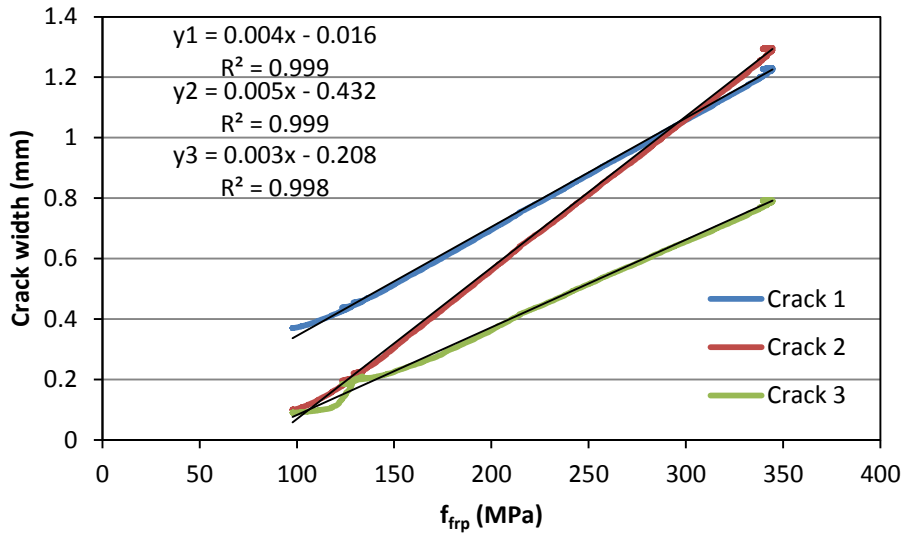
Figure F.31 - Typical cracking behaviour for BA6

F3 PHASE IIB

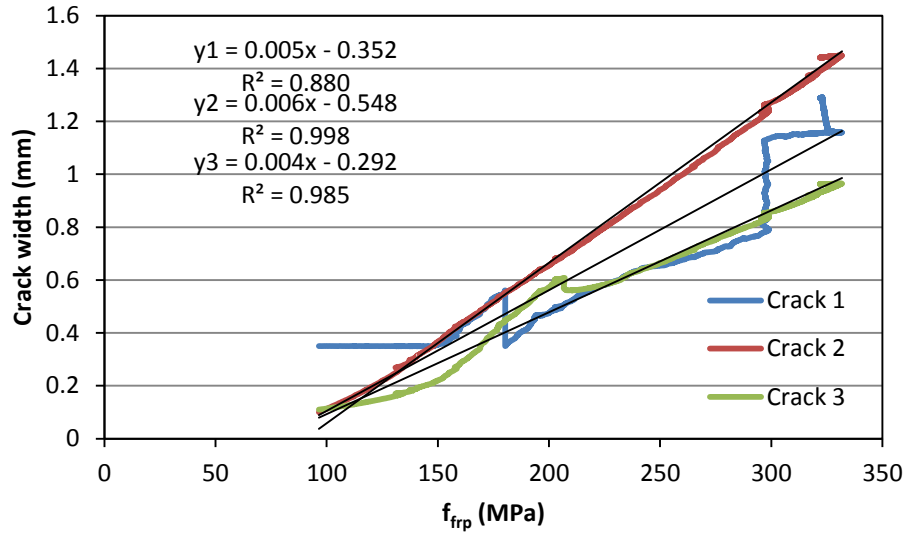**Figure F.32 - Typical cracking behaviour for B38**

Figure F.33 - Typical cracking behaviour for B50

APPENDIX G: CALCULATIONS FOR FRP STRESSES

For this study, the stress in the FRP reinforcement was calculated using elastic cracked section theory. This theory assumes the section is cracked but remains linear elastic with a strain distribution as shown in Figure G.1. In addition, the concrete in tension is considered to be ineffective while the FRP reinforcement takes all tensile stress.
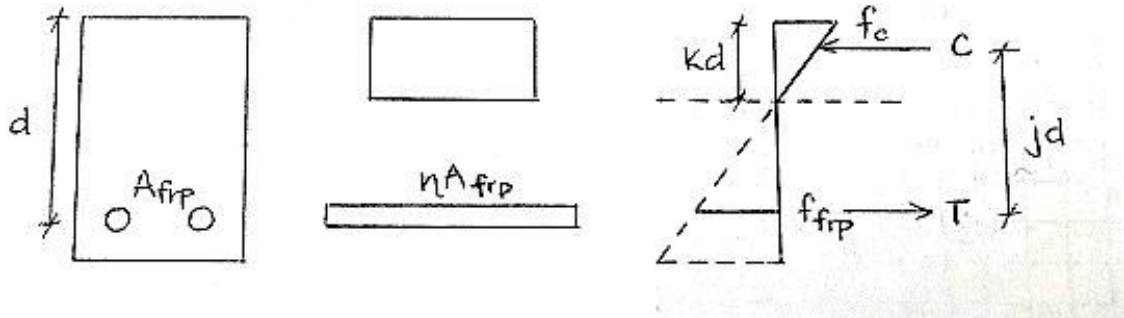

Figure G.1 - Assumed strain distribution

The location of the neutral axis (kd) can be determined by calculating k using Equation [G.1]. The moment arm (jd) between the tension and compression force can be found using relationships between j and k, as shown in Equation [G.2].

$$k = \sqrt{2\rho\eta + (\rho\eta)^2} - \rho\eta \qquad \text{[G.1]}$$

where,

η is the modular ratio (E_{frp}/E_c)

ρ is the FRP reinforcement ratio

$$j = 1 - \frac{1}{3}k \qquad \text{[G.2]}$$

The moments can then be computed using the compression force (Equation [G.3]) or the tension force (Equation [G.4]), which give equivalent values.

$$M = \frac{1}{2}kjf_cbd^2 \qquad \text{[G.3]}$$

$$M = A_{frp}f_{frp}jd \qquad \textbf{[G.4]}$$

To determine the stresses in the concrete (f_c) and the FRP reinforcement (f_{frp}), the following equations can then be used:

$$f_c = 2\frac{M}{kj}bd^2 \qquad \textbf{[G.5]}$$

$$f_{frp} = \frac{M}{A_{frp}jd} \qquad \textbf{[G.6]}$$